國立成功大學
太空與電漿科學研究所
碩士論文

National Cheng Kung University
Institute of Space and Plasma Sciences
Master Thesis

利用高壓產生電漿的極紫外光源中電漿羽流之開發

Development of the plasma plume for an extreme ultraviolet light source using discharged-produced plasma

研究生 (Author)：劉致賢 Chih-Hsien Liu
指導老師 (Advisor)：張博宇博士 Dr. Po-Yu Chang
中華民國一百一十二年七月 July, 2023

國立成功大學

碩士論文

利用高壓產生電漿的極紫外光源中電漿羽流之開發

Development of the plasma plume for an extreme ultraviolet light source using discharged-produced plasma

研究生：劉致賢

本論文業經審查及口試合格特此證明

論文考試委員：

張博宇　曲宏洋

劉耀德

指導教授：張博宇

單位主管：電機所所長 河森榮一郎

（單位主管是否簽章授權由各院、系（所、學位學程）自訂）

中 華 民 國 112 年 7 月 5 日

摘要

本篇論文主要目的是開發氬氣電漿羽流產生器，用於產生極紫外微影所需要的光源。使用極紫外光源的光刻技術是目前半導體最先進的技術之一，我們想透過角向捏縮電漿羽流的方式產生極紫外光刻光源。我們透過放電產生的電漿來產生極紫外光的方式有三個步驟：（1）爲產生氬氣噴流。（2）氬氣噴流通過有高壓之電極後放電，氣體會加溫並游離成電漿羽流，因此溫度會上升至1～10 eV。（3）電漿羽流通過由本實驗室的脈衝功率系統推動的荷姆霍茲線圈（Helmholz coil），透過角向捏縮，以絕熱壓縮的方式將電漿羽流的溫度提升至30 eV，因此產生極紫外光源。在實驗中，我負責的部分爲步驟（1）和（2）。透過噴氣系統（Gas-puff system）噴出氬氣噴流，氬氣噴流經由氣管進入在眞空腔中跨有高壓的游離收斂-擴張噴嘴(Ionization Convergent-Diveregent Nozzle，ICDN），誘發電弧放電，產生電漿羽流，同時透過噴嘴的結構，將氬氣噴流加速至超音速，使氣體在離開噴嘴時的張角(opening angle)比較小， 能夠準直地進入荷姆霍茲線圈，以利後面透過角向捏縮的絕熱壓縮能夠進行。我們在最後的實驗中也看到了氬氣噴流經離收斂-擴張噴嘴形成電漿。我們透過側視相機捕捉到電漿羽流，也透過干涉儀看到了氣體噴流與電漿羽流所造成探測雷射光相位的變化。 這些資訊有利於我們後續光源的設計。

關鍵字： 極紫外微影光源， 氬氣噴流， 噴氣系統， 離收斂-擴張噴嘴

Abstract

As the line width of semiconductor manufacturing becomes narrower and narrower, the importance of extreme ultraviolet (EUV) lithography technology with a light source wavelength of 13.5 nm increases significantly in the reproduction of conductor manufacturing processes. The goal of this thesis is to generate an argon plasma plume for the EUV light source using discharged-produced plasma. The EUV light source has three steps. The first step is to generate argon gas puff. In the second step, the argon gas puff passes through an electrode pair with a high voltage across it. An arc discharge is initiated so the gas is ionized and heated. At this time, the temperature rises to 1-10 eV. The third step is to compress the plasma when it passes through the Helmholtz coil driven by the pulsed-power system. The plasma is heated through the adiabatic compression. Finally, the plasma plume radiates EUV light when it is heated to ∼30 eV. In this thesis, my goal was to accomplish the first and the second step. An argon gas puff was generated by the gas-puff system. The gas puff was delivered to the ionization convergent-divergent nozzle (ICDN) in the vacuum chamber through the gas tube. A high voltage was provided across the electrode pair in the ICDN. Therefore, an arc discharge was initiated. Therefore, the gas puff was ionized and heated. Meanwhile, the CDN in the ICDN accelerated the plasma plume to supersonic speed. In experiments, the plasma plume was generated and observed from the side-view camera. We also used the interferometer to measure the phase shift of the probe laser beam due to the gas puff/plasma plume. We will use the experimental results to design our EUV light source in the future.

Keywords: Extreme ultraviolet lithography light source, argon gas jet, gas-puff system, convergent-divergent nozzle, opening angle.

Contents

1 Introduction **1**

1.1 The extreme ultraviolet lithography . . . 1

1.2 Our EUV light source project . . . 2

1.3 The Gas-puff system . . . 3

1.4 Helmholtz coil . . . 4

1.5 The goal of this thesis . . . 4

2 The experimental platform **5**

2.1 The pulsed-power system . . . 5

2.2 Laser diagnostics . . . 6

3 The gas-puff system **8**

3.1 The design of the gas-puff system . . . 8

3.2 The pulse-valve controller . . . 8

3.3 Testing of the pulse-valve controller . . . 10

3.4 Action test of the pulse valve . . . 12

4 The pulse-valve testing experiment **16**

4.1 Experimental setup for observing the gas puff . . . 16

4.2 Pusle valve with 0.1 mm outlet . . . 17

4.2.1 Glass tube . . . 17

4.2.2 Glass convergent nozzle . . . 19

4.2.3 Plastic convergent-divergent nozzle . . . 21

4.3 Pulse valve with 1-mm outlet . . . 22

4.3.1 Chamber pressure at 1 atm . . . 22

4.3.2 Chamber pressure in vacuum . . . 23

4.4 Opening angle analysis . . . 25

5 The plasma-plume generating system **28**

5.1 The gas-puff arcing system . . . 28

5.2 The design of the ionziation convergent-divergent nozzle system . . . 29

5.3 Gas-puff and plasma-plume generations . . . 32

5.3.1 Gas-puff generation . . . 32

5.3.2 Plasma-plume generation . . . 33

5.4 Analysis process of the interferometer images . . . 37

5.5 Analysis result of interferometer images . . . 45

5.6 Opening angle analysis . . . 48

6 Future works **53**

7 Summary **54**

8 Reference **55**

A Appendix **56**

A.1 Pulse valve voice delay test . . . 56

A.2 The gas puff schlieren image 0.1 mm outlet about the laser delay setting from 50.39 ms to 100.39 ms . . . 58

A.3 ICDN system design . . . 62

A.4 super-Gaussing function fitting . . . 65

A.4.1 High voltage(HV)-laser delay time 20 ms-1 (first data) . . . 65

A.4.2 HV-20ms-2 . . . 69

A.4.3 HV-30ms-1 . . . 73

A.4.4 HV-30 ms-2 . . . 77

A.4.5 HV-40 ms . . . 81

A.4.6 No high voltage(HV)-20 ms-1 . . . 85

A.4.7 No HV-20 ms-2 . . . 88

A.4.8 No HV-20 ms -3 . . . 92

A.4.9 No HV- 20 ms-4 . . . 95

A.4.10 No HV-30 ms-1 . . . 98

A.4.11 No HV-30 ms-2 . . . 101

A.4.12 No HV- 30 ms-3 . . . 104

A.4.13 No HV-30 ms-4 . . . 107

A.4.14 No HV-30 ms-5 . . . 109

A.4.15 No HV-40 ms-1 . . . 111

A.4.16 No HV-40 ms-2 . . . 114

A.4.17 No HV-40 ms -3 . . . 117

A.5 Nas store record . . . 120

List of Figures

1 The process of semiconductor manufacturing [Ref 1] . . . 2
2 The EUV light source experiment schematic diagram [Ref 2] . . . 3
3 The Argon gas will undergo ionization when it passes through the electrodes in the system . . . 3
4 Gas-puff system schematic diagram . . . 3
5 The structure of Helmholz coil. From Cheng-Han Du thesis,"Development of the magneric field in a theta pinch in the EUV light source."[Ref 3] . . . 4
6 The-pulse-power system schematic diagram [Ref 4] . . . 5
7 Photo of the pulsed-power system. [Ref 5] . . . 6
8 Laser path [Ref 6] . . . 7
9 Gas-puff system schematic diagram . . . 8
10 Circuit of the pulse-valve cintroller. . . . 9
11 Photo of the pulse-valve controller. . . . 9
12 Layout of the pulse-valve controller. . . . 10
13 Pulse valve circuit delay time test . . . 11
14 The pattern of the wave generator analysis about gas-puff signal and wave signal. . . . 11
15 The gas-puff system. . . . 13
16 Pulse-valve system delay-experiment setup. . . . 13
17 Sound track of 50-ms pulse width. . . . 14
18 Sound track of 5-ms pulse width. . . . 14
19 Pulse valve reaction of time delay statistics. . . . 15
20 (a) schematic of the gas-puff experiments. (b) The photo of the convergent nozzle installed in the chamber. . . . 17
21 Experimental setting processs . . . 17
22 glass tube dimension . . . 18
23 (a) Schileren image: pulse valve was open 50 ms gas, laser delay time setting: 70.39 ms. (b) Schileren image: No gas puff. . . . 18
24 (a) Schileren image: pulse valve was open for 5 sec (b) Schileren image: No gas puff. . . . 18
25 (a): The shadowgraph image: pulse valve was open for 5 sec. (b) Shadowgraph image: No gas puff. . . . 19
26 (a): Interferometer image: pulse valve was open for 5 sec. (b): Interferometer image: No gas puff 19
27 Convergent nozzle dimension . . . 20
28 (a) Schileren image (b) shadowgraph image of the convergent nozzle with chamber pressure at 1 atm. . . . 20
29 The schileren image of the convergent nozzle with chamber pressure at $10^{-3}\,Torr$ . . . 21
30 Interferometer image of the convergent nozzle with chamber pressure at $10^{-3}\,Torr$ . . . 21

31 The shileren image image of the 24-V V8 CDN. From Fig.76 on page of Jia-Kia Liu's thesis, "study of the gas puff in the EUV light source using a theta pinch." {Ref} . . . 22
32 Interfometer image (a)shadowgraph image (b) of the convergent nozzle with chamber pressure at 1 atm. . . . 22
33 Schlieren image of the convergent nozzle with chamber pressure at 1 atm. . . . 23
34 Schlieren image of the convergent nozzle with chamber pressure at 1 atm . . . 23
35 Schlieren image of the gas puff under vacuum 10^{-3}Torr . . . 24
36 Schlieren image of the gas puff under vacuum 10^{-3} Torr . . . 24
37 Schlieren image captured in vacuum environment with gas jet - cutline 600. . . . 26
38 The calculation of the opening angle. . . . 26
39 The opening angle calculated . . . 27
40 Arcing circuit schematic diagram . . . 28
41 The schematic diagram of chamber and 260-mm electrode gas tube . . . 30
42 Electrode gas tube drawing . . . 31
43 Paschen curve of argon [Ref 7] . . . 32
44 No high voltage, laser delay time 30 ms . . . 33
45 The side-view picture . . . 34
46 convergent-divergent nozzle . . . 34
47 convergent-divergent nozzle -1 . . . 35
48 Gas tube burning point . . . 35
49 The voltage oscillation . . . 36
50 High voltage, laser delay time 30ms . . . 37
51 plasma plume arrow image . . . 37
52 Raw interferometer image of the 20 ms laser delay . . . 38
53 The cutline of example . . . 39
54 The analyze data in matlab . . . 40
55 The average array about the cutline data . . . 41
56 The analyze data in matlab rotate by 90 degrees . . . 42
57 The data of columns 450 to 900 on the y-axis average array . . . 43
58 The super gaussian fitting analyze . . . 43
59 The super gaussian fitting analyze . . . 44
60 The super gaussian fitting analyze . . . 44
61 The gas puff displays the extracted regions . . . 45
62 Comparison of phases between the Gas puff and the plasma plume of 20 ms. . . . 47
63 Comparison of phases between the Gas puff and the plasma plume of 30 ms. . . . 47
64 Comparison of phases between the Gas puff and the plasma plume of 40 ms. . . . 48
65 Data analyze of the opening angle . . . 49

66 Use slope to calculate the opening angle-2 . . . 50
67 Use slope to calculate the opening angle-3 . . . 50
68 Use slope to calculate the opening angle-4 . . . 51
69 Use slope to calculate the opening angle-5 . . . 51
70 Use slope to calculate the opening angle-6 . . . 51
71 Pulse valve voice analyze-1 . . . 56
72 Pulse valve voice analyze-2 . . . 57
73 Setting at laser time dealy 50.39 ms schlieren image . . . 58
74 Setting at laser time dealy 55.39 ms schlieren image . . . 59
75 Setting at laser time dealy 60.39 ms schlieren image . . . 59
76 Setting at laser time dealy 70.39 ms schlieren image . . . 60
77 Setting at laser time dealy 80.39 ms schlieren image . . . 60
78 Setting at laser time dealy 90.39 ms schlieren image . . . 61
79 Setting at laser time dealy 100.39 ms schlieren image . . . 62
80 Back electrode design . . . 62
81 Connect base holder.electrode (Brass) design . . . 63
82 Connect electrode plastic sheet . . . 63
83 Electrode gas tube assemble design . . . 64
84 Electrode gas tube assemble design . . . 64
85 X軸:pixel Y軸:phase. Plasma plume, 20ms delay, average of cols 400~900, average of row 50~200. 65
86 X軸:pixel Y軸:phase.Plasma plume, 20ms delay, average of cols 400~900, average of row 200~350 65
87 X軸:pixel Y軸:phase. Plasma plume, 20ms delay, average of cols 400~900, average of row 350~500 66
88 X軸:pixel Y軸:phase Plasma plume, 20ms delay, average of cols 520~750, average of row 50~150 . 66
89 X軸:pixel Y軸:phase. Plasma plume, 20ms delay, average of cols 520~730, average of row 150~250 66
90 X軸:pixel Y軸:phase. Plasma plume, 20ms delay, average of cols 500~750, average of row 250~350 67
91 X軸:pixel Y軸:phase. 合併selction three function blue line (50~150), red line (150~250), green line 250~350 . . . 67
92 Rotate 90 degree image . . . 68
93 FWHM about selction 50~150 (left), 150~250(middle), 250~350 (right). . . . 68
94 X軸:pixel Y軸:phase. Plasma plume, 20ms delay, average of cols 400~900, average of row 50~200 69
95 X軸:pixel Y軸:phase. Plasma plume, 20ms delay, average of cols 400~900, average of row 200~350 69
96 X軸:pixel Y軸:phase. Plasma plume, 20ms delay, average of cols 400~900, average of row 350~500 70
97 X軸:pixel Y軸:phase. Plasma plume, 20ms delay, average of cols 520~750, average of row 50~150 70
98 X軸:pixel Y軸:phase. Plasma plume, 20ms delay, average of cols 520~750, average of row 150~730 70
99 X軸:pixel Y軸:phase. Plasma plume, 20ms delay, average of cols 500~750, average of row 250~350 71
100 X軸:pixel Y軸:phase. 合併selction three function blue line (50~150), red line (150~250), green line 250~350 . . . 71

101 rotate 90 degree image 72
102 X軸:pixel Y軸:phase Plasma plume, 20ms delay, average of cols 500~750, average of row 250~350 72
103 FWHM about selction 50~150 (left), 150~250(middle), 250~350 (right). 73
104 X軸:pixel Y軸:phase. Plasma plume, 30ms delay, average of cols 400~900, average of row 50~200 73
105 X軸:pixel Y軸:phase. Plasma plume, 30ms delay, average of cols 400~900, average of row 200~350 73
106 X軸:pixel Y軸:phase. Plasma plume, 30ms delay, average of cols 400~900, average of row 350 ~500 74
107 X軸:pixel Y軸:phase. Plasma plume, 30ms delay, average of cols 520~750, average of row 50~150 74
108 X軸:pixel Y軸:phase. Plasma plume, 30ms delay, average of cols 520~750, average of row 150~250 74
109 X軸:pixel Y軸:phase. Plasma plume, 30ms delay, average of cols 500~750, average of row 250~350 75
110 X軸:pixel Y軸:phase. 合併selction three function blue line (50~150), red line (150~250), green line 250~350 75
111 rotate 90 degree image 76
112 FWHM about row selction 50~150 (left), 150~250(middle), 250~350 (right). 76
113 X軸:pixel Y軸:phase Plasma plume, 30ms delay, average of cols 400~900, average of row 50~200 . 77
114 X軸:pixel Y軸:phase. Plasma plume, 30ms delay, average of cols 400~900, average of row 200~350 77
115 X軸:pixel Y軸:phase. Plasma plume, 30ms delay, average of cols 400~900, average of row 350~500 78
116 X軸:pixel Y軸:phase. Plasma plume, 30ms delay, average of cols 520~750, average of row 50~150 78
117 X軸:pixel Y軸:phase. Plasma plume, 30ms delay, average of cols 520~750, average of row 150~250 78
118 X軸:pixel Y軸:phase. Plasma plume, 30ms delay, average of cols 500~750, average of row 250~350 79
119 X軸:pixel Y軸:phase. 合併selction three function blue line (50~150), red line (150~250), green line 250~350 79
120 rotate 90 degree image 80
121 y軸:FWHM pixel. FWHM about row selction 50~150 (left), 150~250(middle), 250~350 (right). . 80
122 X軸:pixel Y軸:phase. Plasma plume, 40ms delay, average of cols 400~900, average of row 50~200 81
123 X軸:pixel Y軸:phase. Plasma plume, 40ms delay, average of cols 400~900, average of row 200~350 81
124 X軸:pixel Y軸:phase. Plasma plume, 40ms delay, average of cols 400~900, average of row 350~500 82
125 X軸:pixel Y軸:phase. Plasma plume, 40ms delay, average of cols 520~750, average of row 50~150 82
126 X軸:pixel Y軸:phase. Plasma plume, 40ms delay, average of cols 520~750, average of row 150~250 83
127 X軸:pixel Y軸:phase Plasma plume, 40ms delay, average of cols 500~750, average of row 250~350 83
128 X軸:pixel Y軸:phase. 合併selction three function blue line (50~150), red line (150~250), green line 250~350 83
129 rotate 90 degree image 84
130 y軸:FWHM pixel. FWHM about row selction 50~150 (left), 150~250(middle), 250~350 (right). . 84
131 X軸:pixel Y軸:phase. Gas puff, 20ms delay, average of cols 400~900, average of row 50~200 . . . 85
132 X軸:pixel Y軸:phase. Gas puff, 20ms delay, average of cols 400~900, average of row 200~350 . . . 85
133 X軸:pixel Y軸:phase. Gas puff, 20ms delay, average of cols 400~900, average of row 350~500 . . . 85
134 X軸:pixel Y軸:phase. Gas puff, 20ms delay, average of cols 520~750, average of row 50~150 . . . 86

135 X軸:pixel Y軸:phase. Gas puff, 20ms delay, average of cols 520~750, average of row 150~250 . . . 86
136 X軸:pixel Y軸:phase. Gas puff, 20ms delay, average of cols 500~750, average of row 250~350 . . . 86
137 X軸:pixel Y軸:phase. 合併selction three function blue line (50~150), red line (150~250), green line 250~350 . . . 87
138 rotate 90 degree image . . . 87
139 y軸:FWHM pixel. FWHM about row selction 50~150 (left), 150~250(middle), 250~350 (right). . 88
140 X軸:pixel Y軸:phase. Gas puff, 20ms delay, average of cols 400~900, average of row 50~200 . . . 88
141 X軸:pixel Y軸:phase. Gas puff, 20ms delay, average of cols 400~900, average of row 200~350 . . . 88
142 X軸:pixel Y軸:phase. Gas puff, 20ms delay, average of cols 400~900, average of row 350~500 . . . 89
143 X軸:pixel Y軸:phase. Gas puff, 20ms delay, average of cols 520~750, average of row 50~150 . . . 89
144 X軸:pixel Y軸:phase. Gas puff, 20ms delay, average of cols 520~750, average of row 150~250 . . . 89
145 X軸:pixel Y軸:phase. Gas puff, 20ms delay, average of cols 500~750, average of row 250~350 . . . 90
146 X軸:pixel Y軸:phase. 合併selction three function blue line (50~150), red line (150~250), green line 250~350 . . . 90
147 rotate 90 degree image . . . 91
148 y軸:FWHM pixel. FWHM about row selction 50~150 (left), 150~250(middle), 250~350 (right). . 91
149 X軸:pixel Y軸:phase. Gas puff, 20ms delay, average of cols 400~900, average of row 50~150 . . . 92
150 X軸:pixel Y軸:phase. Gas puff, 20ms delay, average of cols 400~900, average of row 200~350 . . . 92
151 X軸:pixel Y軸:phase. Gas puff, 20ms delay, average of cols 400~900, average of row 350~500 . . . 92
152 X軸:pixel Y軸:phase. Gas puff, 20ms delay, average of cols 520~750, average of row 50~150 . . . 93
153 X軸:pixel Y軸:phase. Gas puff, 20ms delay, average of cols 520~750, average of row 150~250 . . . 93
154 X軸:pixel Y軸:phase. Gas puff, 20ms delay, average of cols 500~750, average of row 250~350 . . . 94
155 X軸:pixel Y軸:phase. 合併selction three function blue line (50~150), red line (150~250), green line 250~350 . . . 94
156 rotate 90 degree image . . . 95
157 y軸:FWHM pixel. FWHM about row selction 50~150 (left), 150~250(middle), 250~350 (right). . 95
158 X軸:pixel Y軸:phase. Gas puff, 20ms delay, average of cols 400~900, average of row 50~200 . . . 95
159 X軸:pixel Y軸:phase. Gas puff, 20ms delay, average of cols 400~900, average of row 200~350 . . . 96
160 X軸:pixel Y軸:phase. Gas puff, 20ms delay, average of cols 400~900, average of row 350~500 . . . 96
161 X軸:pixel Y軸:phase. Gas puff, 20ms delay, average of cols 520~750, average of row 50~150 . . . 96
162 X軸:pixel Y軸:phase. Gas puff, 20ms delay, average of cols 520~750, average of row 150~250 . . . 97
163 X軸:pixel Y軸:phase. Gas puff, 20ms delay, average of cols 500~750, average of row 250~350 . . . 97
164 X軸:pixel Y軸:phase. 合併selction three function blue line (50~150), red line (150~250), green line 250~350 . . . 97
165 rotate 90 degree image . . . 98
166 y軸:FWHM pixel. FWHM about row selction 50~150 (left), 150~250(middle), 250~350 (right). . 98
167 X軸:pixel Y軸:phase. Gas puff, 30ms delay, average of cols 400~900, average of row 50~150 . . . 98

168 X軸:pixel Y軸:phase. Gas puff, 30ms delay, average of cols 400~900, average of row 200~350 . . . 99
169 X軸:pixel Y軸:phase. Gas puff, 30ms delay, average of cols 400~900, average of row 350~500 . . . 99
170 X軸:pixel Y軸:phase. Gas puff, 30ms delay, average of cols 520~750, average of row 50~150 . . . 99
171 X軸:pixel Y軸:phase. Gas puff, 30ms delay, average of cols 520~750, average of row 150~250 . . . 100
172 X軸:pixel Y軸:phase. Gas puff, 30ms delay, average of cols 500~750, average of row 250~350 . . . 100
173 rotate 90 degree image . . . 100
174 X軸:pixel Y軸:phase. 合併selction three function blue line (50~150), red line (150~250), green line 250~350 . . . 101
175 y軸:FWHM pixel. FWHM about row selction 50~150 (left), 150~250(middle), 250~350 (right). . 101
176 X軸:pixel Y軸:phase. Gas puff, 30ms delay, average of cols 400~900, average of row 50~200 . . . 101
177 X軸:pixel Y軸:phase. Gas puff, 30ms delay, average of cols 400~900, average of row 200~350 . . 102
178 X軸:pixel Y軸:phase. Gas puff, 30ms delay, average of cols 400~900, average of row 350~500 . . . 102
179 X軸:pixel Y軸:phase. Gas puff, 30ms delay, average of cols 520~750, average of row 50~150 . . . 102
180 X軸:pixel Y軸:phase. Gas puff, 30ms delay, average of cols 520~750, average of row 150~250 . . . 102
181 X軸:pixel Y軸:phase. Gas puff, 30ms delay, average of cols 500~750, average of row 250~350 . . . 103
182 X軸:pixel Y軸:phase. 合併selction three function blue line (50~150), red line (150~250), green line 250~350 . . . 103
183 rotate 90 degree image . . . 103
184 X軸:pixel Y軸:phase. Gas puff, 30ms delay, average of cols 520~750, average of row 50~150 . . . 104
185 X軸:pixel Y軸:phase. Gas puff, 30ms delay, average of cols 400~900, average of row 50~200 . . . 104
186 X軸:pixel Y軸:phase . . . 104
187 X軸:pixel Y軸:phase. Gas puff, 30ms delay, average of cols 400~900, average of row 200~350 . . . 105
188 X軸:pixel Y軸:phase. Gas puff, 30ms delay, average of cols 520~730, average of row 150~250 . . . 105
189 X軸:pixel Y軸:phase. Gas puff, 30ms delay, average of cols 500~750, average of row 250~350 . . . 105
190 X軸:pixel Y軸:phase. 合併selction three function blue line (50~150), red line (150~250), green line 250~350 . . . 106
191 rotate 90 degree image . . . 106
192 y軸:FWHM pixel. FWHM about row selction 50~150 (left), 150~250(middle), 250~350 (right). . 106
193 X軸:pixel Y軸:phase. Gas puff, 30ms delay, average of cols 400~900, average of row 50~200 . . . 107
194 X軸:pixel Y軸:phase. Gas puff, 30ms delay, average of cols 400~900, average of row 200~350 . . . 107
195 X軸:pixel Y軸:phase. Gas puff, 30ms delay, average of cols 400~900, average of row 350~500 . . . 107
196 X軸:pixel Y軸:phase. Gas puff, 30ms delay, average of cols 520~730, average of row 150~250 . . . 108
197 X軸:pixel Y軸:phase. Gas puff, 30ms delay, average of cols 500~730, average of row 250~350 . . . 108
198 X軸:pixel Y軸:phase. 合併selction three function blue line (50~150), red line (150~250), green line 250~350 . . . 108
199 y軸:FWHM pixel. FWHM about row selction 50~150 (left), 150~250(middle), 250~350 (right). . 109
200 X軸:pixel Y軸:phase. Gas puff, 30ms delay, average of cols 400~900, average of row 50~200 . . . 109

201 X軸:pixel Y軸:phase. Gas puff, 30ms delay, average of cols 400~900, average of row 200~350 . . . 109
202 X軸:pixel Y軸:phase. Gas puff, 30ms delay, average of cols 400~900, average of row 350~500 . . . 110
203 X軸:pixel Y軸:phase. Gas puff, 30ms delay, average of cols 520~750, average of row 50~150 . . . 110
204 X軸:pixel Y軸:phase. Gas puff, 30ms delay, average of cols 520~750, average of row 150~250 . . . 110
205 rotate 90 degree image . . . 111
206 y軸:FWHM pixel. FWHM about row selction 50~150 (left), 150~250(middle), 250~350 (right). . 111
207 X軸:pixel Y軸:phase. Gas puff, 40ms delay, average of cols 400~900, average of row 50~200 . . . 111
208 X軸:pixel Y軸:phase. Gas puff, 40ms delay, average of cols 400~900, average of row 200~350 . . . 112
209 X軸:pixel Y軸:phase. Gas puff, 40ms delay, average of cols 400~900, average of row 350~500 . . . 112
210 X軸:pixel Y軸:phase. Gas puff, 40ms delay, average of cols 520~750, average of row 50~150 . . . 112
211 X軸:pixel Y軸:phase. Gas puff, 40ms delay, average of cols 520~750, average of row 150~250 . . . 112
212 X軸:pixel Y軸:phase. Gas puff, 40ms delay, average of cols 500~750, average of row 250~350 . . . 113
213 X軸:pixel Y軸:phase. 合併selction three function blue line (50~150), red line (150~250), green line 250~350 . . . 113
214 rotate 90 degree image . . . 113
215 X軸:pixel Y軸:phase. Gas puff, 40ms delay, average of cols 400~900, average of row 50~200 . . . 114
216 X軸:pixel Y軸:phase. Gas puff, 40ms delay, average of cols 400~900, average of row 200~350 . . . 114
217 X軸:pixel Y軸:phase. Gas puff, 40ms delay, average of cols 400~900, average of row 350~500 . . . 114
218 X軸:pixel Y軸:phase. Gas puff, 40ms delay, average of cols 520~750, average of row 50~150 . . . 114
219 X軸:pixel Y軸:phase. Gas puff, 40ms delay, average of cols 520~750, average of row 150~250 . . . 115
220 X軸:pixel Y軸:phase. Gas puff, 40ms delay, average of cols 500~750, average of row 250~350 . . . 115
221 X軸:pixel Y軸:phase. 合併selction three function blue line (50~150), red line (150~250), green line 250~350 . . . 116
222 rotate 90 degree image . . . 117
223 y軸:FWHM pixel. FWHM about row selction 50~150 (left), 150~250(middle), 250~350 (right). . 117
224 X軸:pixel Y軸:phase. Gas puff, 40ms delay, average of cols 400~900, average of row 50~200 . . . 117
225 X軸:pixel Y軸:phase. Gas puff, 40ms delay, average of cols 400~900, average of row 200~350 . . . 118
226 X軸:pixel Y軸:phase. Gas puff, 40ms delay, average of cols 400~900, average of row 350~500 . . . 118
227 X軸:pixel Y軸:phase. Gas puff, 40ms delay, average of cols 520~750, average of row 50~150 . . . 118
228 X軸:pixel Y軸:phase. Gas puff, 40ms delay, average of cols 520~750, average of row 150~250 . . . 119
229 X軸:pixel Y軸:phase. Gas puff, 40ms delay, average of cols 500~750, average of row 250~350 . . . 119
230 X軸:pixel Y軸:phase. 合併selction three function blue line (50~150), red line (150~250), green line 250~350 . . . 119
231 rotate 90 degree image . . . 120
232 y軸:FWHM pixel. FWHM about row selction 50~150 (left), 150~250(middle), 250~350 (right). . 120

List of Tables

1 The pulse valve circuit time dealy average and statistics 12

2 The experiment about pulse valve reaction average and the standard deviation statistics 15

3 Pulse valve experiment setting combinations 16

4 Minimum valve of fitting function 46

5 Average and standard deviations of fitting function for plasma plume 46

6 Slope of the FWHM versus y position of the gas puff 52

7 Slope of the FWHM versus y position of the plasma plume 52

8 The no high voltage average slope to calculate the opening angle 52

9 Experiment data record in NAS 120

1 Introduction

Extreme ultraviolet (EUV) light sources became extremely important in semiconductor fabrications. We are building the EUV light source by compressing the plasma plume via theta pinches. The plasma temperature will potentially reach 30 eV so that the EUV light will be radiated. In this chapter, we will introduce the EUV lithography in section 1.1. In section 1.2, our design of the EUV light source is given. The gas-puff system will be introduced in 1.3. Finally, the goal of the thesis will be given in 1.4.

1.1 The extreme ultraviolet lithography

For many years, the development of semiconductor manufacturing technologies has rapidly progressed. As predicted by the Moore's Law, the number of transistors in an integrated circuit doubles every two years. Over the past decades, the semiconductor manufacturing process has become increasingly complex. Figure 1 shows a schematic diagram of a semiconductor manufacturing process [1]. Optical lithography, where the designed model from photomasks is transferred onto the wafer surface is a crucial step in the semiconductor manufacturing process. Subsequently, the desired circuit model is created on the wafer surface using etching and ion implantation. In recent years, as the line width of the semiconductor manufacturing becomes narrower and narrower, the importance of the EUV lithography technology with a light source 13.5 nm increases significantly in the semiconductor manufacturing processes. Our EUV light source development project aims to innovate a new technique that uses gas-puff theta pinches for producing the 13.5 nm EUV light source.

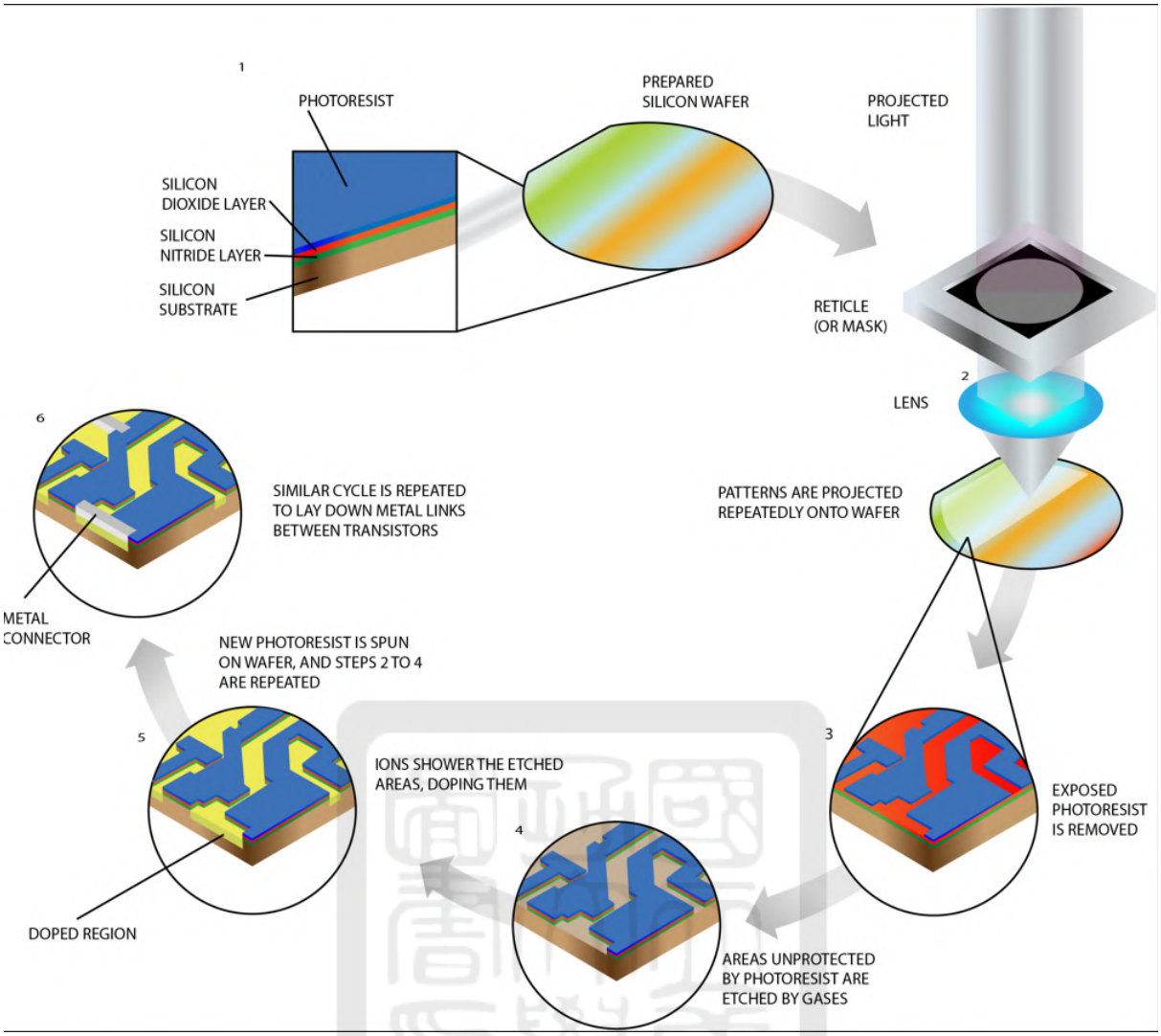

Figure 1: The process of semiconductor manufacturing [Ref 1]

1.2 Our EUV light source project

In Fig. 2, it is a new type of EUV light source. In the first step, an argon gas puff is generated. In the second step, the argon gas jet passes through an electrode pair with high voltage across it so that an arc discharge is induced. Therefore, the gas is ionized and is heated. Temperature supposes to increase to 1∼10 eV. In the third step, the plasma plume passes through a Helmholtz coil, which is driven by a pulsed power system. The peak of the pulse current is 130 kA with a rise time of ∼1.6 μs. Therefore, the plasma plume is adiabatically compressed in the Helmholtz coil, and the plasma temperature increases potentially from 1∼10 eV to 30 eV. Finally, an EUV light at 13.5 nm is radiated if xenon gas is used. To study the heating and radiating process, we use argon gas instead of xenon gas because xenon gas is too expensive.

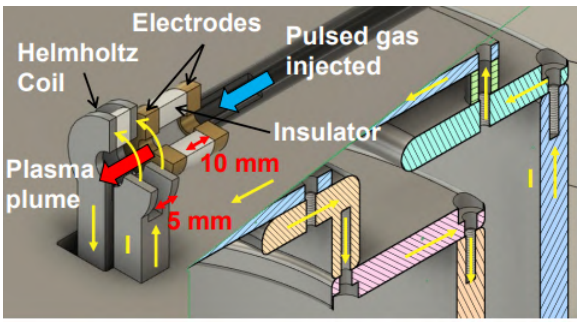

Figure 2: The EUV light source experiment schematic diagram [Ref 2]

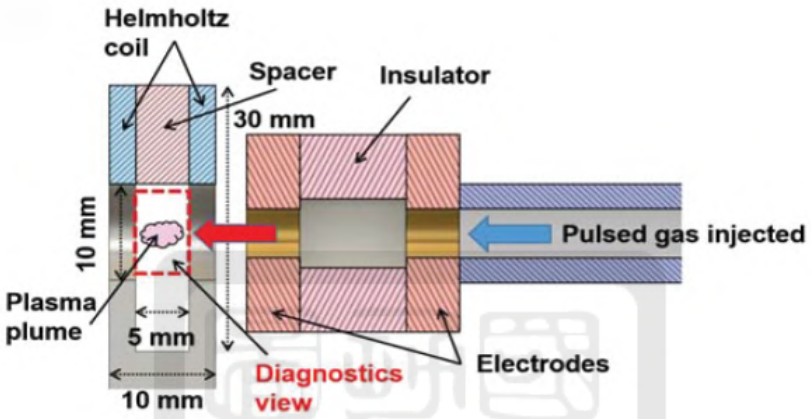

Figure 3: The Argon gas will undergo ionization when it passes through the electrodes in the system

1.3 The Gas-puff system

The gas-puff system is responsible for generating a collimated gas puff. It consists of several components, including a manual valve, a relief valve, a gauge, a reservoir, and a pulse valve. Among these components, the pulse valve plays a crucial role in the gas-puff system.

The main function of the gas-puff system is to deliver the argon gas puff into the system. The pressure of the gas puff is affected by the pressure of the reservoir, the size of the pulse valve's outlet, and how long the pulse valve is open. The first gas-puff system was built by the former student Jia-Kia-Liu. I integrate the system with our pulsed-power system.

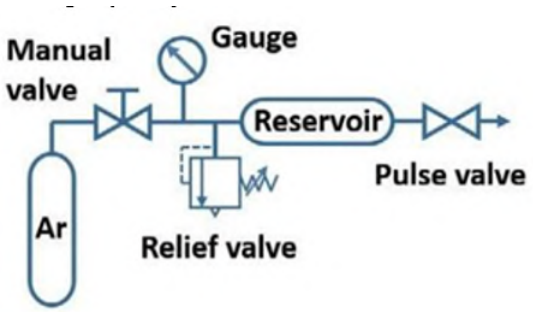

Figure 4: Gas-puff system schematic diagram

1.4 Helmholtz coil

The Helmholtz coil used in the experiment was made of stainless steel. A shown in Fig. 5, it has an inner and an outer radius of 5 mm and 15 mm, respectively. The thickness of each side of the cost is 2.5 mm. The separation between two couls is 5 mm. When driven by the high current supplied by the pulse power system, the Helmholz coil generates a magnetic field at its center. When the Helmholtz coil was driven by our pulse-power system, the measured peak magnetic field at the center position was 11.4 $\pm$ 1.0 T [Ref].

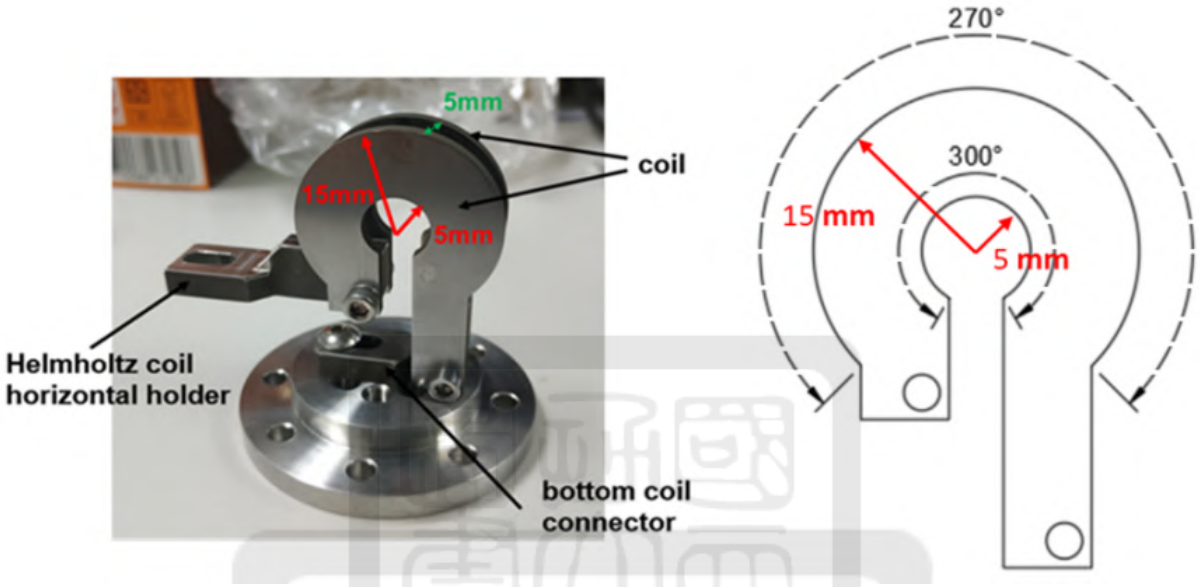

Figure 5: The structure of Helmholz coil. From Cheng-Han Du thesis,"Development of the magneric field in a theta pinch in the EUV light source."[Ref 3]

1.5 The goal of this thesis

As depicted in the Fig. 3, the electrode pairs in our EUV light source are responsible for ionizing the gas puff. This step is crucial for the initial injection and ionization of the gas. The goal of my work is to generate a plasma plume. First, I built a new pulse-valve controller which can sermonized with our laser diagnostics. Second, I designed a new convergent-divergent nozzle. It is also the electrode pair that will be used to ionize the gas puff. Finally, with above design, we successfully generate the plasma plume. The characteristics of the plasma will be presented.

2 The experimental platform

In this section, I will introduce the pulsed-power system and the diagnostic system.

2.1 The pulsed-power system

The pulsed-power system, using a parallel plate capacitor bank (PPCB) [Ref], serves as a platform for generating a high current which can be used to generate plasma in the High-Energy-Density-Plasma (HEDP) regime.

In our EUV light source, the pulsed-power system provides the pulse current to drive the helmoltz coil [Ref]. Although my work did not use the pulsed-power system, the plasma plume system was integrated into the pulsed-power system. It was also the experimental platform for my experiments.

Figure 6and Fig. 7 are the computer-aided design (CAD) drawing and the photo of our system, respectiviely. In Fig. 6, our pulse-power system consists of several components, including 20 capacitors with a capacitance of 1 uF each, two rail-gap switches, two parallel transmission lines, and a vertically oriented cylindrical vacuum chamber. Two capacitors are connected in series as a brickf respectibely [Ref]. There are two wings, the north and the south wings. Five bricks are connected in parallel forming a wing. Finally, two wings are connected in parallel, resulting in a total capacitance of 5 uF. Our pulsed-power system is charged to 20 kV and stories a test energy of 1 kJ. When the system is activeated 20 kV, it produces a pulsed current of 123.5±0.8 kA, with a rise time of 1592±3 ns [Ref 4].

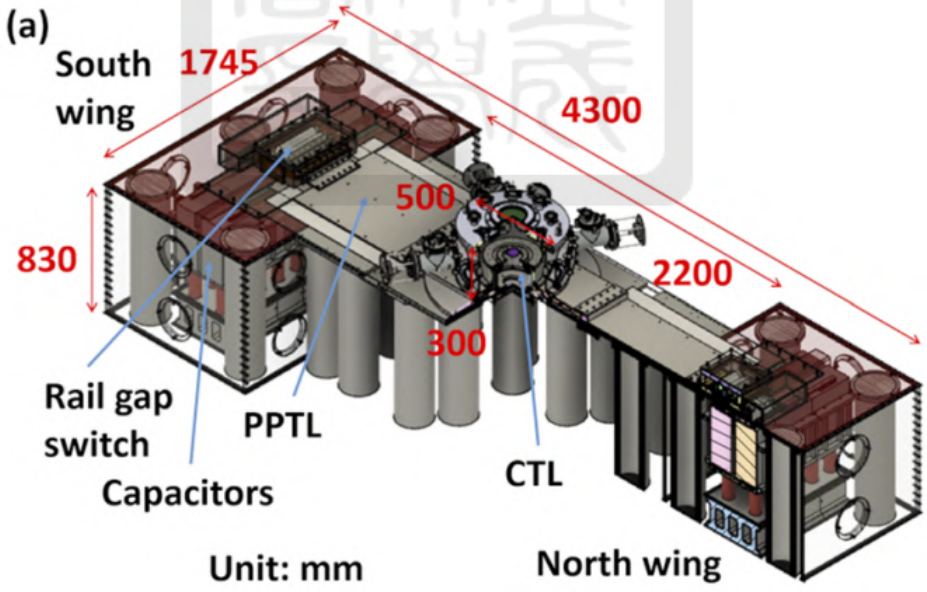

Figure 6: The-pulse-power system schematic diagram [Ref 4]

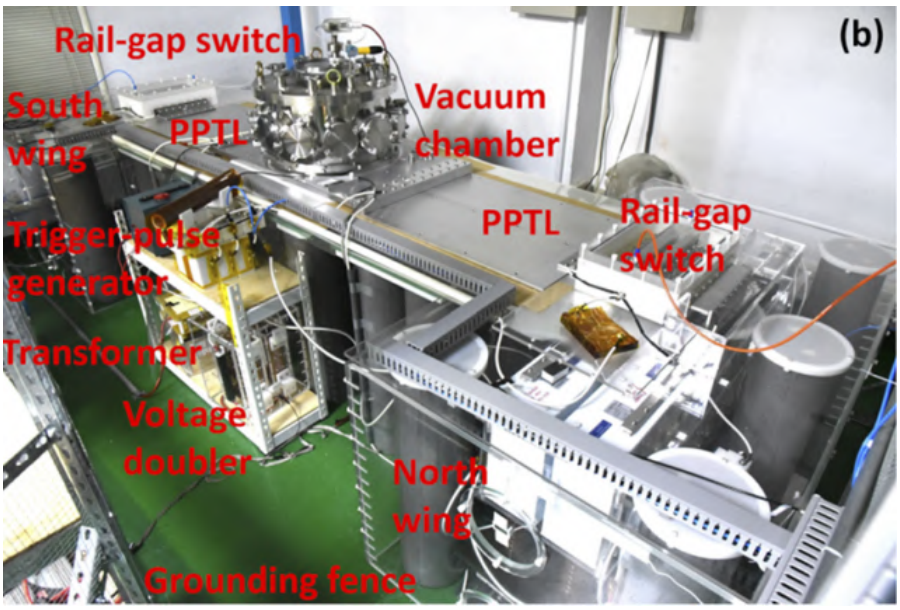

Figure 7: Photo of the pulsed-power system. [Ref 5]

At the center of the pulsed-power system, there is a vacuum chamber. Our gas-puff system will be connected to the vacuum chamber from the side. A gas tube will be inserted into the chamber. We will conduct gas-puff experiments by injecting argon gas into the chamber. The gas puff will be ionized through an arc discharge. It will be observed by laser diagnostics.

2.2 Laser diagnostics

In Fig. 8, our laser diagnostic setup begins with a Q-switch laser. The Q-switch laser operates in a single longitudinal mode at a wavelength of 532 nm and has a pulse width of 5 ns. The laser beam is expanded to provide a field of view with a diameter of 30 mm. We have the capability to capture experimental images, including top-view, side-view, interferometer, shadowgraph, schlieren, and polarimetry images. In our experiments, we primarily use the interferometer camera and the schlieren camera. The interferometer is employed for density measurements. On the other hand, schlieren imaging is mainly used for plasma edge detection, enabling us to visualize the boundaries of the plasma.

Our gas puff system is positioned at the 9 o'clock position of the vacuum chamber, as shown in Fig. 8. The gas puff is directed towards the central point, as indicated by the purple start at the center of the chamber. This arrangement enables us to capture experimental images efficiently.

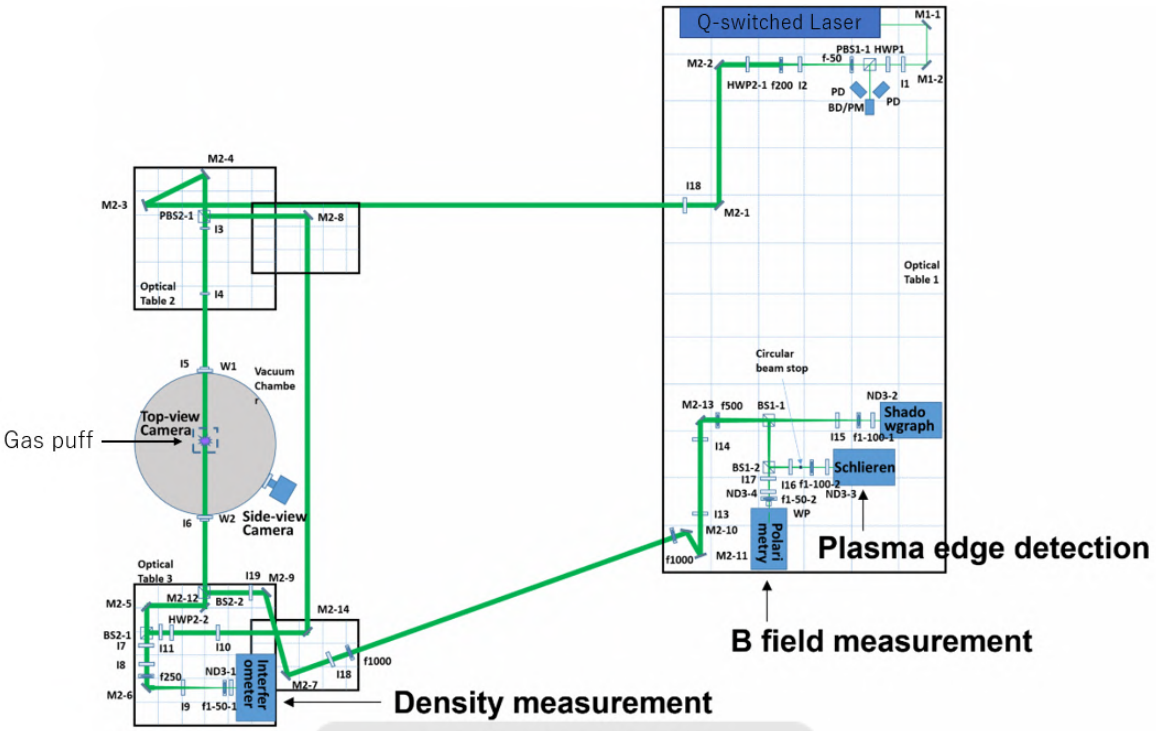

Figure 8: Laser path [Ref 6]

3 The gas-puff system

We built a gas-puff system to generate a puff of argon gas. We designed the system, built it, tested it, and analyzed the experimental data for understanding its performance. In this chapter, we focus on developing the gas-puff controller.

3.1 The design of the gas-puff system

The gas-puff system is responsible for generating a collimated gas puff. It consists of several components, including a manual valve, a relief valve, a gauge, a reservoir, and a pulse valve. Among these components, the pulse valve plays a crucial role in the gas-puff system. Two pulse valve were used. The inner diameters of the outlet were 0.1 mm (part 1) and 1 mm (part). The schematic diagram of the gas-puff system is shown in Fig. 9. The reservoir pressure was always kept at 10 atm. The main function of the system is to deliver argon gas into the chamber.

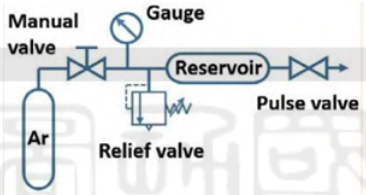

Figure 9: Gas-puff system schematic diagram

3.2 The pulse-valve controller

The pulse-valve controller is to control the pulse valve. It sets the pulse valve opening time in our experiments. The circuit of the pulse-valve controller is given in Fig. 10. The photo of the controller is in Fig. 11. The circuit layout of the controller is shown in Fig. 12. The controller converts an optical square pulse to a 28-V square pulse. The width of the square pulse is determined by the width of the optical square pulse. There are two DC-DC converters in the circuit. One is THN-20-1223. It is used to provide power to drive the pulse valve. The DC-DC converter output is 30 V with a current of up to 667 mA. However, the pulse valve needs only 28 V with a current of 20∼30 mA. Therefore, we use zener diodes to provide the output voltage at 28 V and connect it to pin 8 of the FOD-3184V, which is generally used as a gate driver for an IGBT. The 28-V Zenor diode is obtained by using five 5-V, 5-W zenor diodes and one 3-V, 5-W zenor diode connected in series. The second DC-DC converter, SCWN03A-05, is used to provide the power for the fiber receiver HFBR-2528Z. The voltage is 5 V. The output of the fiber receiver is connected to pin 2 of FOD-3184V. Pin 3 and pin 5 of the FOD-3184V are connected to the ground. Pin 6 of the FOD-3184V is the signal output. Finally, the signal output is connected to the pulse valve.

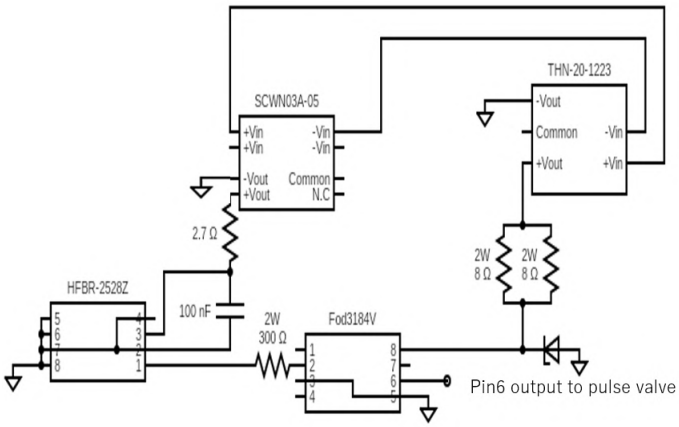

Figure 10: Circuit of the pulse-valve cintroller.

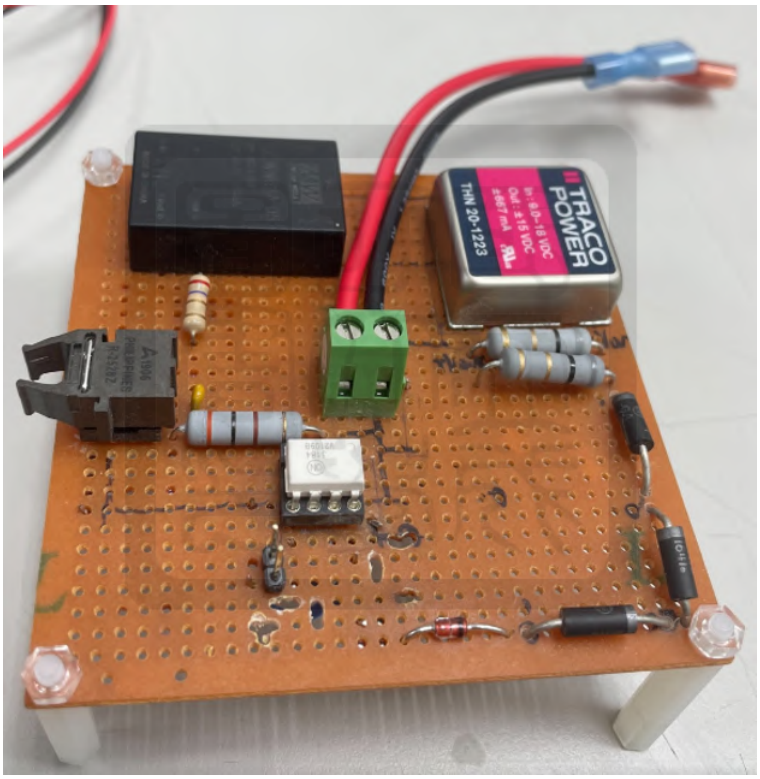

Figure 11: Photo of the pulse-valve controller.

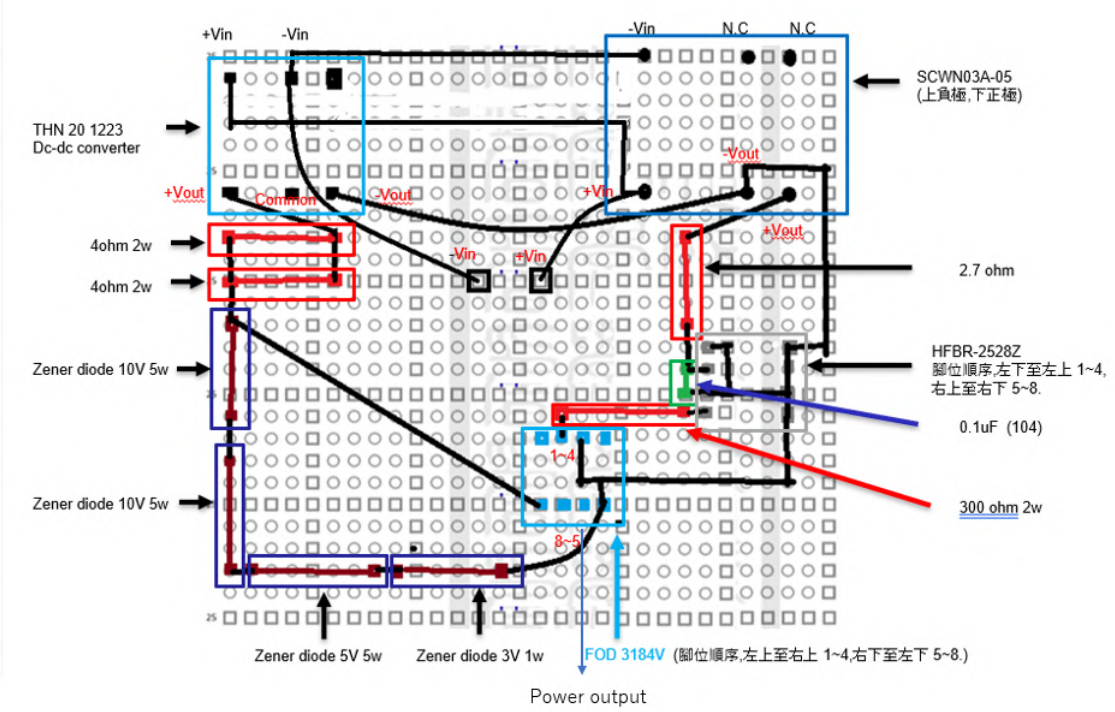

Figure 12: Layout of the pulse-valve controller.

3.3 Testing of the pulse-valve controller

We tested if the optical square pulse can be converted to a 28-V electrical square pulse first. The experiment setup is shown in Fig. 13. First, the function generator generates two identical square pulses at the same time. The first signal is sent to the electrical-to-optical (E→O) converter. The signal is converted from an electrical signal to an optical signal. Then, the optical signal is sent to the pulse-valve controller. The optical signal is converted back to the electrical signal in the controller. Finally, the electrical signal is sent to CH3 of the oscilloscope from pin 6 of the FOD3184V in the pulse-valve controller. The second signal is sent to CH1 of the oscilloscope from the function generator. Therefore, we can compare the CH1 signal with the CH3 signal and obtain the delay time and the width of the signal. I tested the system with six different square pulses. The width of the squares were 25 ns, 100 ns, 1 us, 10 us, 100 us, and 1 ms.

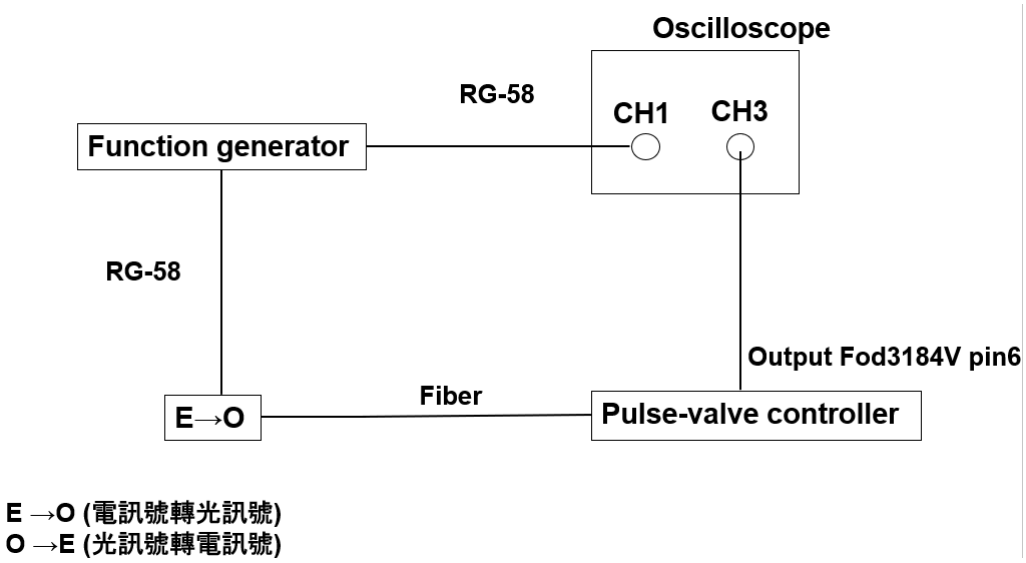

Figure 13: Pulse valve circuit delay time test

Definitions of the ``Function generator reaction width", the ``Gas-puff reaction width", the ``Gas-puff reaction start time", the ``Function generator reaction start time" and the ``Signal delay time" are shown in Fig. 20. The analyzed result is shown in Table 1. Ten data for each condition were obtained for statistics. The raw data is given shown in the Appendix (section A.1).

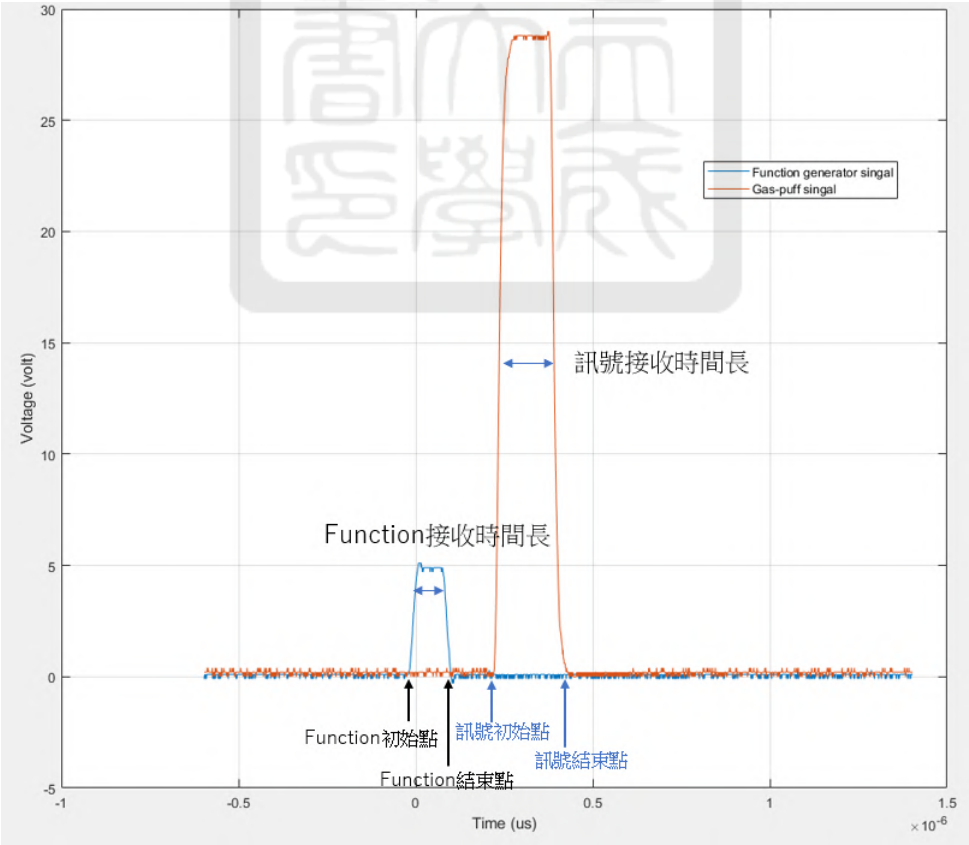

Figure 14: The pattern of the wave generator analysis about gas-puff signal and wave signal.

Table 1: The pulse valve circuit time dealy average and statistics

	Fuction 初始點	Function 結束點	Function 時間長	訊號 初始點	訊號 結束點	訊號接收 時間長
100 ns	-2.10e-08	1.03e-06	1.23e-07±1.80e-08	2.25e-07	4.39e-07	2.14e-07±3.99e-09
200 ns	-2.16e-08	2.01e-07	2.23e-07±3.61e-09	2.25e-07	5.39e-07	3.12e-07±3.98e-09
2 us	-2.03e-08	2.01e-06	2.03e-06±9.95e-09	2.34e-07	2.33e-06	2.09e-06±1.54e-08
20 us	-3.43e-08	2.00e-05	2.00e-05±3.51e-08	2.30e-07	2.03e-05	2.01e-05±4.55e-08
200 us	-3.11e-09	2.00e-04	2.00e-04±2.49e-08	2.26e-07	2.00e-04	2.00e-04±3.23e-08
2 ms	-2.49e-08	2.00e-03	2.00e-03±2.70e-08	2.60e-07	2.00e-03	2.00e-03±3.02e-07

3.4 Action test of the pulse valve

We would like to test the reaction time of the pulse valve. The pulse valve was integrated into the vacuum chamber as shown in Fig. 15. We used a cell phone to record the sound from the action of the pulse valve. By measuring the time difference between the sound from the opening action and from the closing action of the pulse valve, we can know how fast the pulse valve reacts.

As shown in Fig. 16, the function generator generated a square pulse. The electrical signal was sent to the electrical-to-optical (E→O) converter. The electrical signal was converted to the optical signal in the E→O converter. The optical signal was sent to the pulse-valve controller and the optical signal was converted to the electrical signal in the controller. Then, the electric signal was sent to the pulse valve and the pulse valve would react to the signal. I used the cellphone to record the beep sounds from the opening and the closing of the pulse valve in the format of ``m4a". Then, I converted the data to the ``wav" format. Finally, I used Matlab to analyze the sound data.

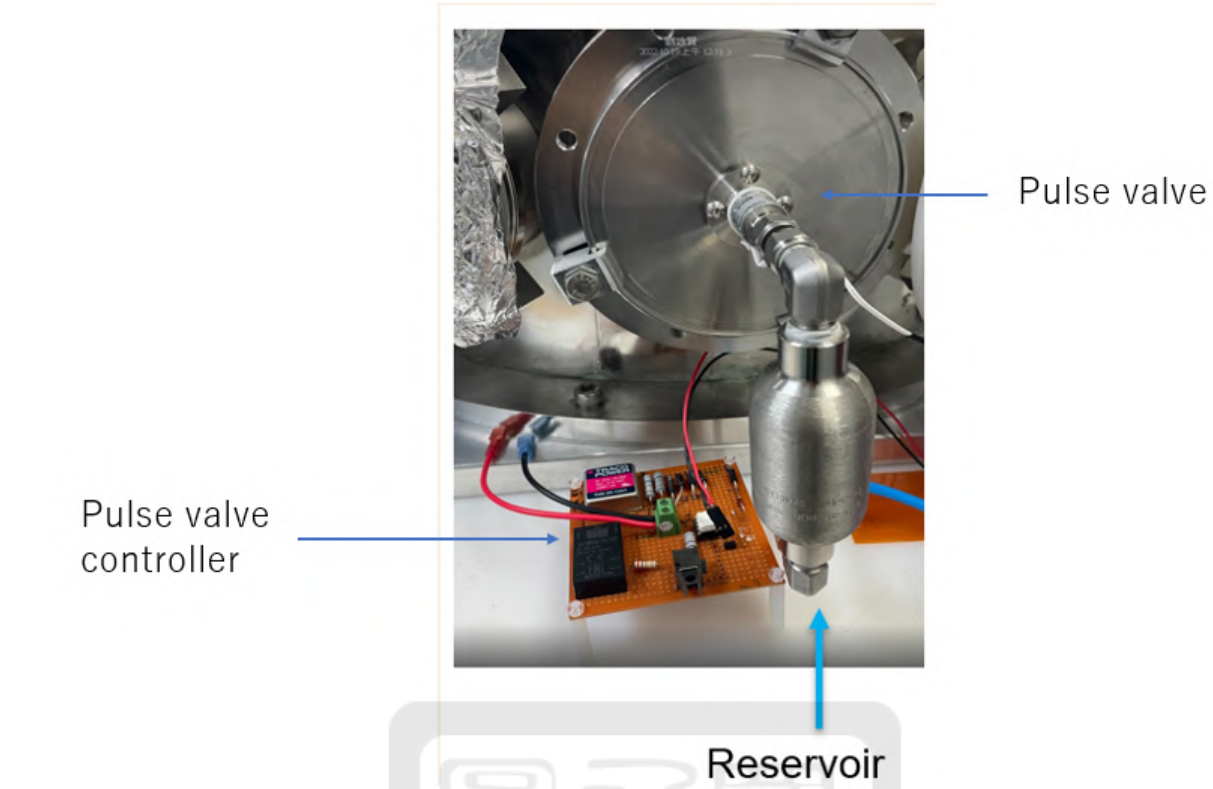

Figure 15: The gas-puff system.

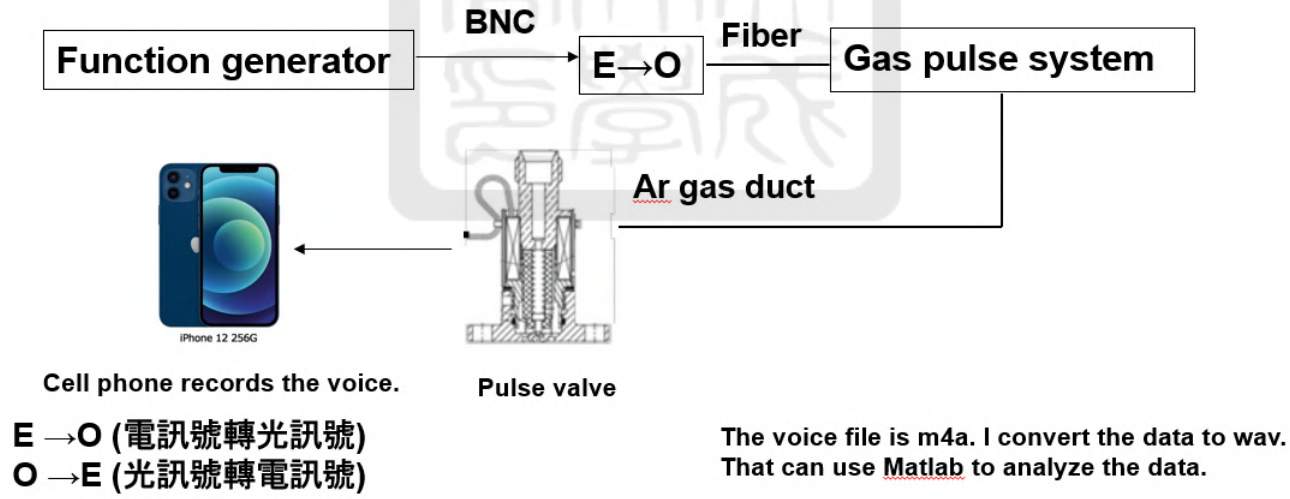

Figure 16: Pulse-valve system delay-experiment setup.

I recorded the action sounds of 9 different pulse widths. They were 2.5 ms, 5 ms, 10 ms, 25 ms, 50 ms, 100 ms, 250 ms, 500 ms, and 1 s. Each experiment was repeated 5 times. Figure 17 and 18 are the cases of 50 ms and 5 ms, respectively, as examples for data analysis. In the examples, the separation of two beeps are more clear in the case of 50 ms then that of 5 ms.

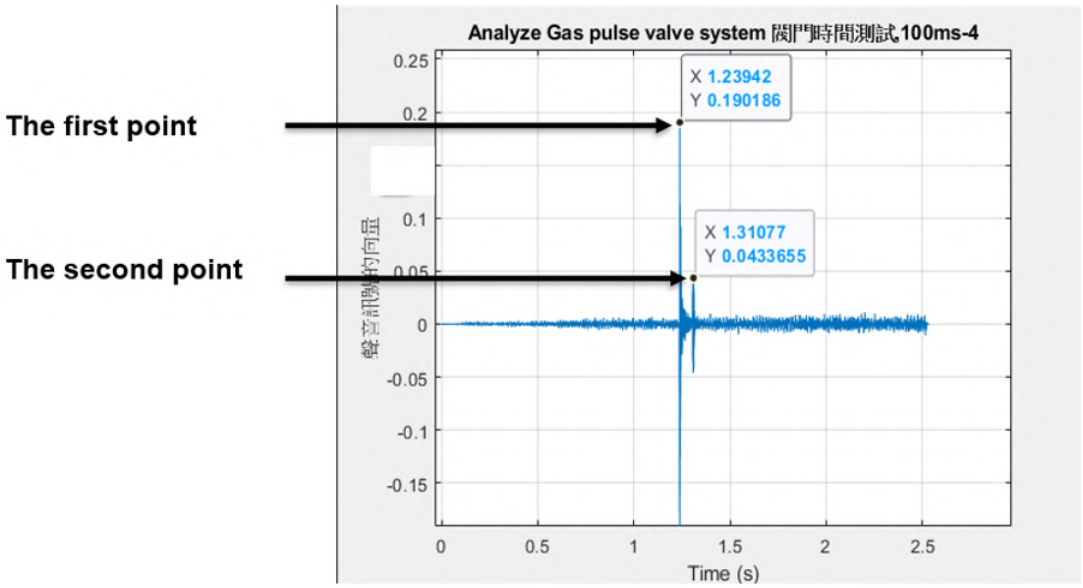

Figure 17: Sound track of 50-ms pulse width.

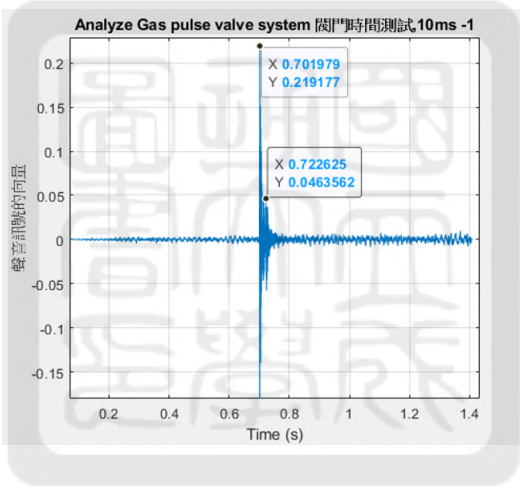

Figure 18: Sound track of 5-ms pulse width.

In Fig. 17 and Fig. 18. I defined the difference between the first point and the second point as the pulse valve reaction time interval. They are the maximum valve of each peak. The time of the first peak is defined as the opening time of the pulse valve. The second peak is defined as the closing time of the pulse valve.

Figure 19 shows the measured action time of the pulse valve as a function of the width of the square pulse. When the pulse width was less than 0.1 s, the time difference between two beep sounds from the action of the pulse valve was much more than the setting time. Therefore, the minimum pulse width we suppose to use is 0.1 second.

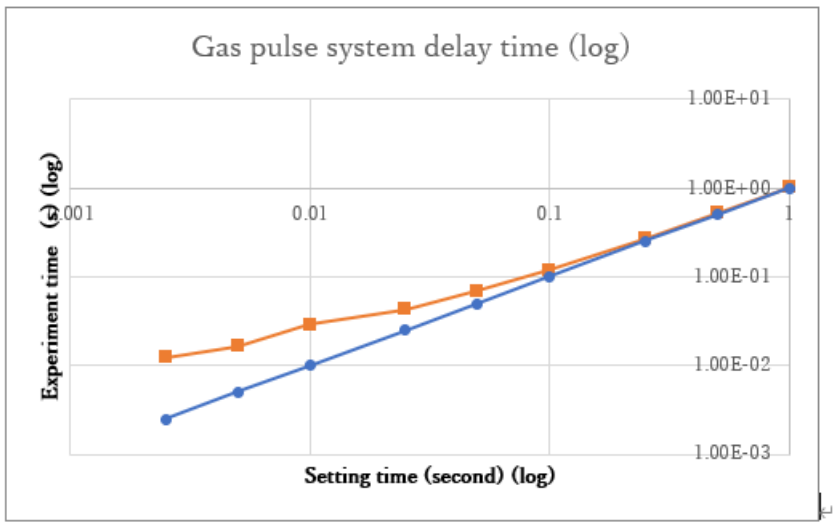

Figure 19: Pulse valve reaction of time delay statistics.

Table 2: The experiment about pulse valve reaction average and the standard deviation statistics

Setting time	平均值	標準差
1 sec	1.02e+0	1.23e-03
500 ms	5.18e-01	1.26e-03
250 ms	2.67e-01	1.56e-03
100 ms	1.19e-01	2.07e-03
50 ms	6.94e-02	1.50e-03
25 ms	4.30e-02	1.38e-03
10 ms	2.88e-02	2.4e-03
5 ms	1.64e-05	8.15e-03
2.5 ms	1.24e-02	2.92e-03

4 The pulse-valve testing experiment

I observed the gas puff by taking schlieren images, interferometer images, and shadowgraph images of the gas puff. One glass tube and two nozzles were tested. The glass tube was a straight glass tube. One nozzle was a convergent nozzle made of a glass tube. The other one was a convergent-divergent nozzle which was used in the former student Jia-Kai Liu's work. The pressure of the reservoir was 10 atm in all experiments. The test was to verify that a gas puff can be generated and can be observed using our diagnostic. Due to the inability to observe the gas puff, we have replaced the original pulse valve with a new one. The outlet diameter of the new pulse valve has been increased from 0.1 mm to 1 mm, which allows more gas to be released. We believe this will improve the observation of the gas puff.

We have tried combinations of different pulse valves, nozzle and chamber pressure. They ares summerized in Table. 3.

Table 3: Pulse valve experiment setting combinations

Using tube	Pulse valve output	Background pressure	pulse valve opening time
Glass tube	0.1 mm	1 atm	50 ms
	0.1 mm	1 atm	5 sec
Glass tube convergent nozzle	0.1 mm	1 atm	5 sec
	0.1 mm	10^{-3}Torr	5 sec
Plastic convergent-divergent nozzle	0.1 mm	1 atm	5 sec
	0.1 mm	10^{-3}Torr	5 sec
Glass convergent nozzle	1 mm	1 atm	5 sec
	1 mm	10^{-3}Torr	5 sec

4.1 Experimental setup for observing the gas puff

In Fig. 20(a), we can see the schematic diagram of the gas-puff experiment viewed from the top. There are three cameras. One is for taking schlieren images. One is for interferometer images. The other one is for taking shadowgraph images. The gas-puff system is in the direction of twelve o'clock in the figure. The gas puff is generated at the chamber center (C.C, the purple star in the figure). The laser passes through the C.C, from the direction of 3 o'clock to the direction of 9 o'clock. To capture images, shutters of all cameras open 15 seconds. Within the 15 seconds that the shutters are open, the laser is triggered and passes through the C.C. The camera will capture anything happens within these 15 seconds.

The experimental signal diagram is shown in Fig. 21. There are three subsystems in the system. They are the camera system, the gas-puff system, and the laser system. In the camera system, the 12-V battery powers the pulse-valve controller. The camera is controlled by a Raspberry Pi while the Raspberry Pi is controlled by a computer via wifi. When the camera is activated, three will be a 60-s countdown followed by a 15-s shutter opening. On the other hand, in the gas-puff system, the pulse-valve controller is powered by another 12-V battery. Within the 15-s shutter opening, The function generator 1 provides 5-second square pulse to pulse-valve controller for generating the gas puff. Finally, in the laser system, the function generator 2 triggers the laser as the backlight for taking images, during the time the pulse valve is open.

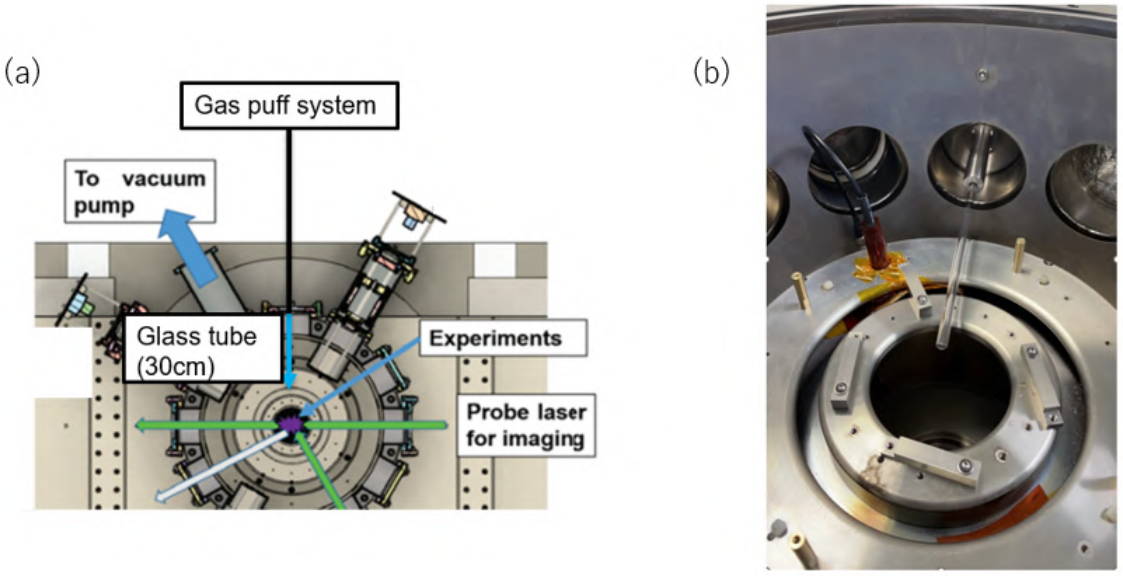

Figure 20: (a) schematic of the gas-puff experiments. (b) The photo of the convergent nozzle installed in the chamber.

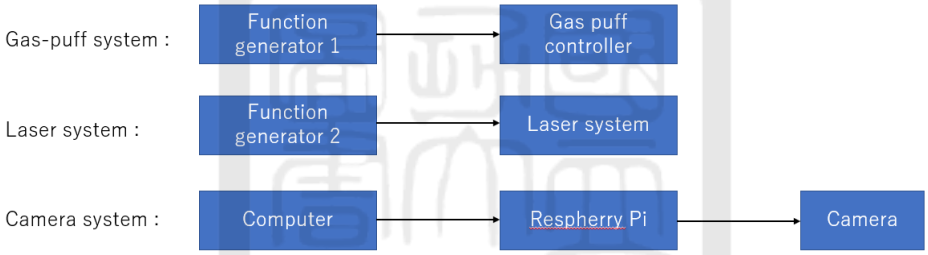

Figure 21: Experimental setting processs

4.2 Pusle valve with 0.1 mm outlet

We used three tubing components for the gas-puff experiment: (1) a 300 mm long glass tube with a 5 mm diameter, (2) a 300 mm tube equipped with a convergent nozzle at the end, and (3) a plastic convergent-divergent nozzle created by Jia-Kai Liu.

4.2.1 Glass tube

We first tested the glass tube. The dimension of the glass tube is shown in Fig. 22. The glass tube was attached to the flange using the connecter shown in Fig. 22. The pulse valve was open for 50 ms and the laser was triggered at 50.39 ms ~ 100.39 ms. We took the photo with and without gas-puff for comparison as shown in the Fig. 23. In Fig. 23, the laser was triggered at 70.39 ms. However, we couldn't observe any gas-puff phenomenon. Then, we repeated the experiment with opening the pulse valve for 5 second and took images within the 5 second. The Schlieren images with and without the gas puff are shown in Fig. 24. The intensity range was linearly scaled from 0∼40 to 0∼255 using the software GIMP. We also checked the shadowgraph images and the interferometer images as shown in Fig. 25 and Fig. 26. However, we couldn't observe any gas

puff either.

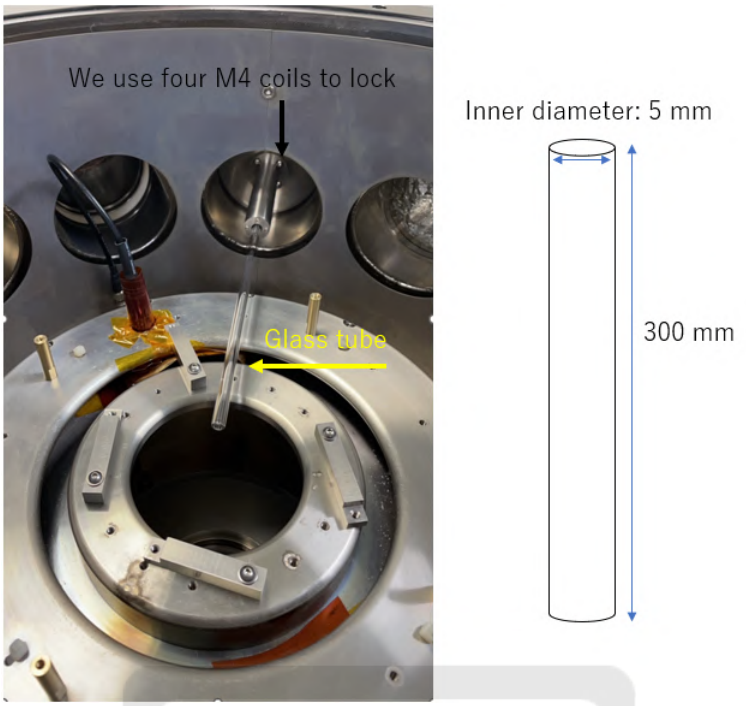

Figure 22: glass tube dimension

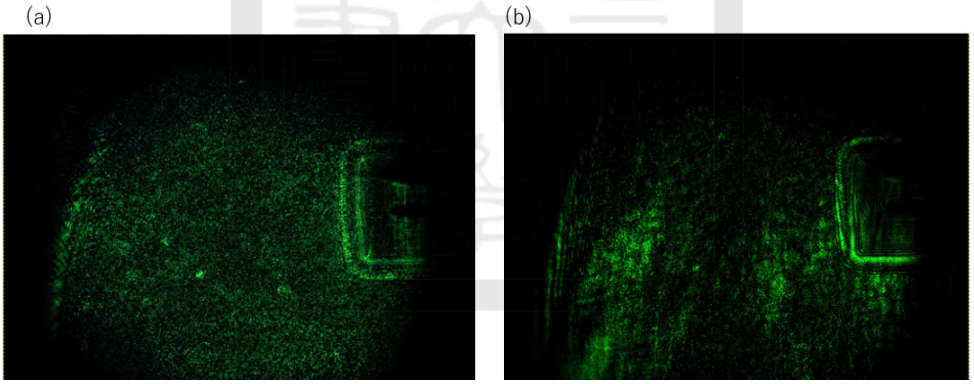

Figure 23: (a) Schileren image: pulse valve was open 50 ms gas, laser delay time setting: 70.39 ms. (b) Schileren image: No gas puff.

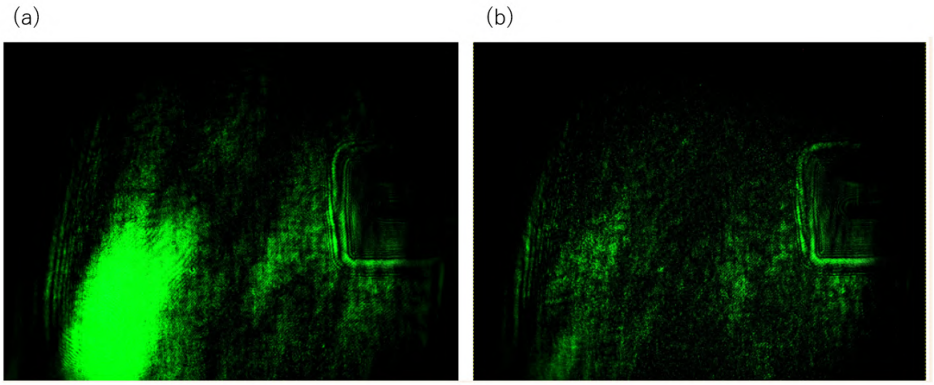

Figure 24: (a) Schileren image: pulse valve was open for 5 sec (b) Schileren image: No gas puff.

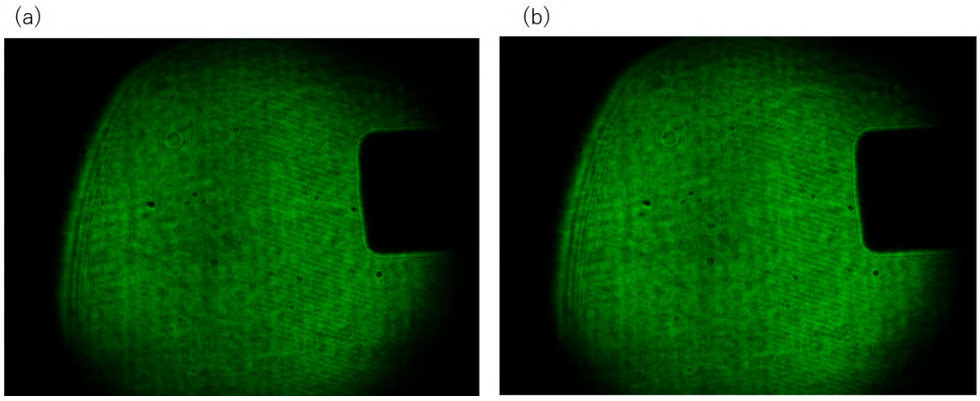

Figure 25: (a): The shadowgraph image: pulse valve was open for 5 sec. (b) Shadowgraph image: No gas puff.

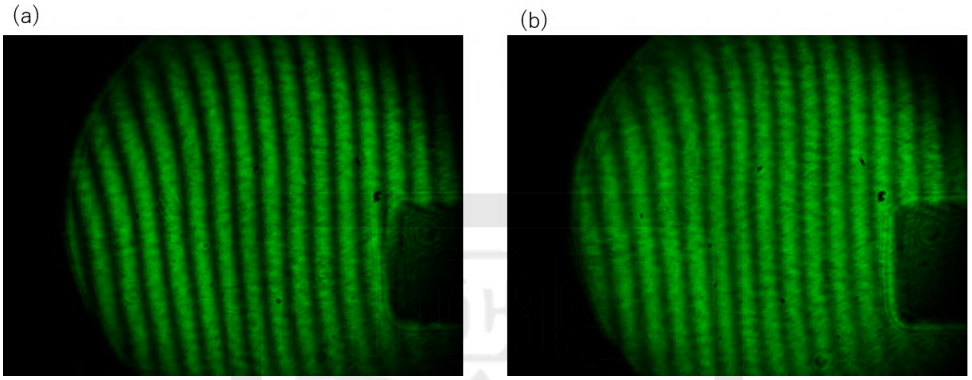

Figure 26: (a): Interferometer image: pulse valve was open for 5 sec. (b): Interferometer image: No gas puff

4.2.2 Glass convergent nozzle

We used a convergent nozzle to conduct a gas-puff experiment and see if we can observe the gas puff. The design of the glass convergent nozzle is shown in Fig.27. The glass tube inner of the diameter convergent from 5 mm to 1 mm in a length of 6 mm. The experiment process of the pulse valve was open for 5 second. The laser was triggered within the 5 second.

4.2.2.1 Chamber pressure at 1 atm We first condition the experiment with the chamber pressure at 1atm. Shown in Fig. 28 are the Schlieren image (Fig. 28 (a)) and the shadowgraph image (Fig. 28 (b)). The intensity range was linearly scaled from 0~20 to 0~255 using the software GIMP. Unfortunately, we could not observe the gas puff.

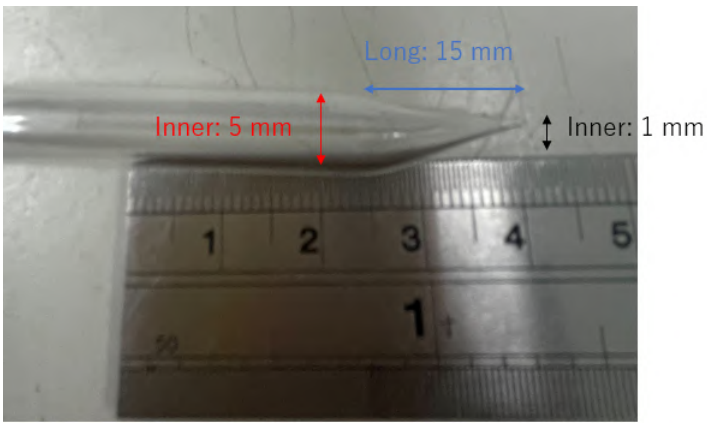

Figure 27: Convergent nozzle dimension

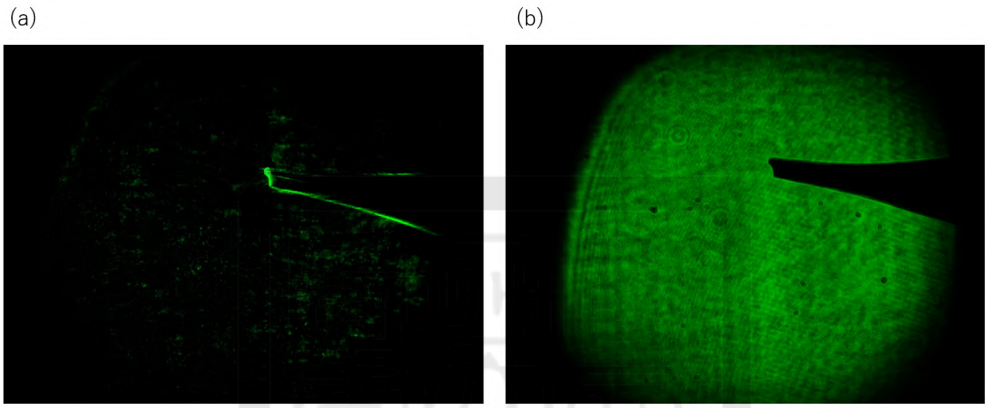

Figure 28: (a) Schileren image (b) shadowgraph image of the convergent nozzle with chamber pressure at 1 atm.

4.2.2.2 Chamer pressure at vaccum Additionally, we took into consideration the potential impact of atmospheric pressure on the visibility of the gas plume in our experiments. To address this, we conducted a gas-puff experiment in a low-vacuum environment 10^{-3} Torr. However, even under the low-vacuum conditions, we were unable to observe the gas puff. The Fig. 29 and Fig. 30 are the schlieren image and interferometer image in low-vacuum experiment.

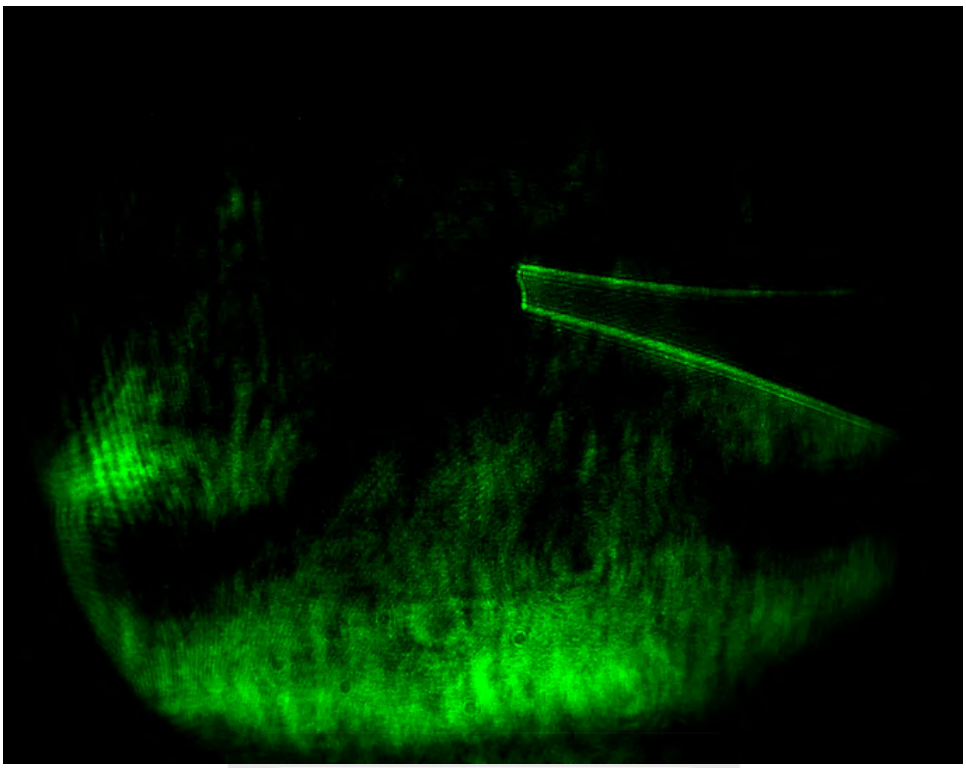

Figure 29: The schileren image of the convergent nozzle with chamber pressure at $10^{-3}\,Torr$

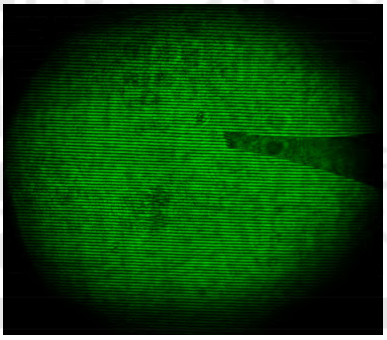

Figure 30: Interferometer image of the convergent nozzle with chamber pressure at $10^{-3}\,Torr$

4.2.3 Plastic convergent-divergent nozzle

Since we could not observe the gas puff using neither the glass tube nor the convergent nozzle, we replaced them with a convergent-divergent nozzle and repeated the experiment at 1 atm. I used the V6A convergent-divergent nozzle made by the former student Jia-Kai Liu for this experiment {Ref}. We would like to repeat his works and obtain the similar results as shown in Fig. 31. Figure 32 (a) is the interferometer image and Fig. 32 (b) is the shadowgraph image. Unfortunately, we did not observe the gas puff like that in Fig. 32. We suspected that the outlet of the pulse valve was too small because the opening angle of the pulse valve in outlet in Fig. 32 was 5.5 mm in diameter.

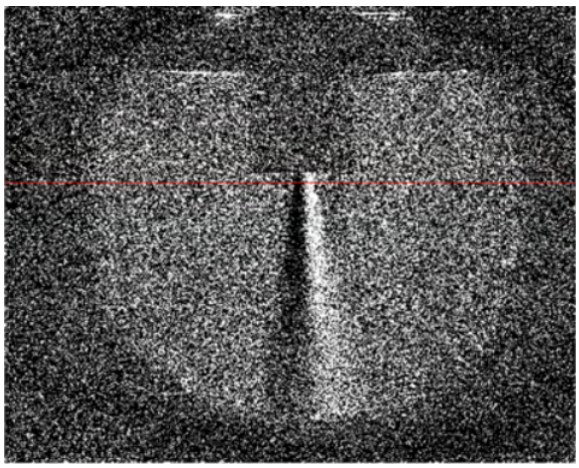

Figure 31: The shileren image image of the 24-V V8 CDN. From Fig.76 on page of Jia-Kia Liu's thesis, "study of the gas puff in the EUV light source using a theta pinch." {Ref}

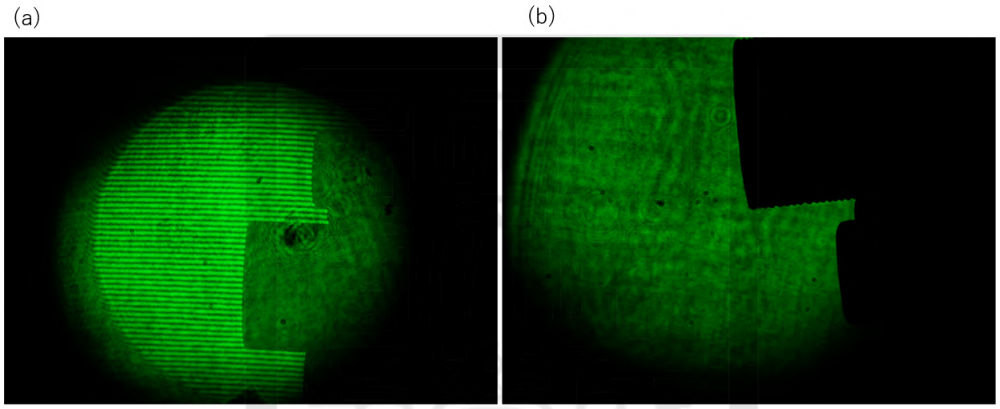

Figure 32: Interfometer image (a)shadowgraph image (b) of the convergent nozzle with chamber pressure at 1 atm.

4.3 Pulse valve with 1-mm outlet

We made two improvements to the experiment and kept using the same glass convergent nozzle used in section 4.2.2. First, we reinstalled the glass convergent nozzle more carefully. We made sure no gas leakage at the condition between the glass convergent nozzle and the flange. Second, we replaced the pulse valve with a new one that had a gas 1-mm outlet diameter. After making the two improvements mentioned above, we finally observed the gas puff in experiments.

4.3.1 Chamber pressure at 1 atm

We first tested the gas puff with keeping the chamber pressure at 1 atm. Figure 33 and fig. 34 are shileren images from two different shots. We can observe a straight gas puff spraying out of the glass nozzle. This is the first time we have observed the gas puff. We can see the turbulence of the gas puff. We can estimate the Reynolds number of the gas puff. Reynolds' number is defined as $R_e \equiv \frac{\rho * u * L}{\mu}$ where ρ is the density, u is the flow velocity, L is the characteristic linear dimension, and μ is the dynamic viscosity. Assuming the argon gas

pressure already dropped down to near 1 atm when it left the glass convergent nozzle, i.e, $\rho = 1.63$ kg/m^3 . The diameter of the glass convergent nozzle is $\sim$ 1 mm, i.e., $L \sim 10^{-3}$ m. For Argon, $\mu = 2.23 * 10^{-5}$ Pa-s. Therefore, $R_e > 73u$. Since we have observeed turbulence, i.e, $R_e > 2000$. Therefore, $u \geqq 30$ m/sec, which is about $\frac{1}{10}$ of the sound speed.

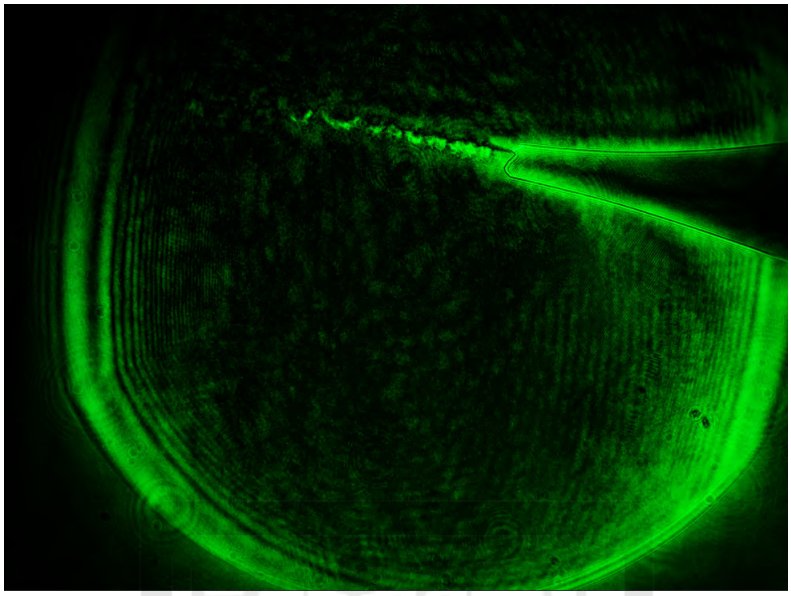

Figure 33: Schlieren image of the convergent nozzle with chamber pressure at 1 atm.

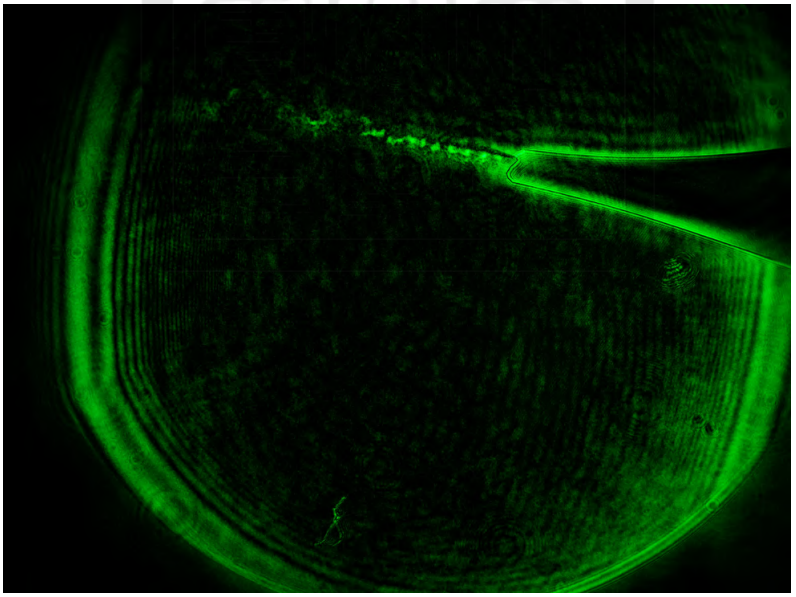

Figure 34: Schlieren image of the convergent nozzle with chamber pressure at 1 atm

4.3.2 Chamber pressure in vacuum

After observing the gas puff under atmospheric background pressure, we decided to conduct another experiment to investigate whether the gas jet can also be observed under vacuum condition or not. Therefore, we replaced experiments in section 4.3.1 with pumping the vacuum pressure down to $\sim 10^{-3}$ Torr. Shown in Fig. 35 and 36 are schlieren images of two shots. We observed faint lines at the exit of the glass convergent nozzle, which

we believed it was the of gas puff. The boundaries of the gas puff were straight. Different from the gas puff observed in the atmosphere (Fig. 33 and Fig. 34), the gas puff expended when it went downstream. It is not surprised since the background pressure was much less than 1 atm. It indicated that the gas puff was a laminar flow.

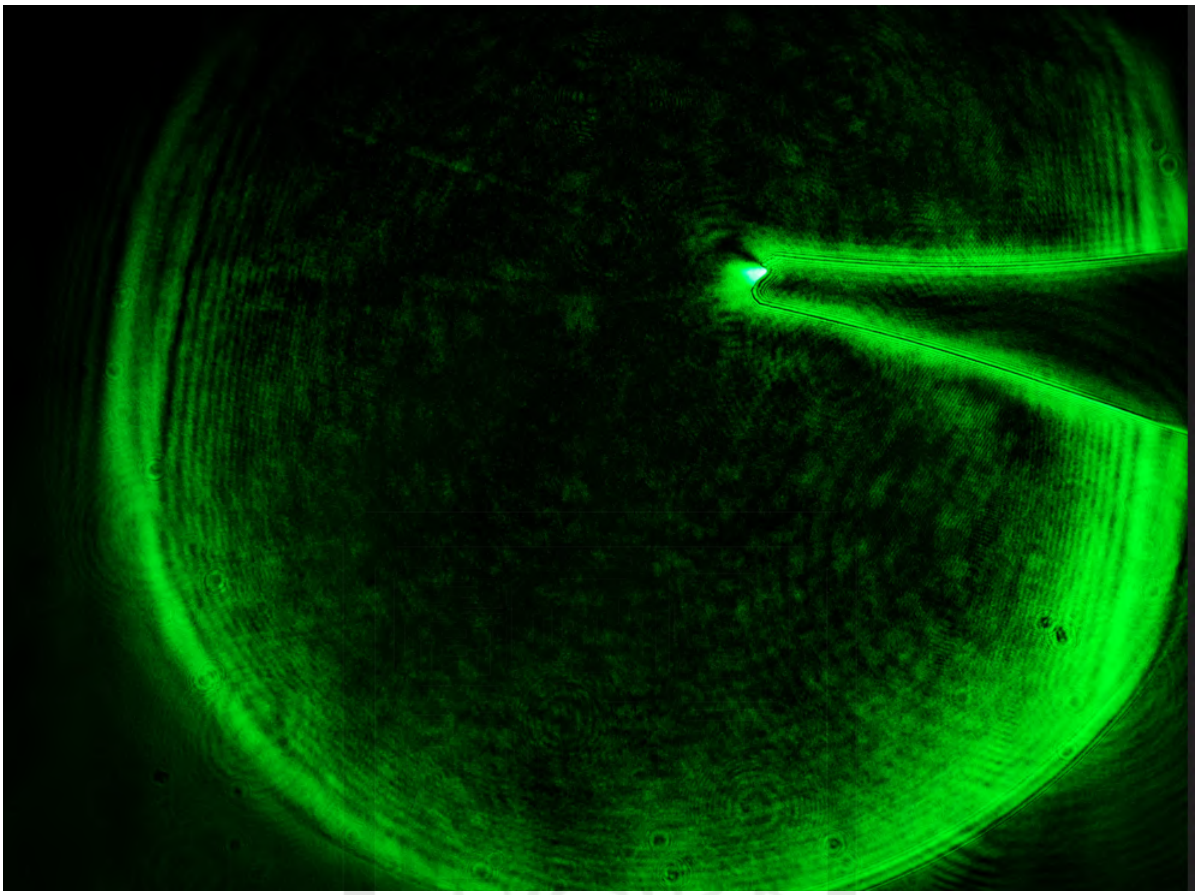

Figure 35: Schlieren image of the gas puff under vacuum 10^{-3}Torr

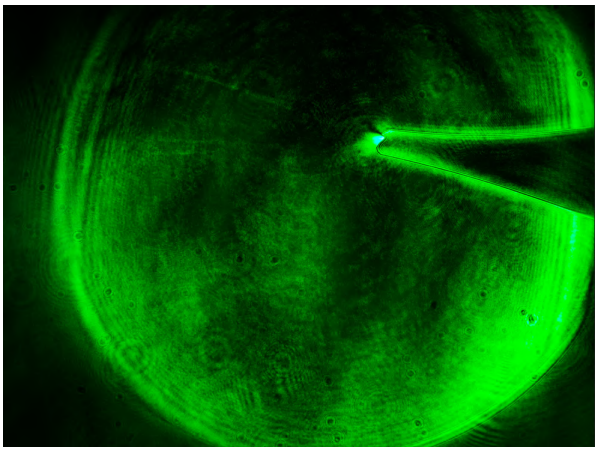

Figure 36: Schlieren image of the gas puff under vacuum 10^{-3} Torr

4.4 Opening angle analysis

We need to have a collimated gas puff and thus a collimated plasma plume for our EUV light source. Therefore, the plasma plume can go straight through the Helmholtz coil for being pinched in the future. Therefore, it is important to obtain the opening angle of the gas puff.

I used Matlab to analyze the schlieren image. The analyzing process is as follows:

(1) Load the image into Matlab.

(2) Convert the color image into a gray image with intensity range of 0 to 255 as shown in Fig. 37.

(3) After importing the image into MATLAB and processing it, I obtained the (x, y) pixel coordinates of the gas puff by using the mouse to record the coordinate. By clicking points on the boundary using the mouse, we can obtain a series of (x,y) which are points at the boundary.

(4) Exporting these coordinates to Excel allows me to further analyze the data. Plot series of boundary points (x_i, y_i) in Excel as shown in Fig. 38. By calculating the slope of the gas puff in Excel, I can gain insights into its direction and behavior.

(5) Fit the data plotted in excel using a linear function $y = ax + b$ as the blue dashed line shown in Fig. 38. Then the titled angle of the boundary is $\Theta = tan^{-1}(a)$.

(6) Finally, the opening angle $\alpha = 180 - (\Theta_1 + |\Theta_2|)$ as shown in Fig. 39.

Shown in Fig. 38 are the location of the boundary in Fig. 37 as an example. The fitting function of each side of the boundary is $y = 4.71x - 9847.7$ and $y = -6.58x + 2430.2$, respectively. The corresponding titled angles are $\Theta_1 = 78.01^\circ \pm 3.5^\circ$ and $\Theta_2 = -81.36^\circ \pm 0.6^\circ$. Therefore, the opening angle was $20.7^\circ \pm 4.1$. Similarly, opening angles of the other two repeated shots were $16.9^\circ \pm 6.6^\circ$ and $17.3^\circ \pm 5.4^\circ$. Finally, the averaged opening angle was $18.3^\circ \pm 5.4^\circ$ from three shots.

Figure 37: Schlieren image captured in vacuum environment with gas jet - cutline 600.

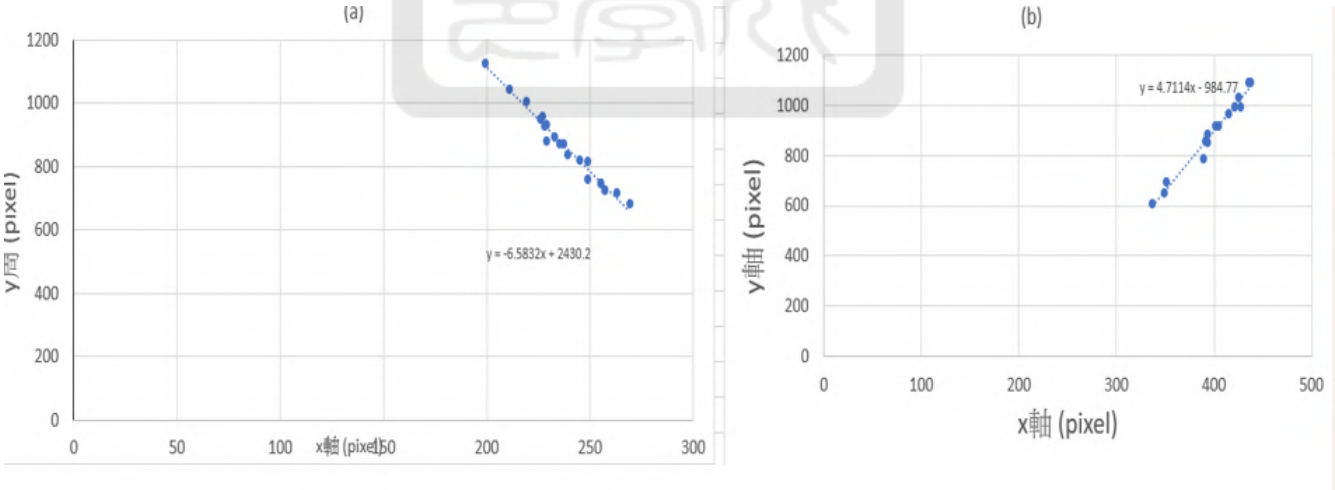

Figure 38: The calculation of the opening angle.

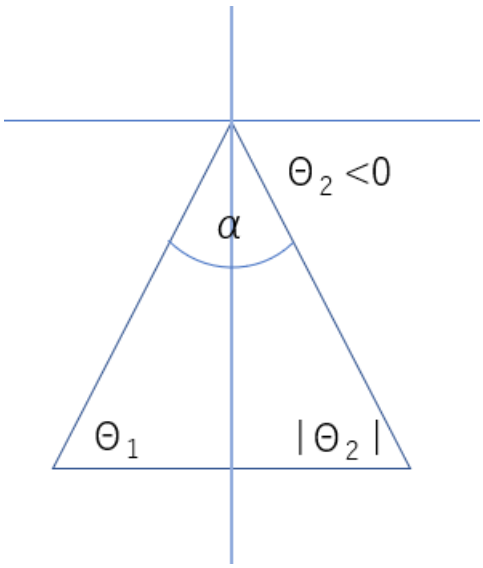

Figure 39: The opening angle calculated

5 The plasma-plume generating system

In this chapter, I will introduce how we ionized the gas puff and observed the plasma plume. The plasma-plume generating system consists of two subsystems: the gas-puff arcing system and the ionization convergent-divergent nozzle (ICDN) system. Section 5.1 will introduce the gas-puff arcing system that I have installed. Section 5.2 describes the design of the ICDN. Section 5.3 discusses the process of ionizing the argon gas jet during the experiment. In section In section 5.4 and 5.5, we analyzed the interferometer image using by Matlab. In section 5.6, I analyzed the opening angle of the plasma plume observed at the outlet of the ICDN.

5.1 The gas-puff arcing system

The gas-puff arcing system is primarily used to provide the electrical energy to ionize the argon gas puff passing through the ICDN. Figure 40 is the schematic diagram of the gas-puff arcing system. The system consists of a DC power supply, a DC high-voltage power supply, one 7.5-uF high voltage capacitor, and two resistors. The power supply provides a voltage of 24 V to drive the DC high-voltage power supply. Then, the DC high-voltage power supply provides a voltage of 1.05 kV to the system. Finally, the capacitor is charged to ∼1 kV through the 2-MΩ resistor. The 100-MΩ resistor, on the other hand, is connected to the capacitor in parallel. In the circuit, we have included two resistors in the system. The 2-MΩ resistor is to protect the power supply. The 100-MΩ resistor primarily serves as the safety discharge device. The energy in the capacitor is dissipated when the power supply is turned off. These two resistors also determine the charging time and the energy dissipation time.

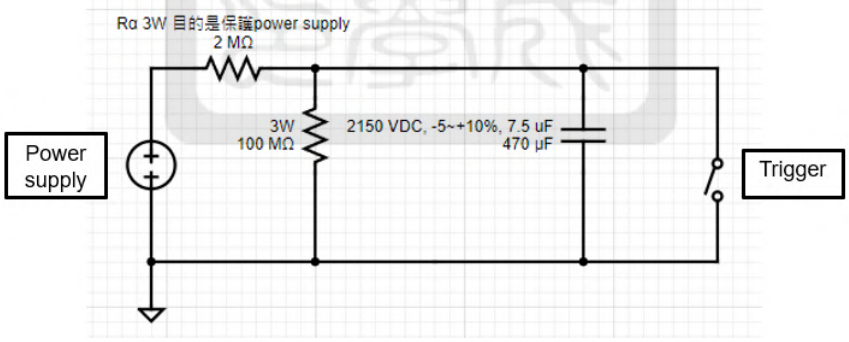

Figure 40: Arcing circuit schematic diagram

To charge the capacitor, it takes us 75 seconds to charge from 0V to ∼1 kV. It's estimated by $\tau = 5RC$

$$.\tau = 5RC = 5(2 \times 10^{6})(7.5 \times 10^{-6}) = 75 \quad \text{second} \tag{1}$$

For safety purposes, we have set the energy dissipation time to 3750 seconds. The formula is $\tau = 5RC$.

$$\tau = 5RC = 5 * (100 \times 10^{6}) * (7.5 \times 10^{-6}) = 3750 \quad seconds = 62.5 \quad \text{minutes.} \tag{2}$$

Notice that the 100-MΩ resistor is always connected to the capacitor in parallel. In other words, when the

capacitor is fully charged to ∼1 kV, a current I = 1 kV/1 MΩ = 1 mA keeps flowing through the resistor. Therefore, we can calculate the ohmic-heating power of the resistor.

$$P = \frac{V^2}{R} = \frac{(1.05 \times 10^3}{100 \times 10^6} = 0.011 \qquad \text{W} \tag{3}$$

. Therefore, the 3-W resistor we use will not be damaged.

5.2 The design of the ionziation convergent-divergent nozzle system

The ionization convegent-divergent nozzle (ICDN) system has two purposes: (1) deliver the gas to the ICDN; (2) generate a plasma plume. The first requirement for designing our ICDN system is to integrate the system to the pulsed-power system chamber. I have divided the ICDN system into two parts. The first part is the gas tube from the reservoir to the ICDN, which mainly transports the gas from the reservoir to the ICDN. The second part is the ICDN system, which serves two purposes. The first purpose is to ionize the argon gas. The second is the geometry of a convergent-divergent nozzle that can accelerate the argon gas puff to supersonic speed.

Let me introduce the gas tube first. In order to match the size of the pulsed-power system chamber, the length of the gas tube needs to be between 295 mm and 300 mm, as shown in the Fig. 41. Therfore, the plasma plume can be observed by the laser diagnostic. The pulse valve with an outlet of 1 mm is attached to the flange from outside. The connection between the gas tube and the flange is a plastic disk with a diamter of 40 mm. The inner diameter of the gas tube is 3 mm and the outer diameter of the gas tube is 10 mm. The material of the gas tube is stainless steel. It is able to hold the designed argon gas pressure of 10 atm. Nevertheless, we expect the pressure of the argon gas drops below 10 atm when the gas flow along the gas tube while the pulse valve is open.

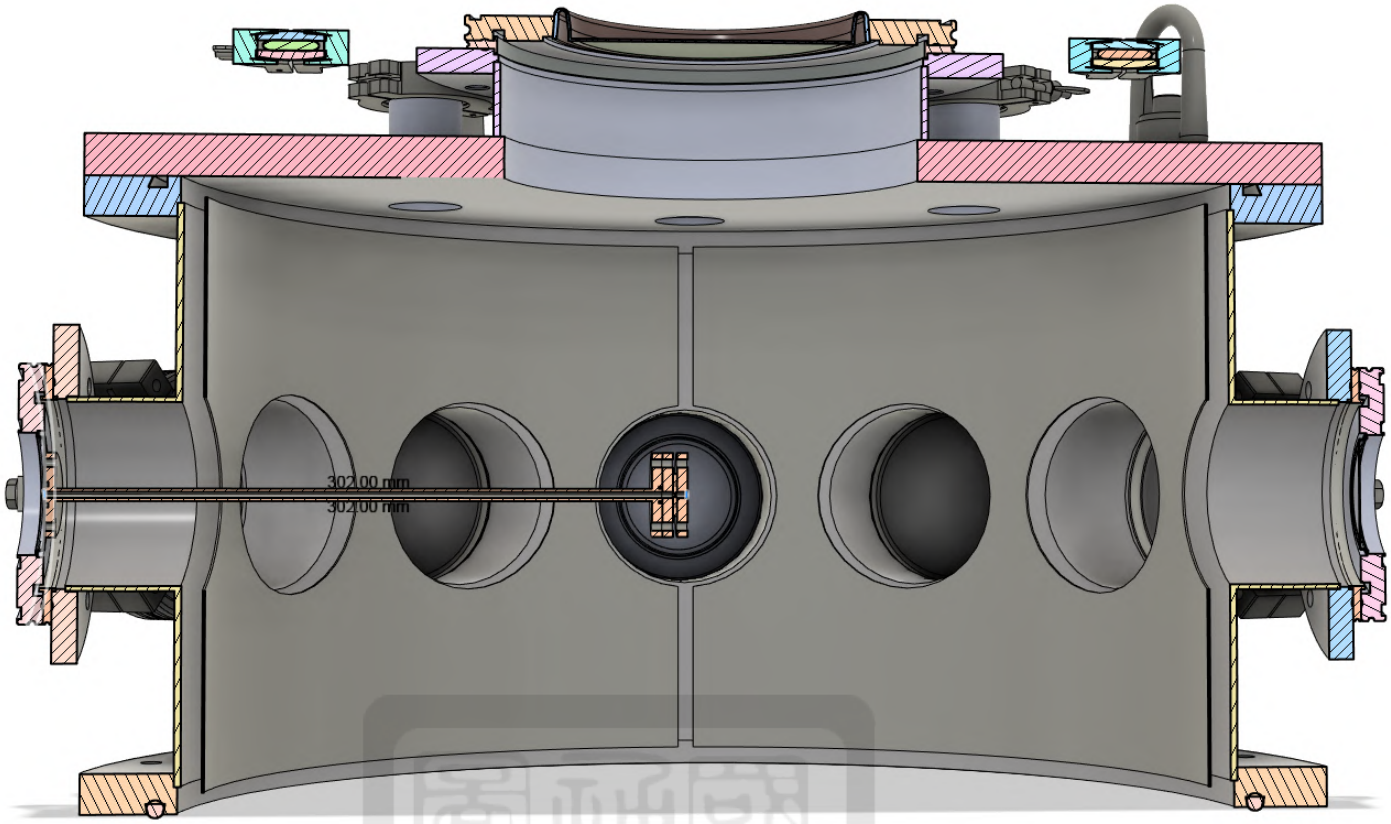

Figure 41: The schematic diagram of chamber and 260-mm electrode gas tube

Figure 42 is the ICDN system comprising four components: the gas tube, two brass plates, and a Teflon plate sandwiched between the brass plates. The gas tube's head is attached to the chamber using M4 vacuum screws. The other end of the gas tube is fastened to brass plates and the Teflon plate with M4 plastic screws to prevent electrical flashover through the screws during the discharge process.

Now let's move on to the second part, which is the ICDN. First, let me introduce the ionization process of the argon gas puff. Our design comprises three disks with coalign holes at the center stack on each other. The first and third disks serve as electrodes, In between, the second disk is the insulator. It is made of Teflon. Additionally, the hole at the center of the Teflon disk acts as a converging-diverging nozzle to accelerate the argon gas puff to supersonic speed. The detailed engineering drawing is given in Appendix (section A.3).

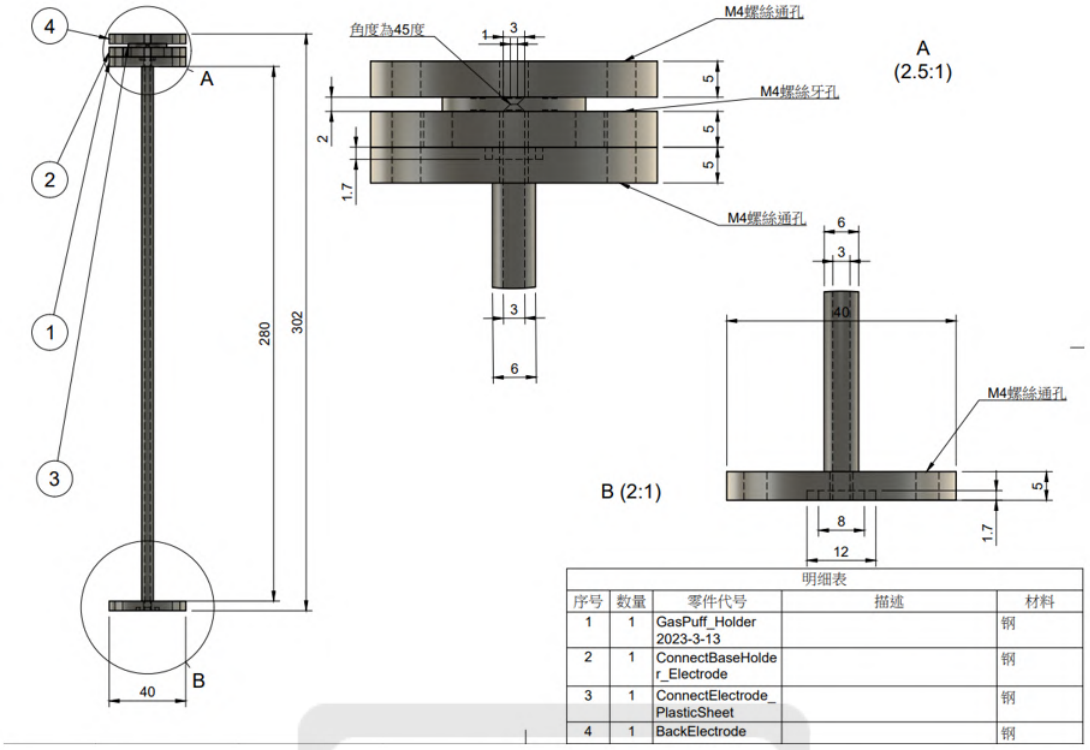

明细表

序号	数量	零件代号	描述	材料
1	1	GasPuff_Holder 2023-3-13		钢
2	1	ConnectBaseHolder_Electrode		钢
3	1	ConnectElectrode_PlasticSheet		钢
4	1	BackElectrode		钢

Figure 42: Electrode gas tube drawing

To assess the possibility of arcing, we can refer to the Paschen curve, which determines the electrical breakdown of argon at 10^{-6} Torr under a voltage of 1 kV. The Paschen curve is defined by the formula $V = P * d$ where V represents the breakdown voltage, P is the gas pressure, and d is the gap distance. Figure 43 show the Paschen curve function. The value of d estimated as to the diagonal length of the ICDN depicted in the diagram, which is $2 \times 2^{0.5}$ mm in width. First, our vacuum condition is on the left side of the Paschen curve We charged the capacitor to 1050 V. According to the curve, argon does not breakdown at 1 kV in high vacuum conditions. When the pulse valve opens, the argon gas flow through the gas tube and reaches the ICDN. As a result, the voltage of 1 kV across the ICDN exceeds the breakdown voltage since the pressure increases when the gas flow reaches the ICDN.

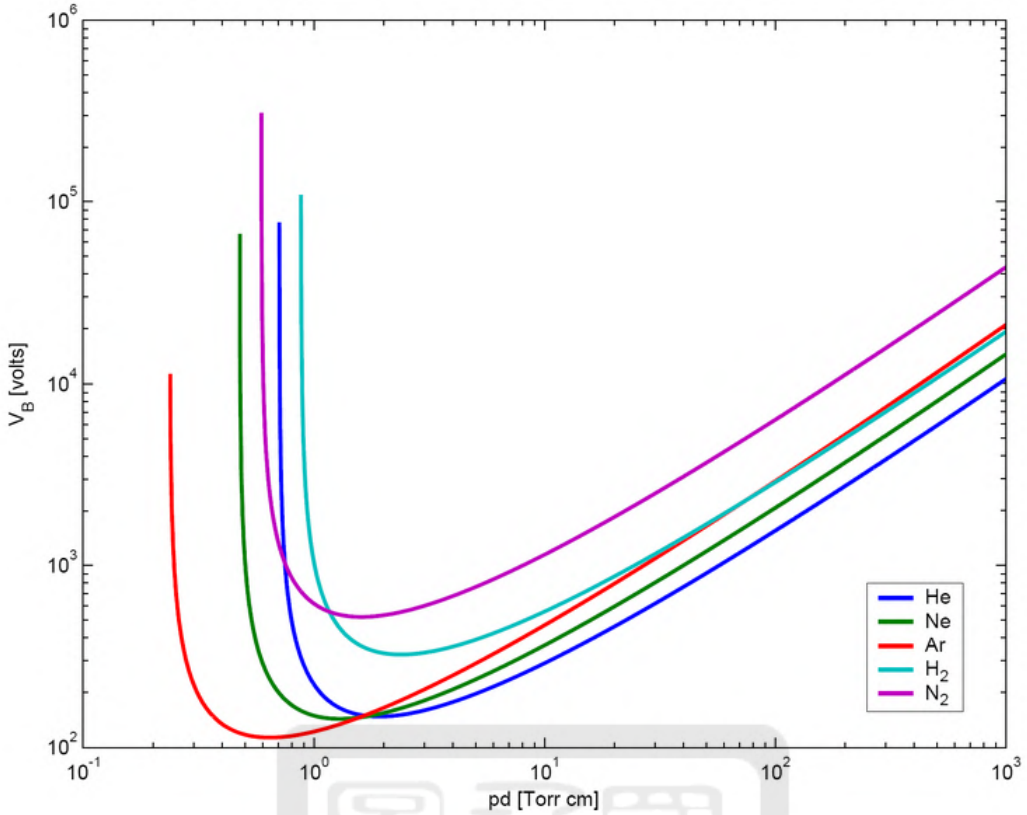

Figure 43: Paschen curve of argon [Ref 7]

5.3 Gas-puff and plasma-plume generations

After installing the ICDN system to the chamber, we tested the performance of the plasma-plume generating system. The vacuum chamber is pumped down 10^{-6} Torr in all experiments.

5.3.1 Gas-puff generation

First, we would like to check if the gas puff is generated by the ICDN system. We reassembled the plasma-plume generating system more carefully to avoid any gas leakage. Before conducting experiments in vacuum, we ensured that the gas puff was generated under atmospheric pressure conditions by puffing a tissue at the outlet of the ICDN. Then, we starting to pump the chamber to vacuum prior to conducting following experiments.

In this experiment, we didn't provide the high voltage so that that we can observe the gas puff. The pulse valve open for 50 ms. We set the delay time of the laser relative to the opening time of the pulse valve to be between 10, 20, 30, and 40 ms. In Fig. 44, it is a schlieren image of the gas puff with a laser delay time of 30 ms relative to the opening time of the pulse valve. We can see the gas puff indicated by the arrow in Fig. 44. We found that the gas puff was captured only for delay time larger than 20 ms. In other words, it took 20 ms for the gas puff to propagate from the pulse valve to the outlet of the ICDN.

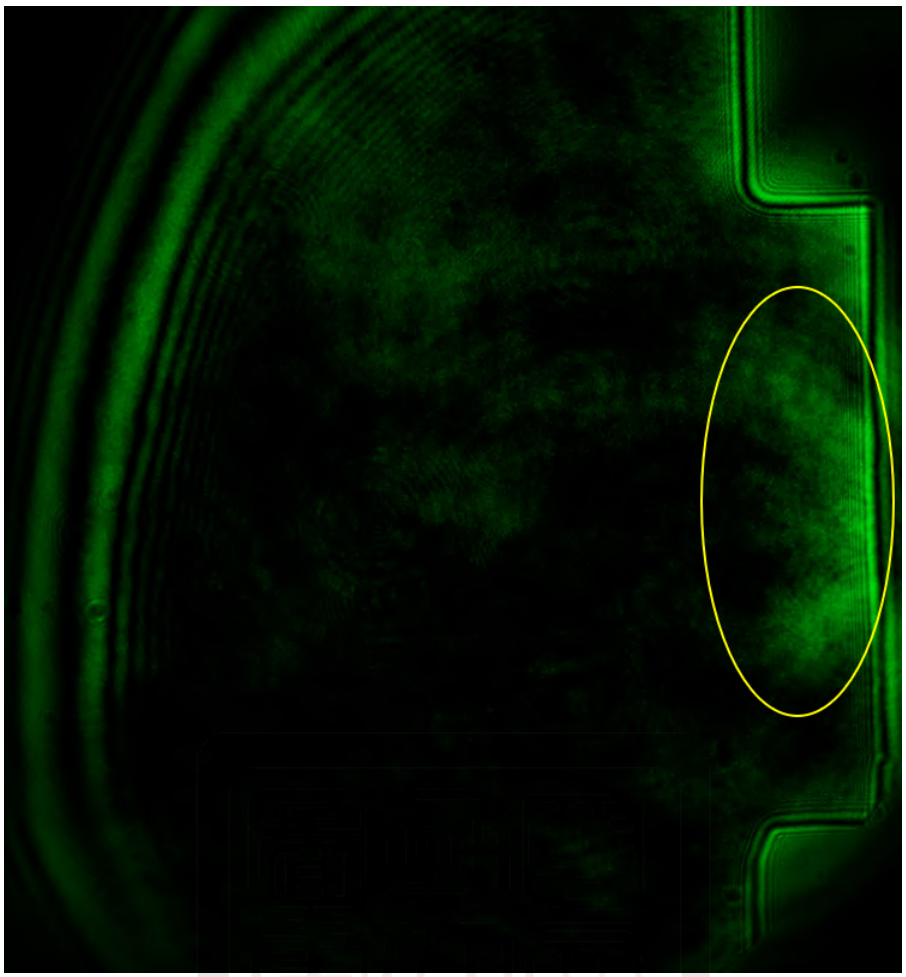

Figure 44: No high voltage, laser delay time 30 ms

5.3.2 Plasma-plume generation

After confirming that the gas puff was generated, we proceeded with the experiment with the capacitor of the gas-arcing system charged.

In order to confirm the presence of arcing and ionization in the argon gas puff, we used a side-view camera to capture experimental images. In Fig. 45, the red and blue light was observed, indicating the generation of plasma. The green light was due to the laser for diagnosis. However, precise determination of the timing and duration of plasma formation was not possible just using the side-view camera. Nevertheless, the experiments confirmed that plasma can indeed be generated in the system.

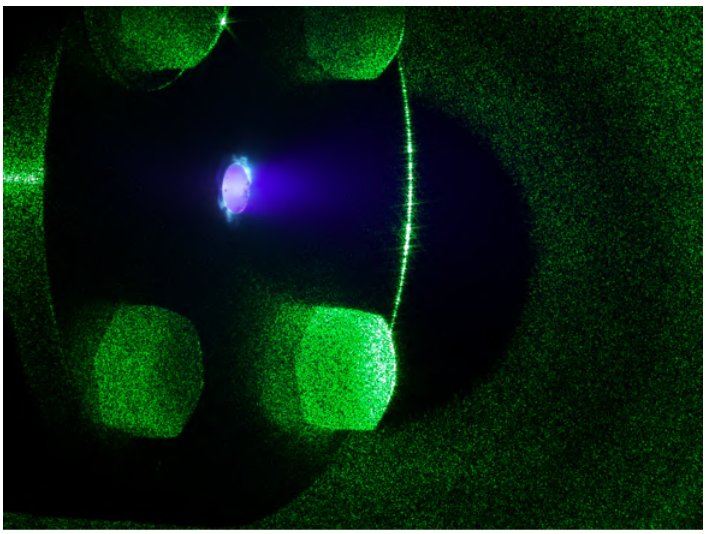

Figure 45: The side-view picture

After experiments, we disassembled the ICDN and made several significant observations, as Fig. 46 and Fig. 47. A burn mark is visible at the center, indicating that the discharge current was through the center of the nozzle of the ICDN.

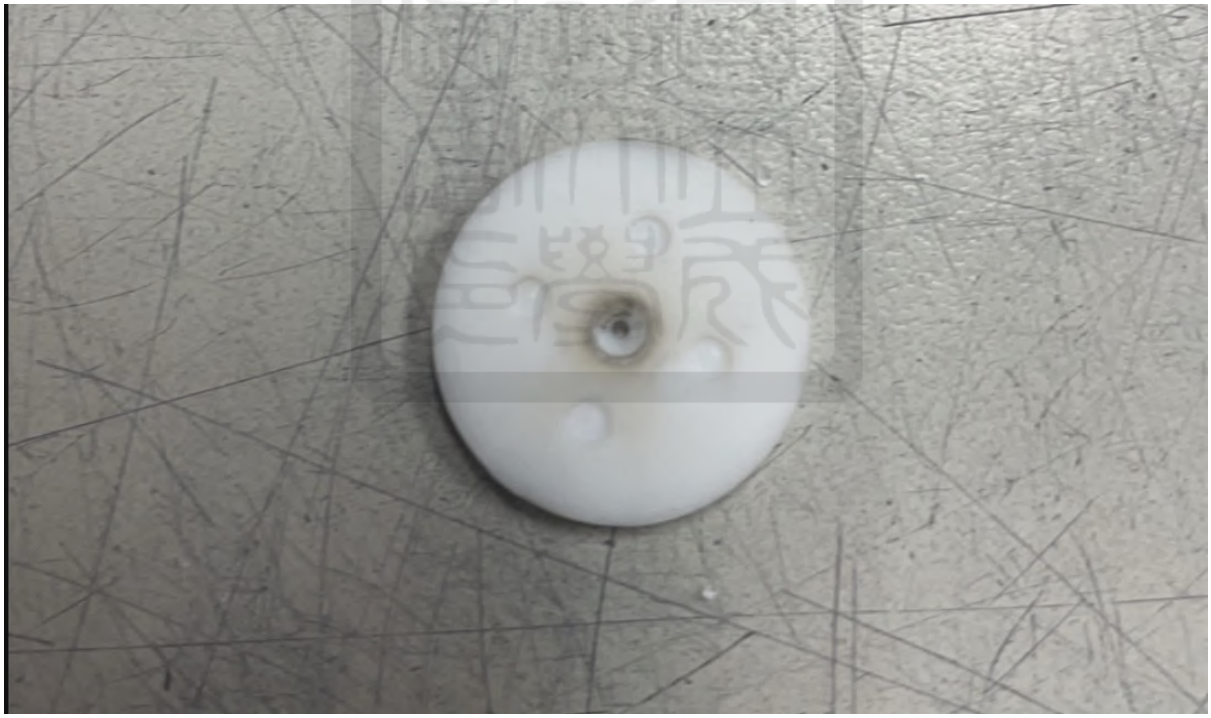

Figure 46: convergent-divergent nozzle

Figure 47: convergent-divergent nozzle -1

Additionally, we observed distinct burn marks at the locations where the one of the electrical O-rings was located as shown in Fig.48. We suspected that these burn masks came from the contact between the electrical O-ring to the brass plate being not firm enough. It was solved by making a better contact when we tightened the O-ring.

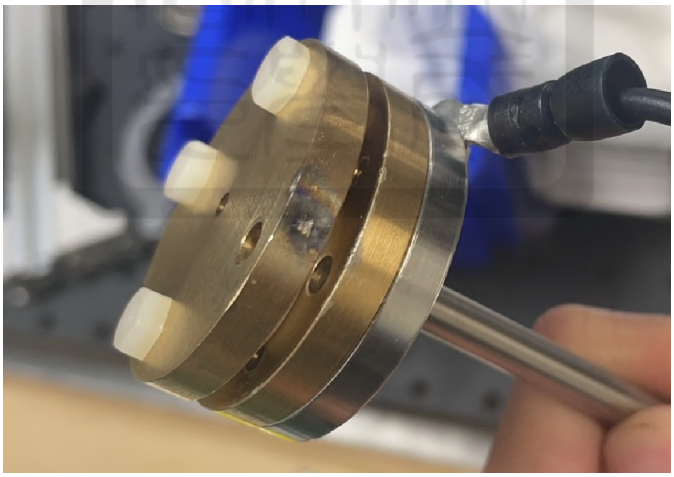

Figure 48: Gas tube burning point

We didn't measure the discharge current. Nevertheless, we measured the voltage of the capacitor during each discharge. We can use voltage measurement to estimate the peak current. We can begin by using the formula

$$\omega = \frac{2\pi}{T} = \frac{1}{(LC)^{\frac{1}{2}}} \tag{4}$$

, where "ω" represents the angular frequency, T denotes the period of the discharge voltage, L stands for the inductance of the system, and C represents the capacitance. The current peak can then be estimated using the

formula

$$I_{peak} = \frac{V}{\left(\frac{L}{C}\right)^{\frac{1}{2}}}. \tag{5}$$

. In our case, the voltage was ~ 1 kV and the capacitance was 7.5 uF. Figure 49 shows one of the discharge voltage. The period was 36 us. Therefore, the inductance and the discharge peak current was ~1300 A.

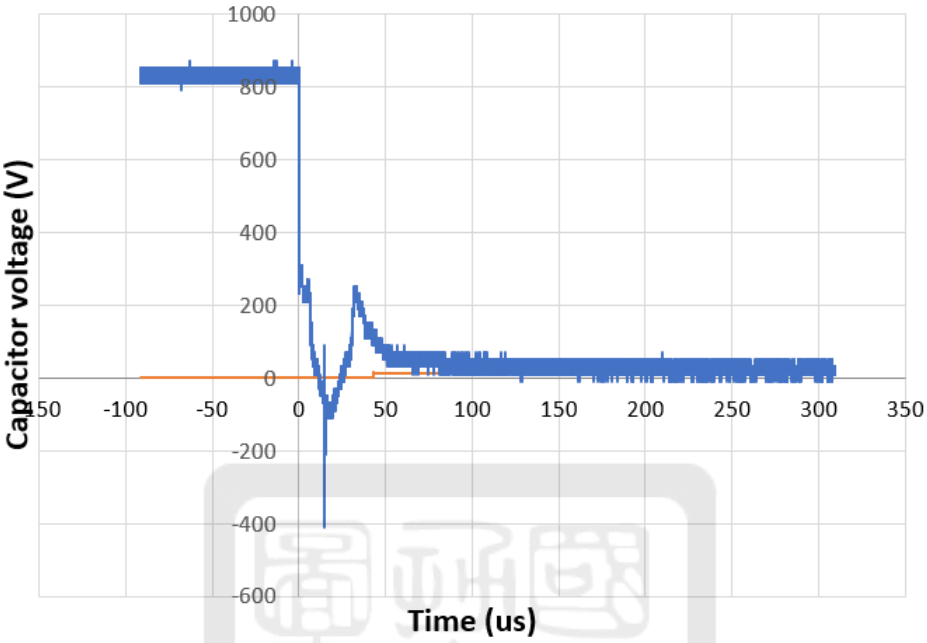

Figure 49: The voltage oscillation

After confirming that an arc inside the ICDN was initiated, we tried to capture the plasma plume. We conducted experiments with varying laser delay times of 10 ms, 20 ms, 30 ms, and 40 ms relative to the pulse-valve opening time. The pulse valve open for 50 ms. Finally, we observed the plasma plume. Figure 50 is the Schlieren image with laser delay of 30 ms as an example. A plasma plume can be observed pointed out by an arrow in Fig. 51.

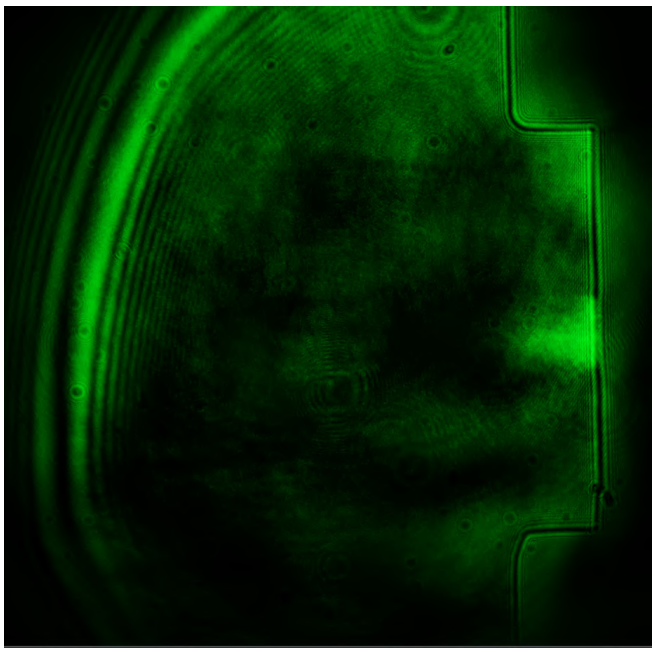

Figure 50: High voltage, laser delay time 30ms

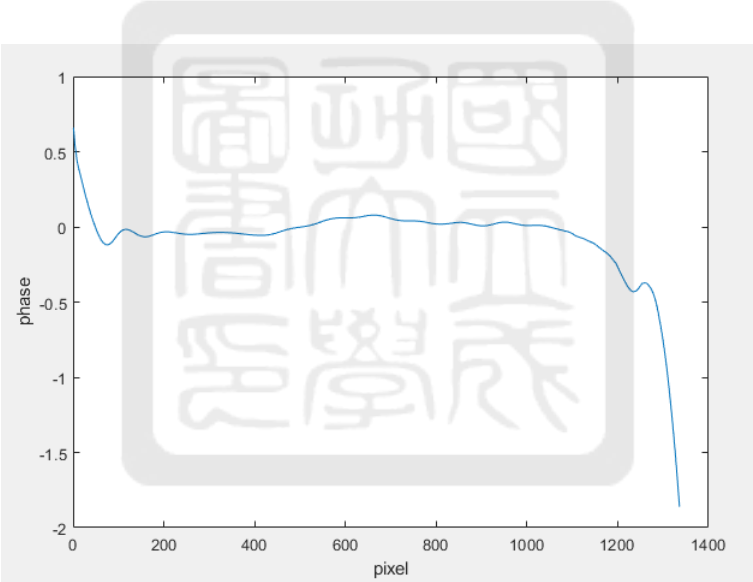

Figure 51: plasma plume arrow image

5.4 Analysis process of the interferometer images

In this section, the interferometer images will be analyzed using MATLAB to calculate the opening angle, full width at half maximum (FWHM), and their respective error bars of the gas puff and the plasma plume. I will demonstrate the analysis process using the interferometer image taken at 20 ms delay as an example. The analysis results of the remaining data will be included in Appendix (section A.4).

First, edges and noises of a raw interferometer image shown in Fig. 52 are removed. Notice that the image is convert to gray level. This can be done by cropping the image to focus on the relevant region of interest as shown in Fig. 53.

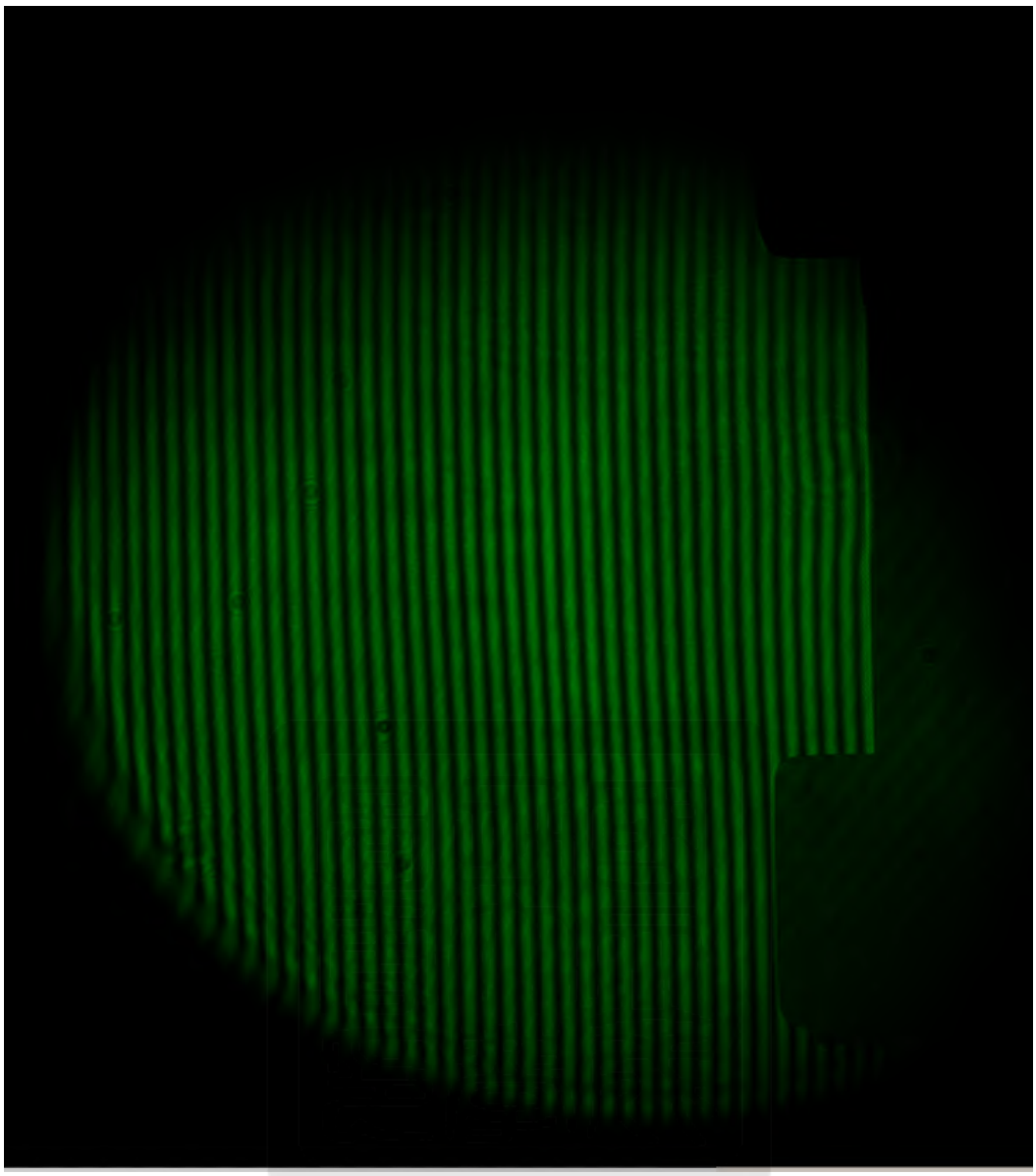

Figure 52: Raw interferometer image of the 20 ms laser delay

Figure 53: The cutline of example

By following the analysis algorithm given in Ref 8, we can obtain the phase changes of the laser light propagating through the gas puff or plasma plume. The line integrated plasma density (n_e) can be obtain from the phase changes: $\int n_e dl = -\frac{2cn_c}{\omega}\Delta\Phi$. Where $\Delta\Phi$ is the phase changes, n_c is the critical density corresponds to the laser light, ω is the angular frequency of the laser light, and c is the speed of the light. However, the neutral gas can also be measured since the refraction index of the argon gas is $n_r = 1.00028287$ at 532 nm. In other words, the gas puff also causes phase changes. Therefore, for fair comparison, we only calculate the phase changes. Finally, the 2D phase-change image is obtained and shown in Fig. 54.

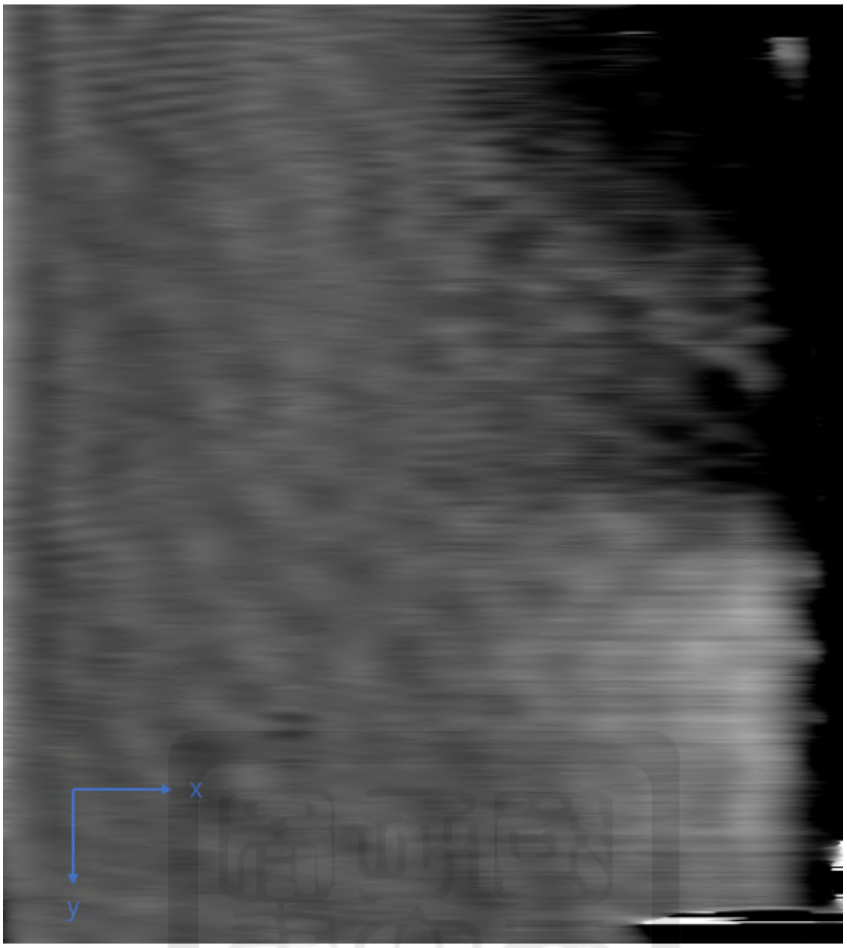

Figure 54: The analyze data in matlab

We have observed that the dark region pointed out by the arrow corresponds to the gas puff in Fig. **??**. To quantitatively obtain the profile of the gas puff/plasma plume, we take the average of the 2D phase image. Notice that the averaging calculation in Matlab takes the average from top to down.

Firstly, we directly take the average of Fig. 54. The result is shown in Fig. 55. We can see the drop at x~50 pixel corresponds to the dark boundary on the left side of Fig. 54. On the other hand, the drop at x~1350 pixel corresponds to the nozzle.

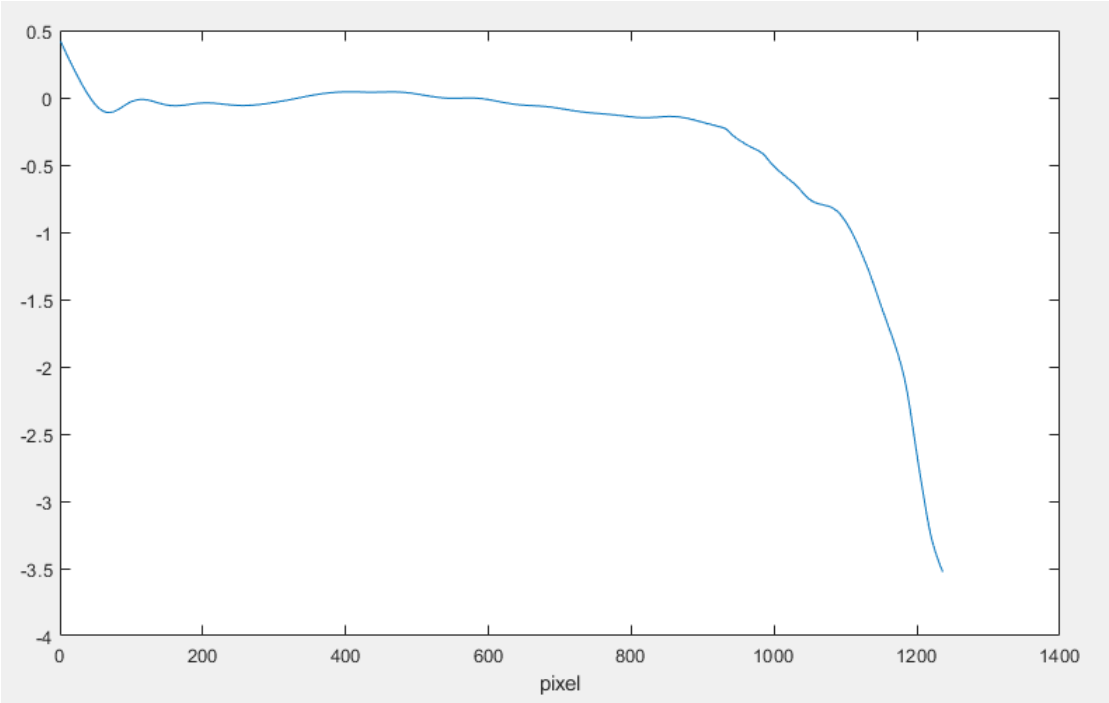

Figure 55: The average array about the cutline data

Secondly, we want to obtain the opening angle of the gas puff/plasma plume. We need to find the widths of the gas puff/plasma plume at different heights. To obtain the profile of the gas puff/plasma plume at different height, we take the averages of row 50∼150, 150∼250, and 250∼350. In other words, three profiles across the gas puff/plasma plume at different heights are obtainal by Fig. 54. After rotating the image by 90 degrees and taking average of the array allows you to observe the profiles at different height of the gas puff/plasma plume.

To focus on the gas-puff/plasma plume region, we select row 400 to 900 on the y-axis of Fig. 54, i.e., column 400˜900 on the x' axis in Fig. 56. This selection allows us to narrow down our analysis to the relevant portion of the image that captures the gas puff/plasma plume. Shown in Fig. 58 is the averaged profile of row 50∼100 in the range of colume 400∼900 of the Fig. 56 as an example.

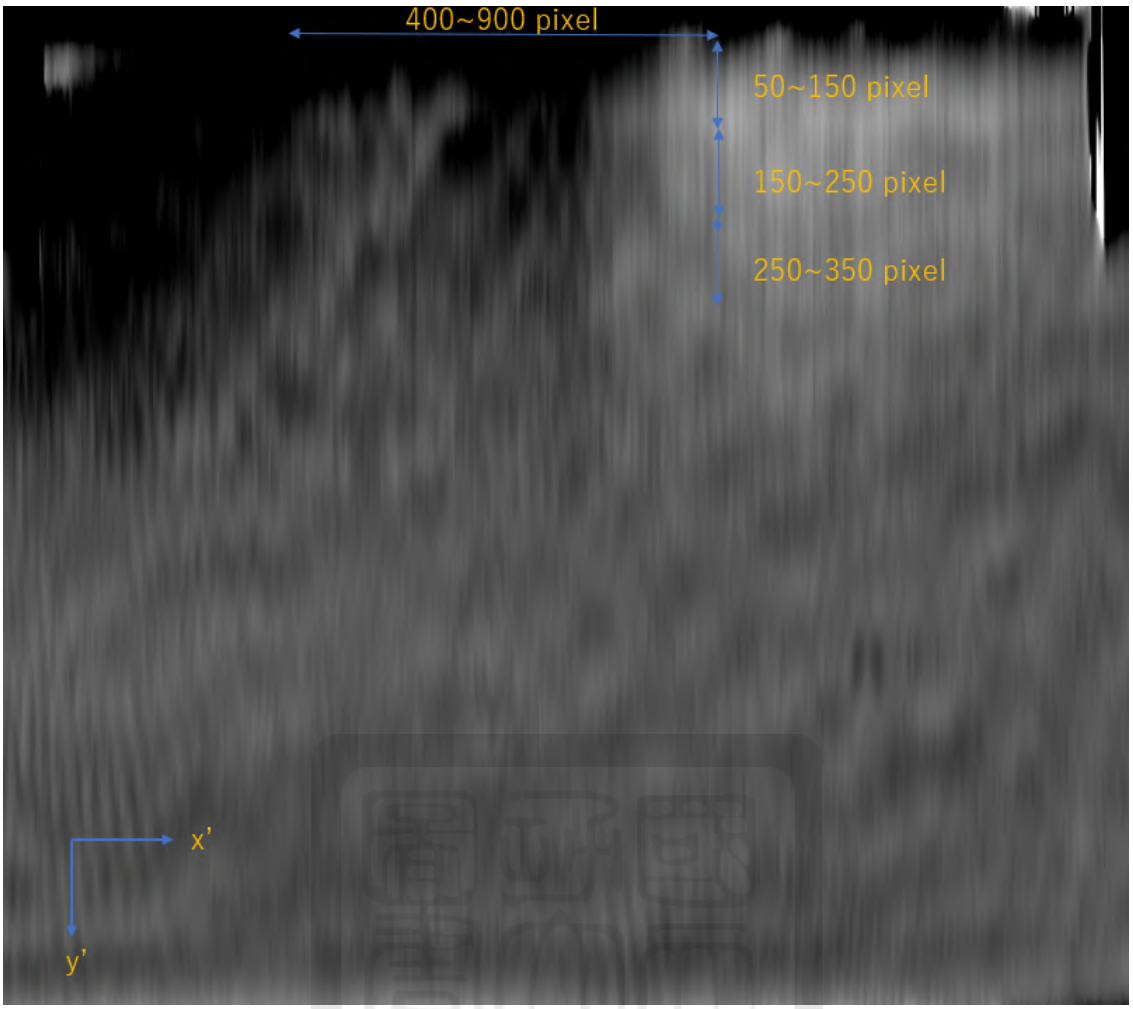

Figure 56: The analyze data in matlab rotate by 90 degrees

To obtain the width and the amplitude of the phase changes, I fit the data with super-Gaussian function. The super-Gaussian function is given in Equation (7).

$$A_0 e^{((\frac{x-b}{c})^2)^e} + d, \tag{6}$$

where $A_0$is the amplitude, b corresponds to the location of the function, c is the width, d is the offset, and e is the power of the Super-gaussian function. Figure 57, Fig. 58, Fig. 59, and Fig. 60 are the fitting results of the profiles at different heights. We can put them together in the same plot as shown in Fig. 61.

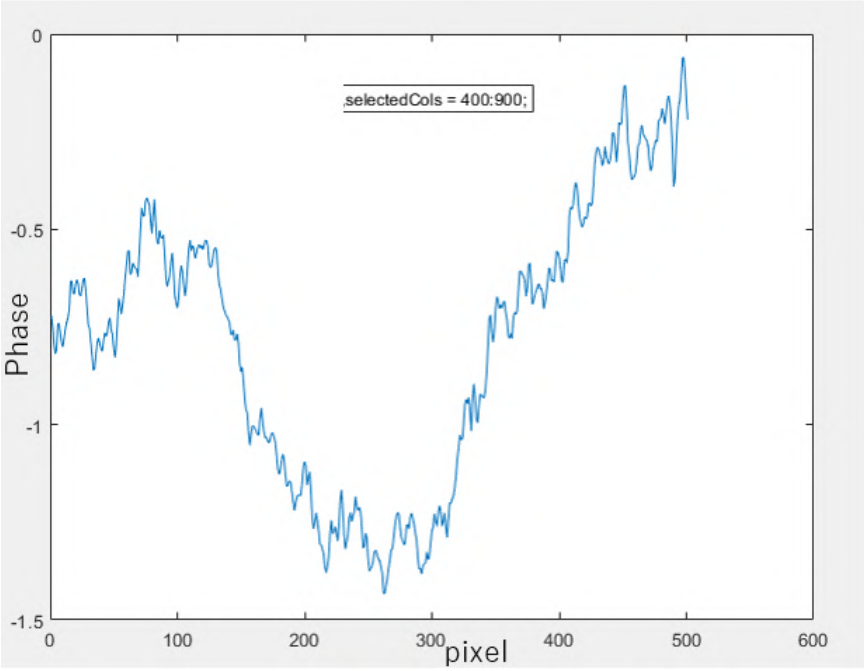

Figure 57: The data of columns 450 to 900 on the y-axis average array

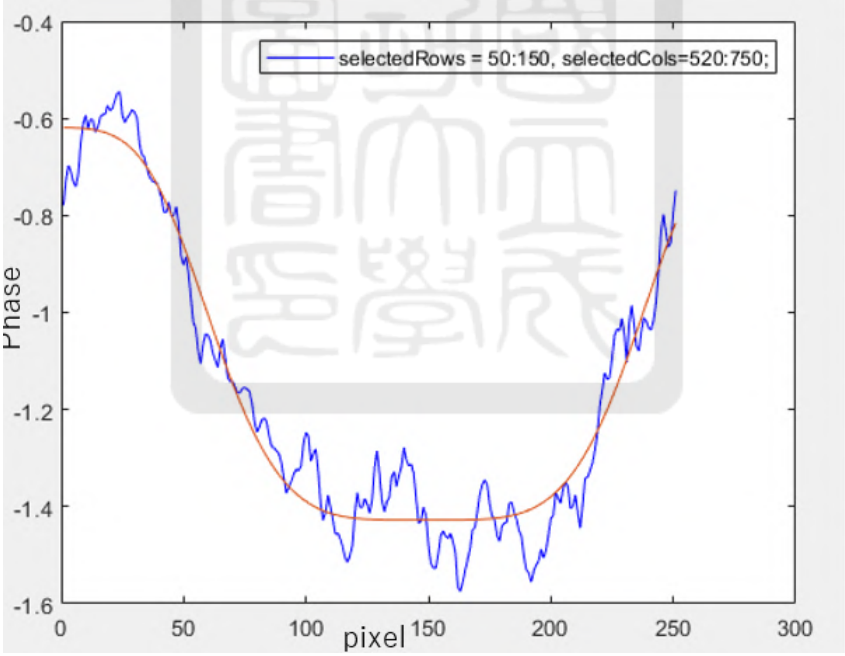

Figure 58: The super gaussian fitting analyze

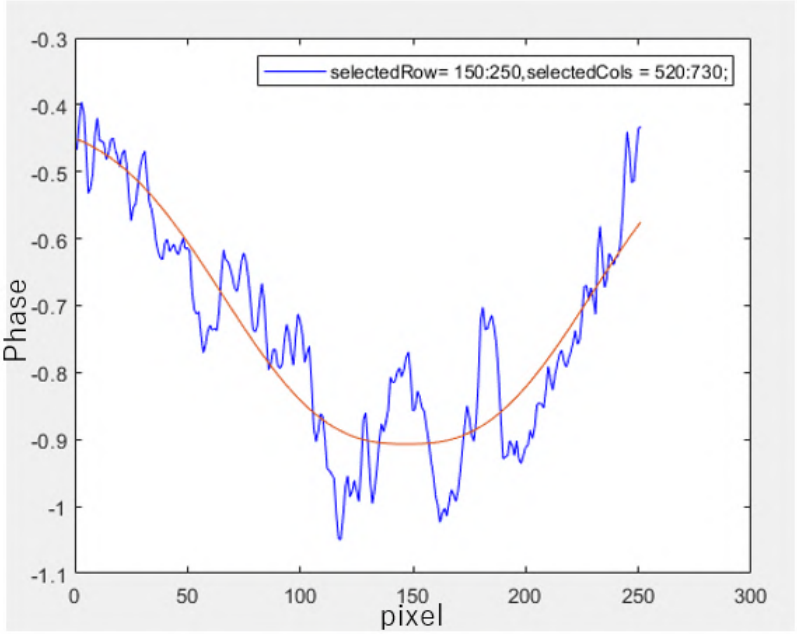

Figure 59: The super gaussian fitting analyze

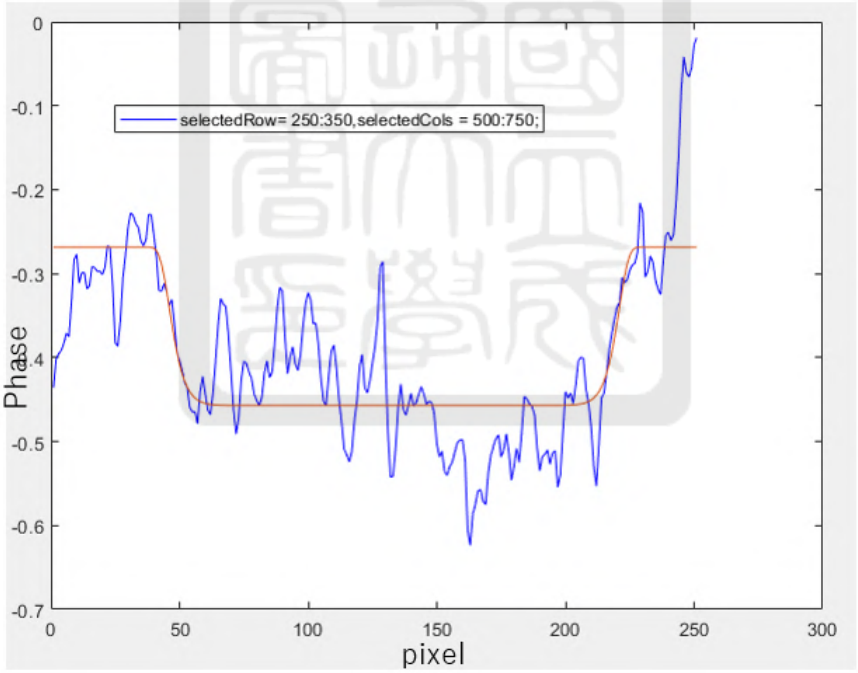

Figure 60: The super gaussian fitting analyze

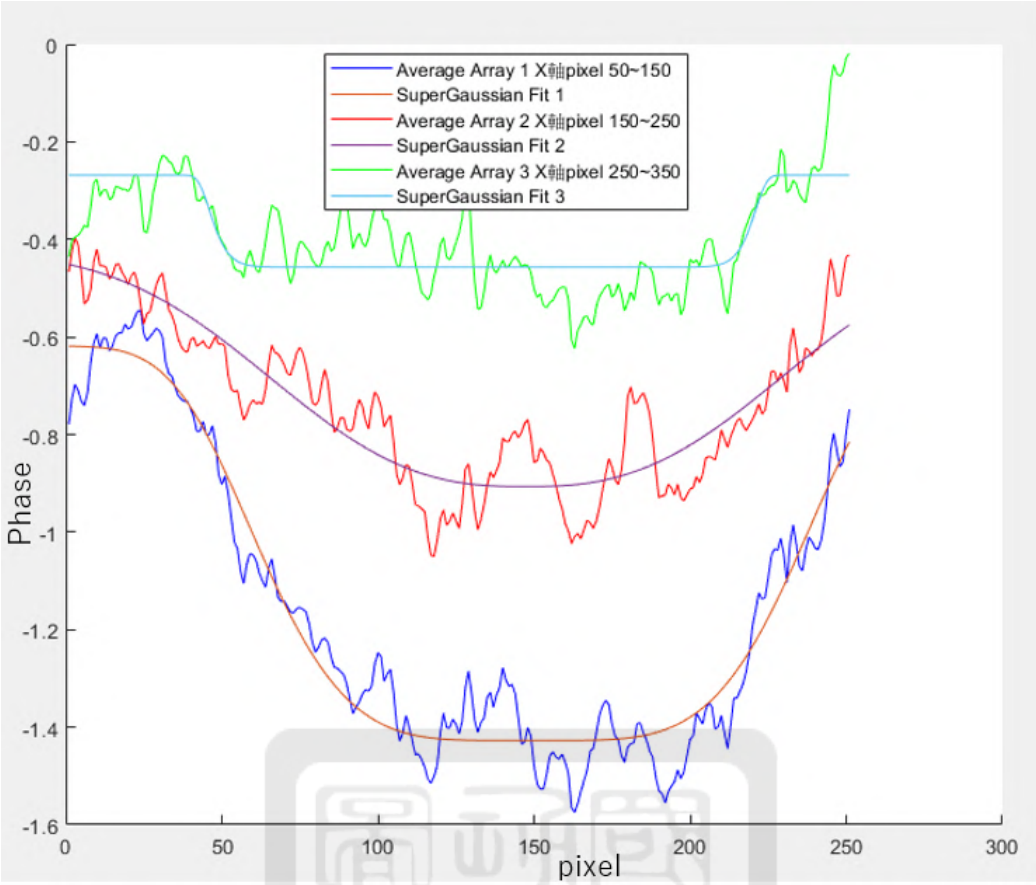

Figure 61: The gas puff displays the extracted regions

5.5 Analysis result of interferometer images

We are now collecting all analyzed results for all cases we have done. All analyzed curves are given in Appendix (section A.4). The curve fitted valves are summarized in Table 4. Notice that the "Gas puff" and the "Plasma plume" correspond to cases without and with charging the capacitor. The interferometer measures phase changes, which can indicate density variations in the gas/plasma. By comparing the minimum values of the fitting functions, we can identify any differences between the two cases. Since we repeated several times for each case, Table 4 show the averaged and the standard deviation of each case. Based on the observation that the gas puff was not visible when the laser delay time was set to less than 20 ms, a decision was made to record data starting from 20 ms and extending up to 40 ms. This range was determined to effectively capture the phenomenon of the gas puff. For fair comparison, the same delays were used for observing the plasma plumes. In fact, we couldn't see the plasma plume with a delay less than 20 ms either.

Table 4: Minimum valve of fitting function

Type	delay	Phase @ 50~150	Phase @ 150~250	Phase @ 250~350
Gas puff	40 ms	-1.9908	-1.3581	-0.8069
		-2.8054	-1.636	-0.8704
		-1.4657	-0.8648	-0.4879
	30 ms	-3.5475	-1.5136	-0.9906
		-2.131	-1.535	-1.1608
		-0.7826	-0.6435	-0.2303
		-1.7582	-1.4097	-0.7643
		-1.2468	-0.9808	-0.5356
	20 ms	-1.4362	-0.9151	-0.4059
		-1.4059	-0.9437	-0.7045
		-2.4329	-0.85	-0.5438
		-1.4162	-0.8023	-0.4605
Plasma plume	40 ms	-2.1458	-1.707	-1.0991
	30 ms	-1.9801	-1.3787	-0.8776
		-0.7615	-0.3956	-0.1413
	20 ms	-2.7274	-2.1134	-1.3389
		-0.7371	-0.6273	-0.4199

Table 5: Average and standard deviations of fitting function for plasma plume

Type	Delay	50～150 pixel	150～250 pixel	150～250 pixel
Gas puff	20 ms	-1.7±1.4	-1.4±1.1	-0.9±0.6
	30 ms	–1.4±0.9	-0.9±0.7	-0.5±0.5
	40 ms	-2.145	-1.707	-1.099
Plasma plume	20 ms	-1.7±0.5	-0.9±0.1	-0.5±0.1
	30 ms	-1.9±1.1	-1.2±0.4	-0.7±0.4
	40 ms	2.1±0.7	-1.3±0.4	-0.7±0.2

We plot the result in Table 5 as shown in Fig. 62～64. We compared the minimum slope values of the gas puff and plasma plume and found that there is little difference between them. Based on this comparison, we were unable to distinguish between the two. Nevertheless, the phase changes were largest (the values were minimum) in both cases indicating that the densities were the highest right at the ICDN outlet in both cases.

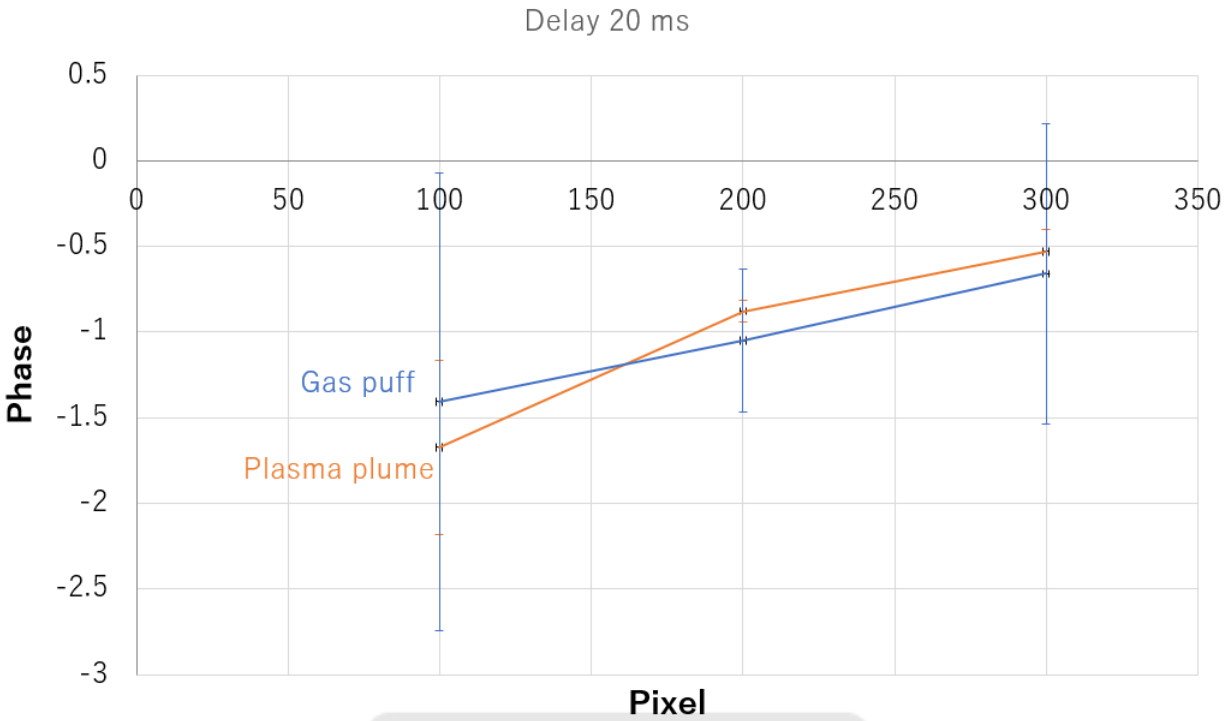

Figure 62: Comparison of phases between the Gas puff and the plasma plume of 20 ms.

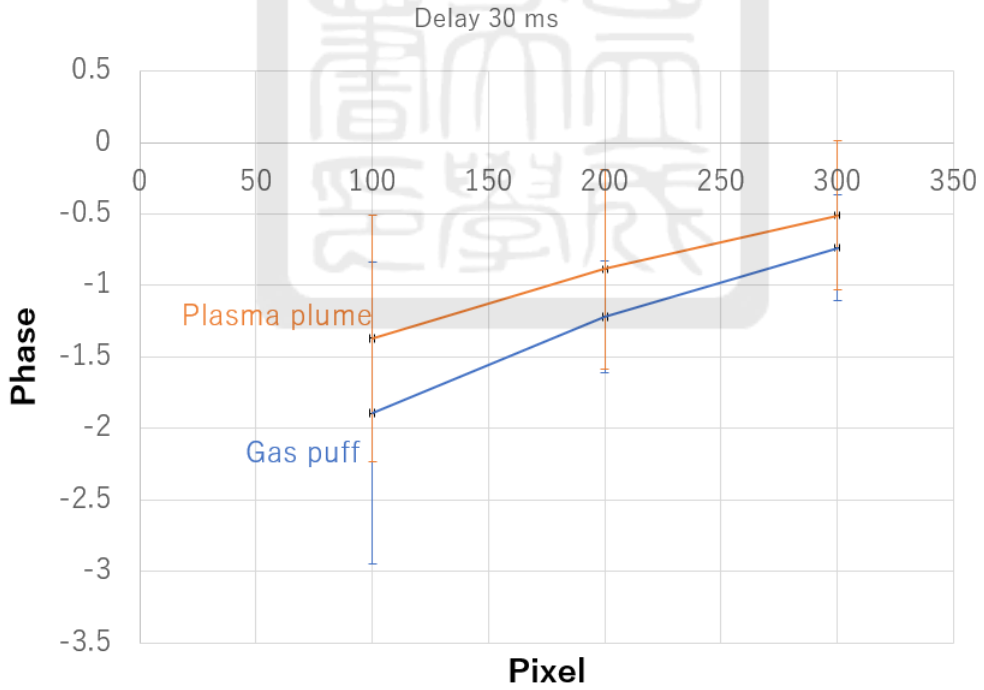

Figure 63: Comparison of phases between the Gas puff and the plasma plume of 30 ms.

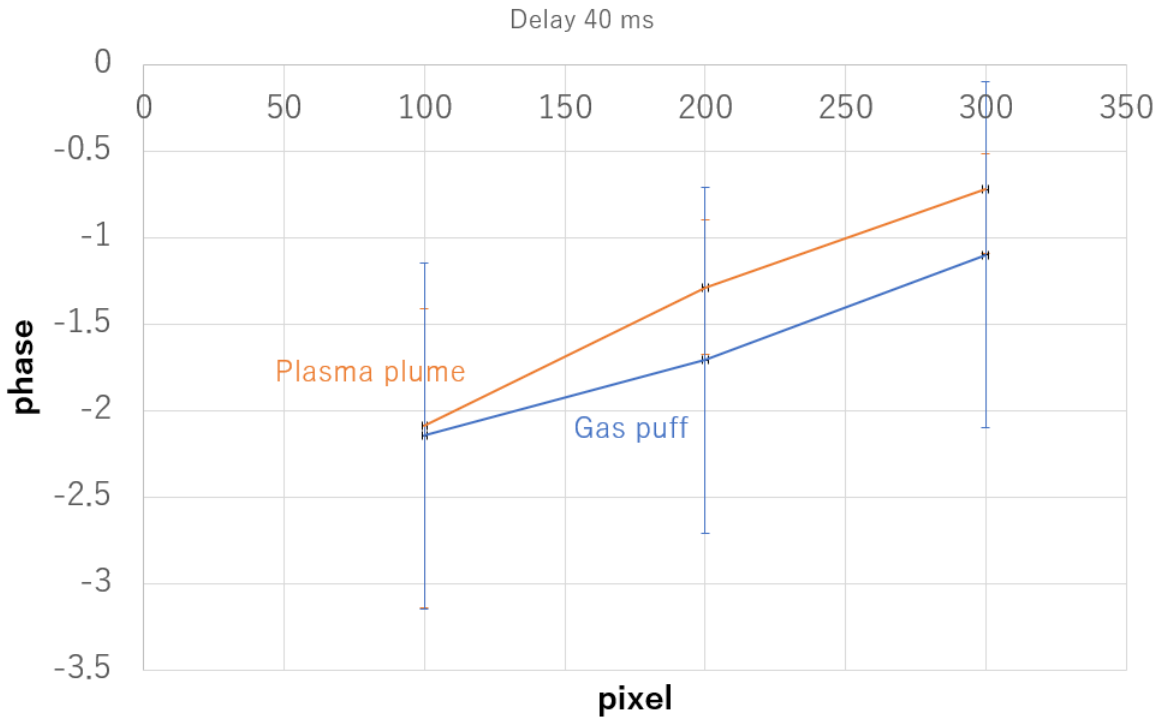

Figure 64: Comparison of phases between the Gas puff and the plasma plume of 40 ms.

5.6 Opening angle analysis

We would like to obtain the opening angle of the gas puff/plasma plume. It is obtained by finding the Full width half maximum (FWHM) of the fitting functions in section 5.4 final as a function of y' position in Fig. 56. The position for the average of rows 50~150 is 100 pixels. Similarly, the position is at 200 and 300 pixels for the average of rows 150~250 and 250~350, respectively. Figure 65 is the condition of 20 ms as an example. We then fit these values with straight lines. After obtaining the slopes of the fitted lines, slope is used to determine the opening angle $\theta = 2tan^{-1}(\frac{m}{2})$.

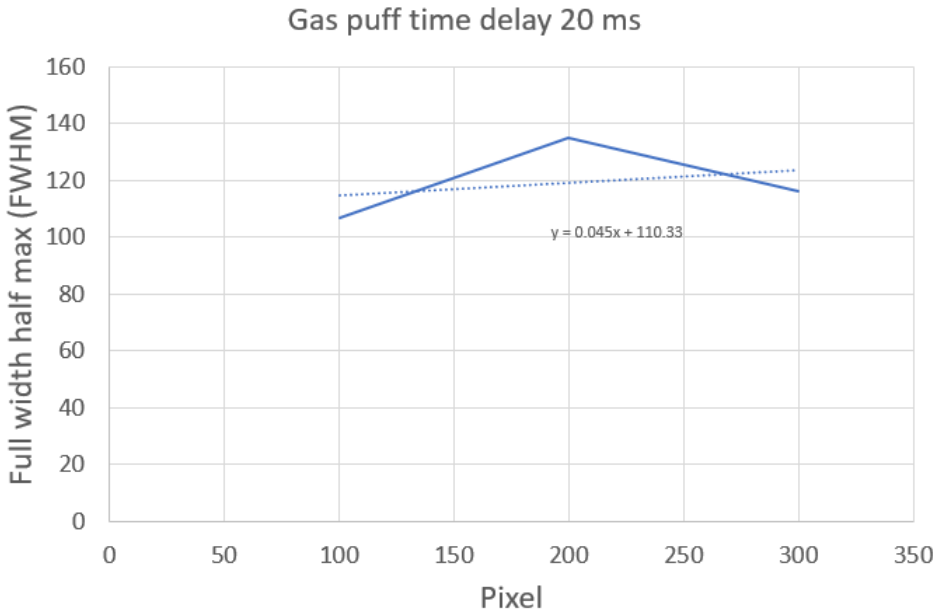

Figure 65: Data analyze of the opening angle

The Table 6 or gas puff and Table and 7 for plasma plume are the summaries of slopes from all experiments. Data of Table 6 and Table 7 are plotted in Fig. 65 - 70. By calculating the averaged slope and take the arctangent of each dataset, we can determine the averaged opening angles. The Table 8 shows the calculated opening angles.

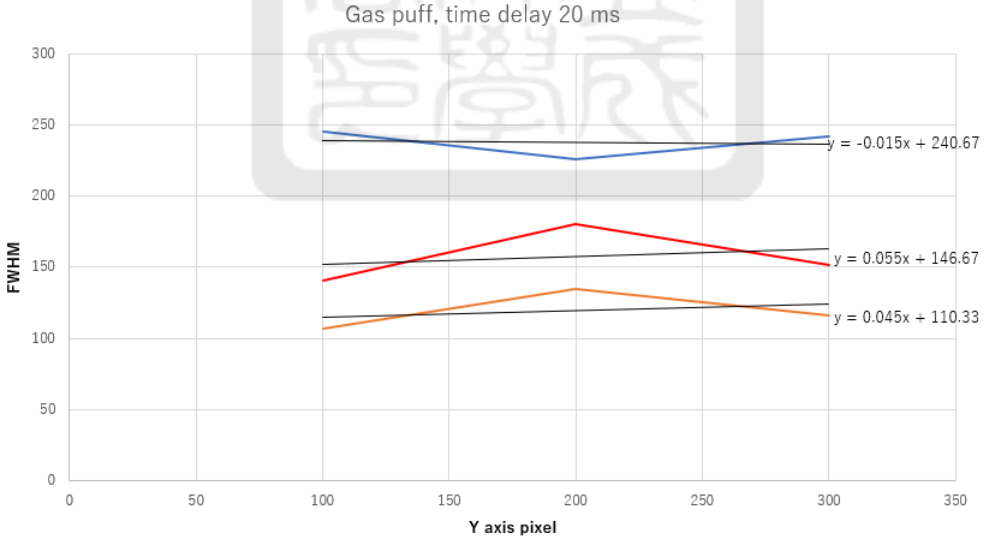

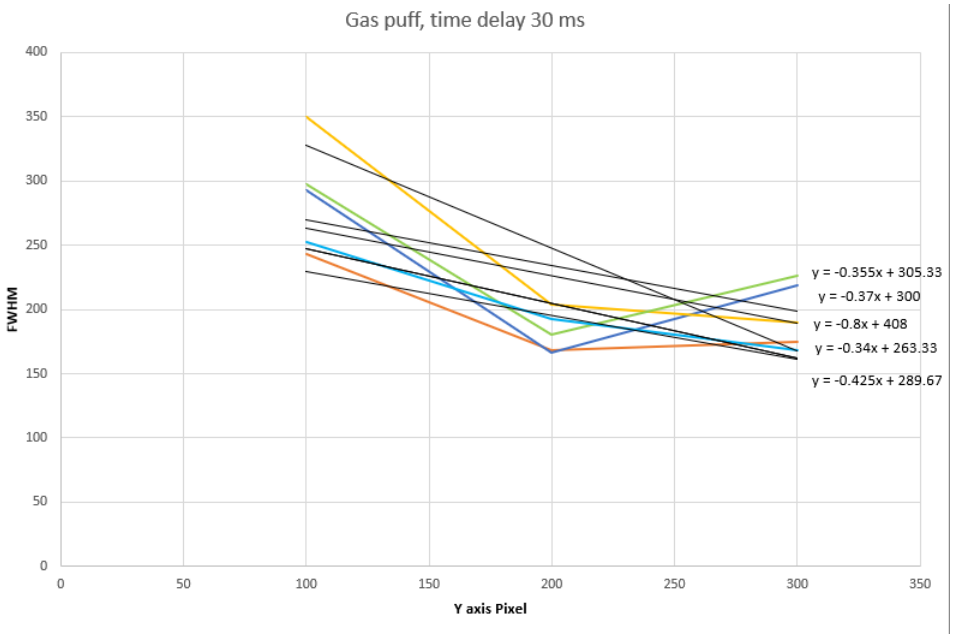

Figure 66: Use slope to calculate the opening angle-2

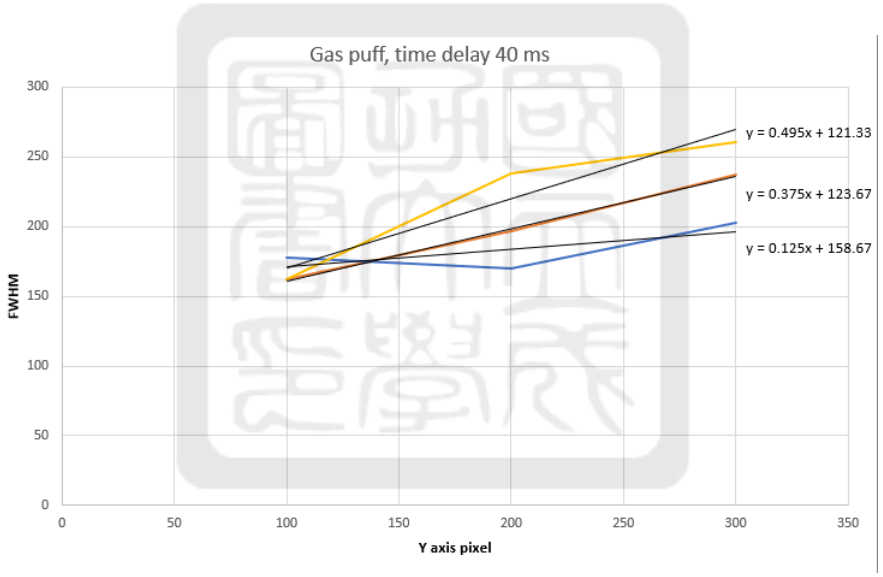

Figure 67: Use slope to calculate the opening angle-3

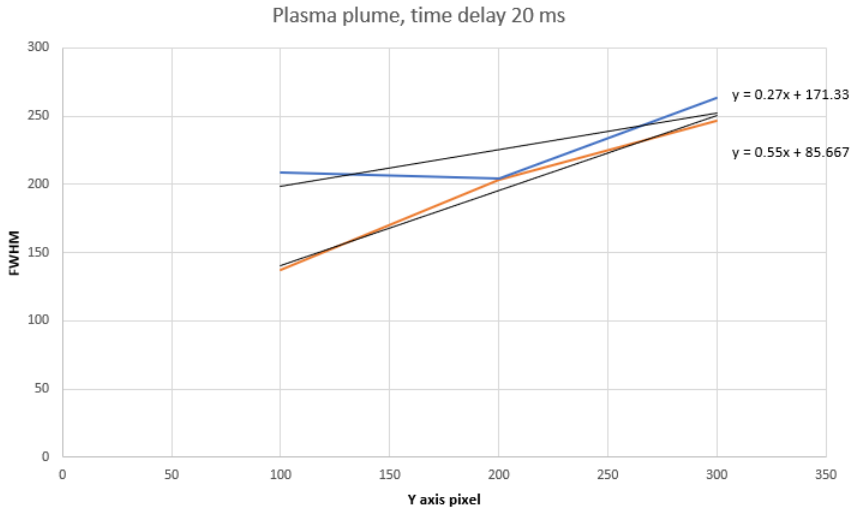

Figure 68: Use slope to calculate the opening angle-4

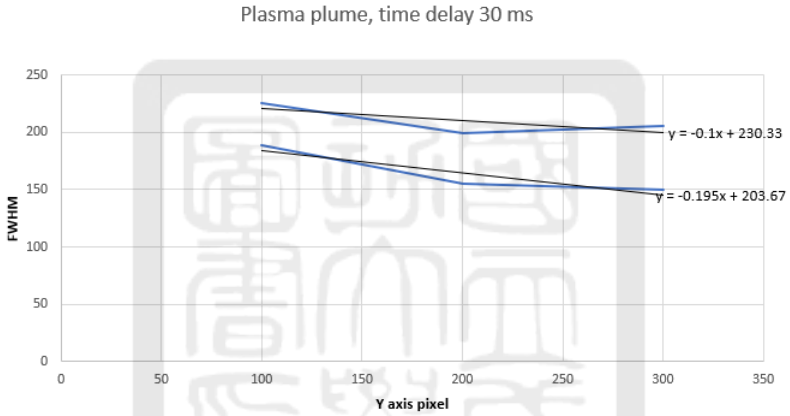

Figure 69: Use slope to calculate the opening angle-5

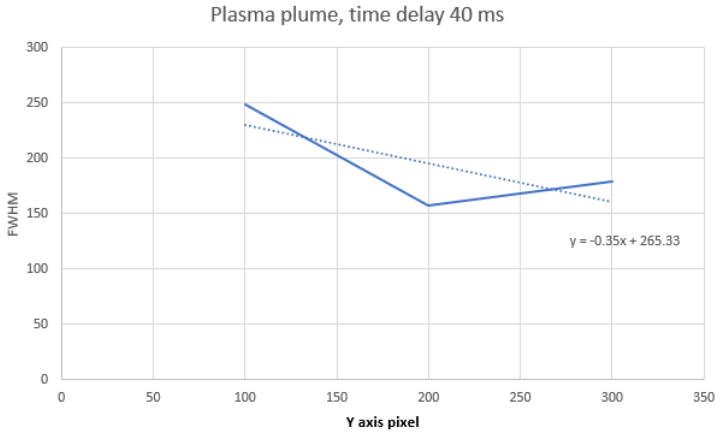

Figure 70: Use slope to calculate the opening angle-6

Table 6: Slope of the FWHM versus y position of the gas puff

	gas puff delay 20 ms	gas puff delay 30 ms	gas puff delay 40 ms
Slope record	-0.015	-0.37	0.495
	0.055	-0.8	0.375
	-0.015	-0.355	0.125
	0.045	-0.425	
		-0.34	
Average	0.02	-0.46	-0.33
standard deviation	0.04	0.20	0.19

Table 7: Slope of the FWHM versus y position of the plasma plume

	gas puff delay 20 ms	gas puff delay 30 ms	gas puff delay 40 ms
Slope record	0.27	-0.1	-0.35
	0.55	-0.195	
		-0.195	
Average	0.41	-0.14	-0.35
standard deviation	0.2	0.07	

Table 8: The no high voltage average slope to calculate the opening angle

		Delay 20 ms	Delay 30 ms	Delay 40 ms
Gas puff	average slope	0.02±0.04	-0.46±0.19	0.33±0.19
	Degree	1.0±2.1	-25.8±10.5	18.8±10.5
Plasma plume	average slope	0.41±0.2	-0.15±0.07	-0.35
	Degree	23.2±10.8	-8.43±3.8	-19.9

6 Future works

We already generated the plasma plume. More measurenents are needed to characterize the plasma plume. For example, we need to know how the plasma density charges with the reservoir pressure. The discharge current ended within 100 us but we can only observe the plasma plume after 20 ms. We need to verify what we see as the future work. We also need to redesign the the gas-puff arcing system so that the current can last longer. Most importantly, we need to know the propagating speed of the plasma plume so that we know how to integrate the plasma plume with the theta pinchl. Finally, we will pinch the plasma plume using the theta pinch for generate the EUV light. We may need to redesign the ICDN and the develop the new Helmholtz coil if necessary.

7 Summary

I developed two systems, namely the gas-puff system and the ionized convergent-divergent nozzle (ICDN) system for our EUV light source.

In the gas-puff system, we conducted experiments to test the functionality of the pulse-valve controller and statistically analyzed the action time of the pulse valve. To observe the gas-puff phenomenon, we used different gas tubes, background pressures, and pulse valves with varying inner diameters. Notably, we couldn't see the gas puff in experiments with a 0.1 mm inner diameter pulse valve, while a gas puff was visible in experiments with a 1.0 mm inner diameter pulse valve. This suggests that the gas flow rate plays a significant role in the visibility of the gas puff.

In the ICDN experiments, we applied high voltage to initiate an electrical discharge in argon gas, resulting in the generation of plasma. Although we saw the plasma plume using both the side-view camera and the interferometer, no strong correlations between the opening angle of the gas puff and that of the plasma plume. It is reasonable since the discharge current ended within 100 us but we can only observe the plasma plume after 20 ms. We need to verify what we see as the future work. We also need to redesign the gas-puff arcing system so that the current can last longer.

8 Reference

[1] https://www.gallagherseals.com/blog/semiconductor-manufacturing-process

[2] https://capst.ncku.edu.tw/PGS/index.php/soft-x-ray-euv-light-source/

[3]Development of the magnetic field in a theta pinch in the EUV light soure, Cheng-Han Du.

[4]https://capst.ncku.edu.tw/PGS/index.php/pulsed-power-generator/

[5]https://capst.ncku.edu.tw/PGS/index.php/pulsed-power-generator/

[6]https://capst.ncku.edu.tw/PGS/index.php/laser-probing/

[7]Paschen_Curve :https://zh.m.wikipedia.org/zh-tw/File:Paschen_Curves.PNG.

[8] M. Hipp, etc., Measurement 3, 55-66 (2004)

A Appendix

A.1 Pulse valve voice delay test

Analyze Gas pulse valve system 閥門時間測試

Duty cycle:50%

測試時間	開啟閥門時間點 (s)	關閉閥門時間點 (s)
1s	0.825	1.344
1s	0.995	1.513
1s	0.828	1.344
1s	0.507	1.025
2s	0.870	1.885
2s	0.5966	1.611
2s	0.947	1.962
2s	0.425	1.442
2s	0.509	1.526
5ms	0.4671	0.4761
5ms	0.4961	0.5091
5ms	0.9333	0.9493
5ms	0.6596	0.6712
10ms	0.7019	0.7148
10ms	1.0055	1.018
10ms	0.6384	0.6510
10ms	1.5316	1.5447
20ms	1.2463	1.2770
20ms	1.0923	1.1186
20ms	1.1025	1.1286
20ms	0.9718	1.0019
20ms	1.0261	1.0571
50ms	1.1654	1.2070
50ms	1.0267	1.0688
50ms	0.5963	0.6388
50ms	0.6915	0.7362
50ms	1.1783	1.2226

Figure 71: Pulse valve voice analyze-1

測試時間	開啟閥門時間點 (s)	關閉閥門時間點 (s)
100ms	1.0633	1.1311
100ms	1.0722	1.1402
100ms	1.2708	1.3411
100ms	1.2394	1.3107
200ms	1.1016	1.2225
200ms	0.9012	1.0211
200ms	1.0990	1.2146
200ms	1.0383	1.1581
200ms	1.1732	1.2915
500ms	0.9935	1.2616
500ms	1.0842	1.3504
500ms	1.0760	1.3420
500ms	1.1572	1.4262
500ms	1.0334	1.2987
測試時間	平均值 (s)	標準差 (s)
1s	5.18e-01	1.26e-0
2s	1.02e+0	1.23e-03
5ms	1.24e-02	2.92e-03
10ms	1.64e-02	8.15e-03
20ms	2.88e-02	2.43e-03
50ms	4.30e-02	1.38e-03
100ms	6.94e-02	1.50e-03
200ms	1.19e-01	2.07e-03
500ms	2.67e-01	1.56e-03

Figure 72: Pulse valve voice analyze-2

A.2 The gas puff schlieren image 0.1 mm outlet about the laser delay setting from 50.39 ms to 100.39 ms

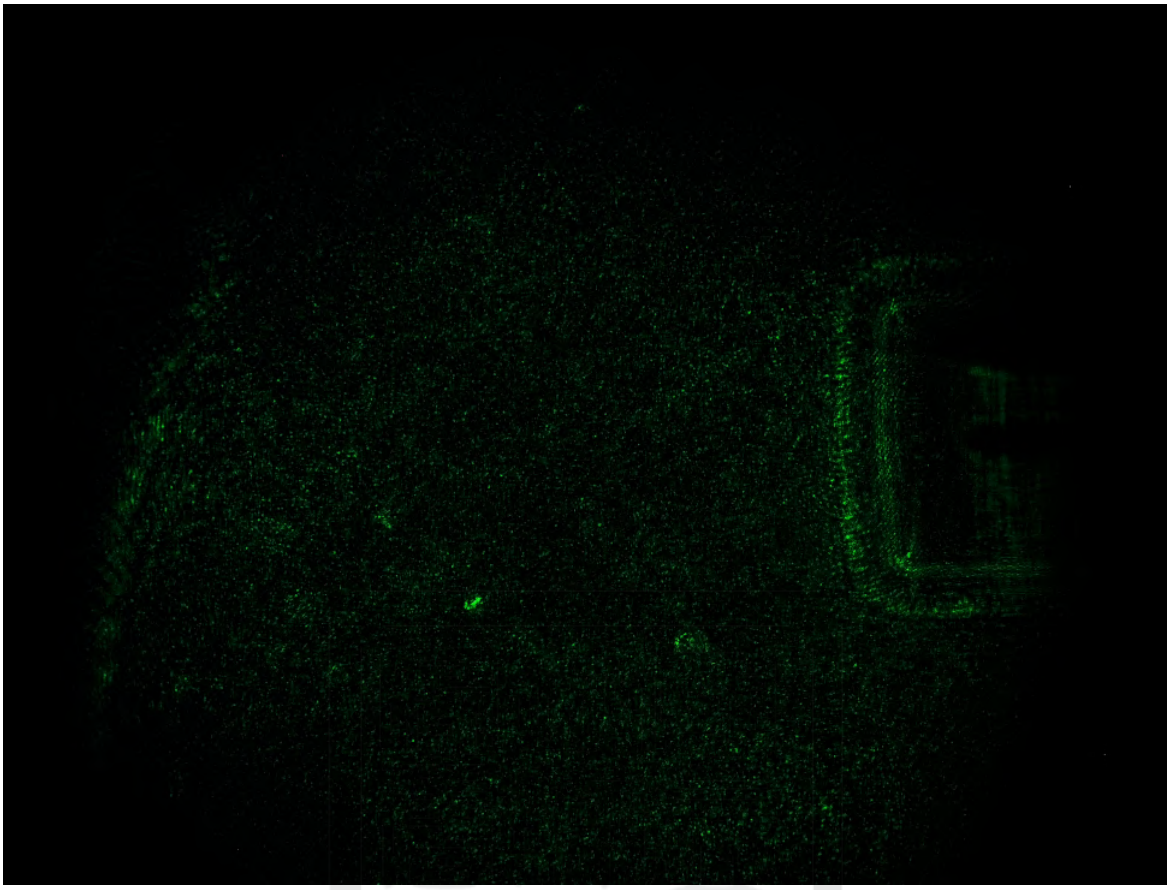

Figure 73: Setting at laser time dealy 50.39 ms schlieren image

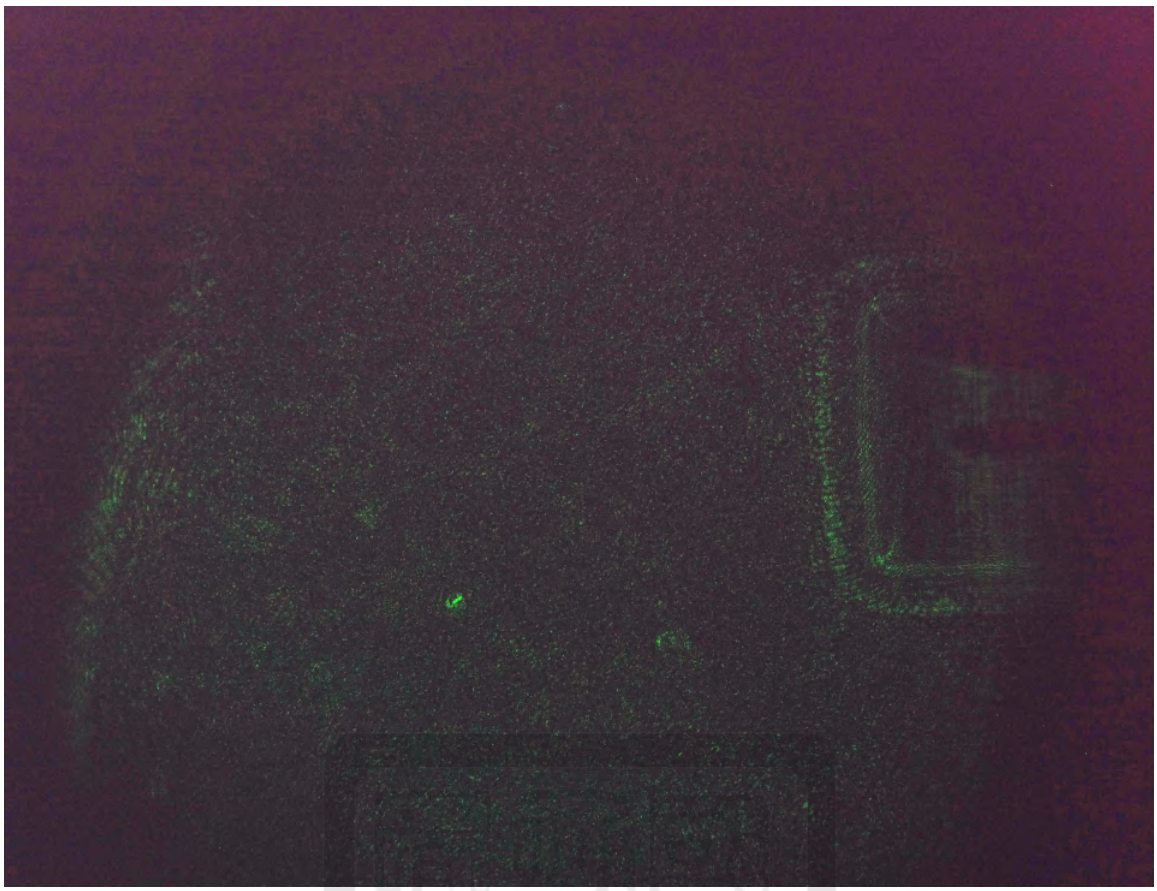

Figure 74: Setting at laser time dealy 55.39 ms schlieren image

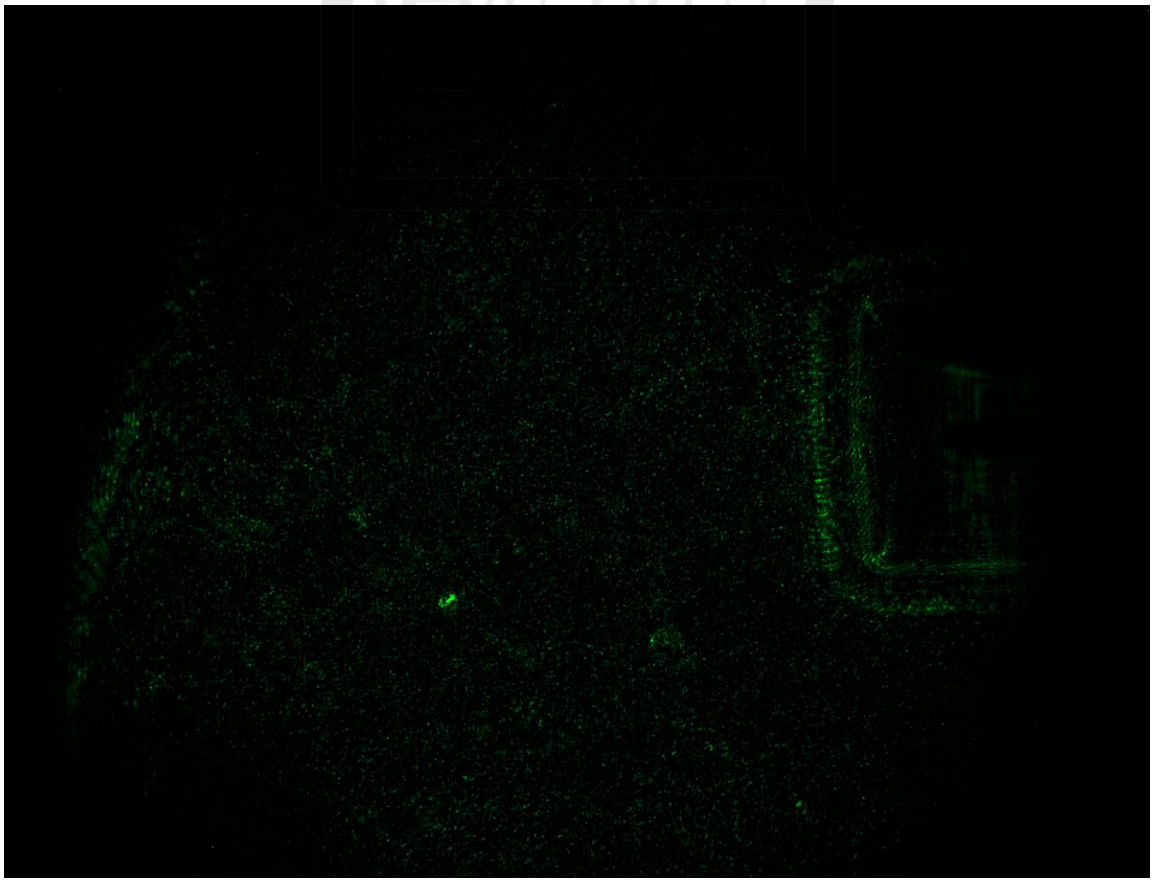

Figure 75: Setting at laser time dealy 60.39 ms schlieren image

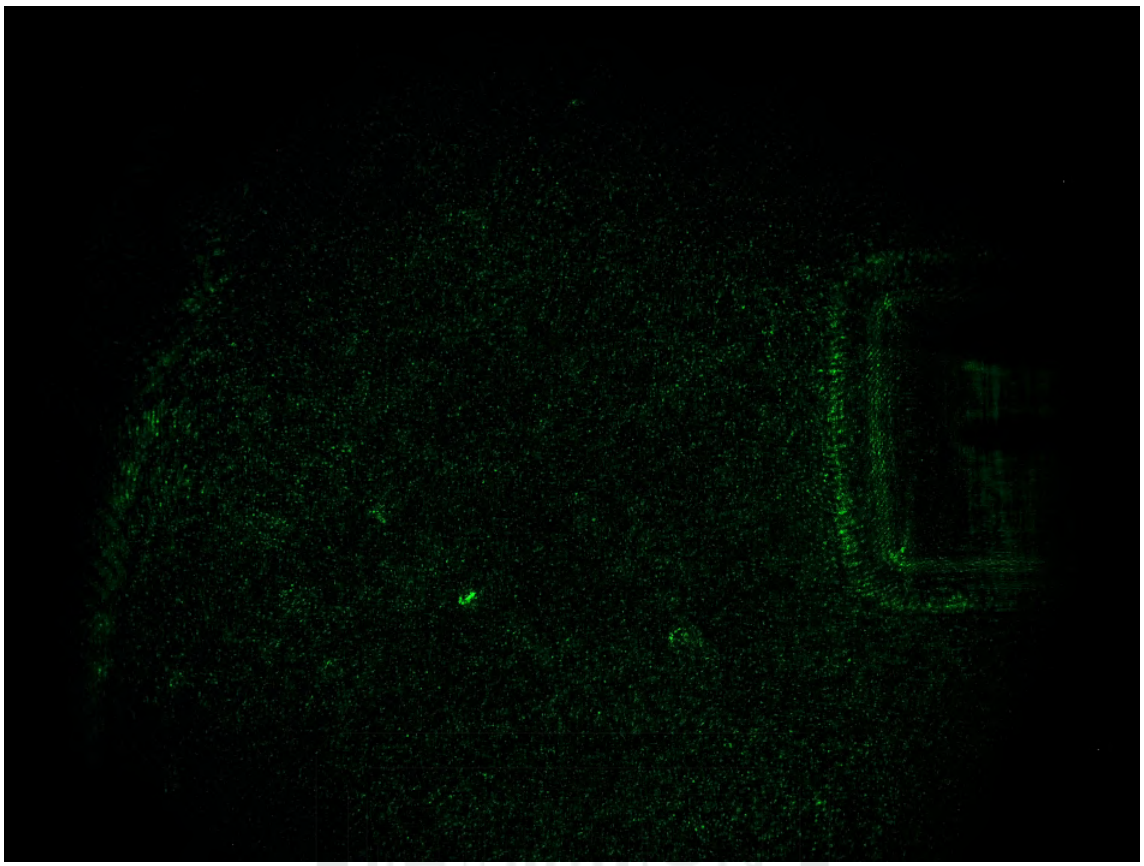

Figure 76: Setting at laser time dealy 70.39 ms schlieren image

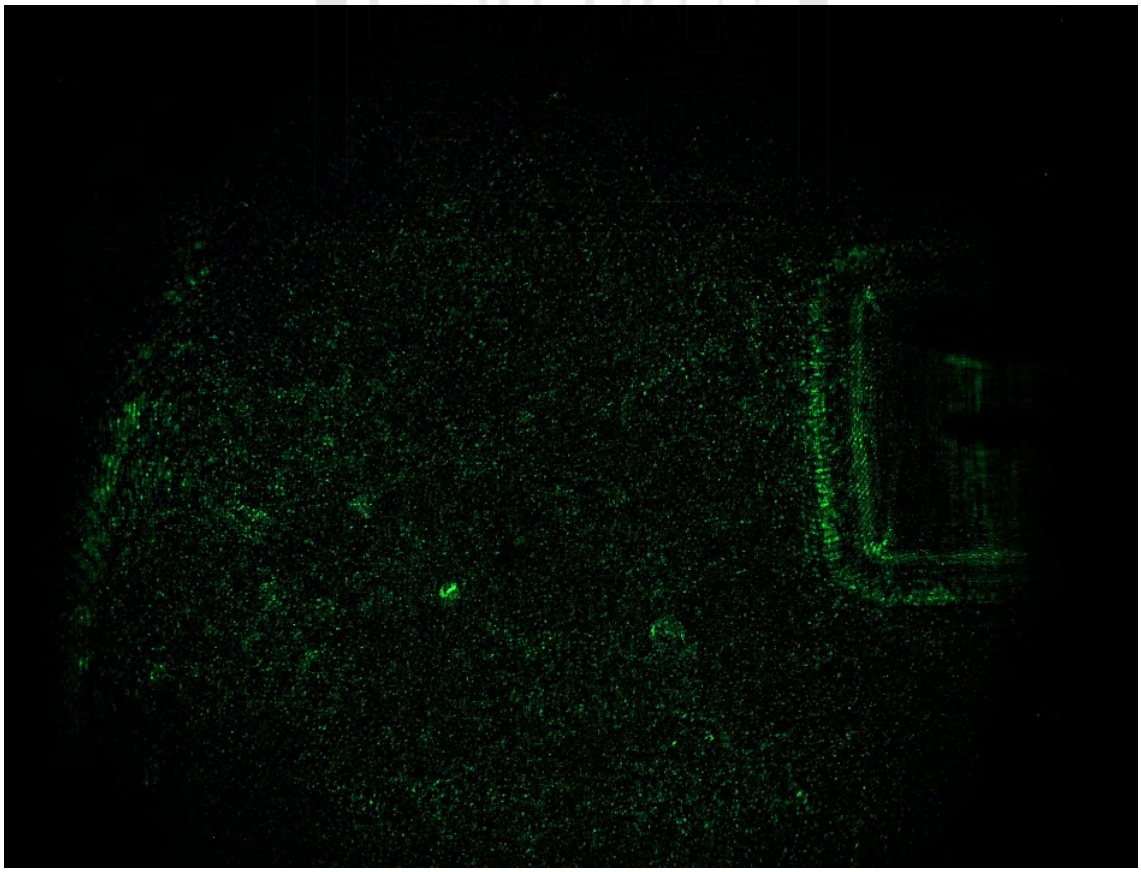

Figure 77: Setting at laser time dealy 80.39 ms schlieren image

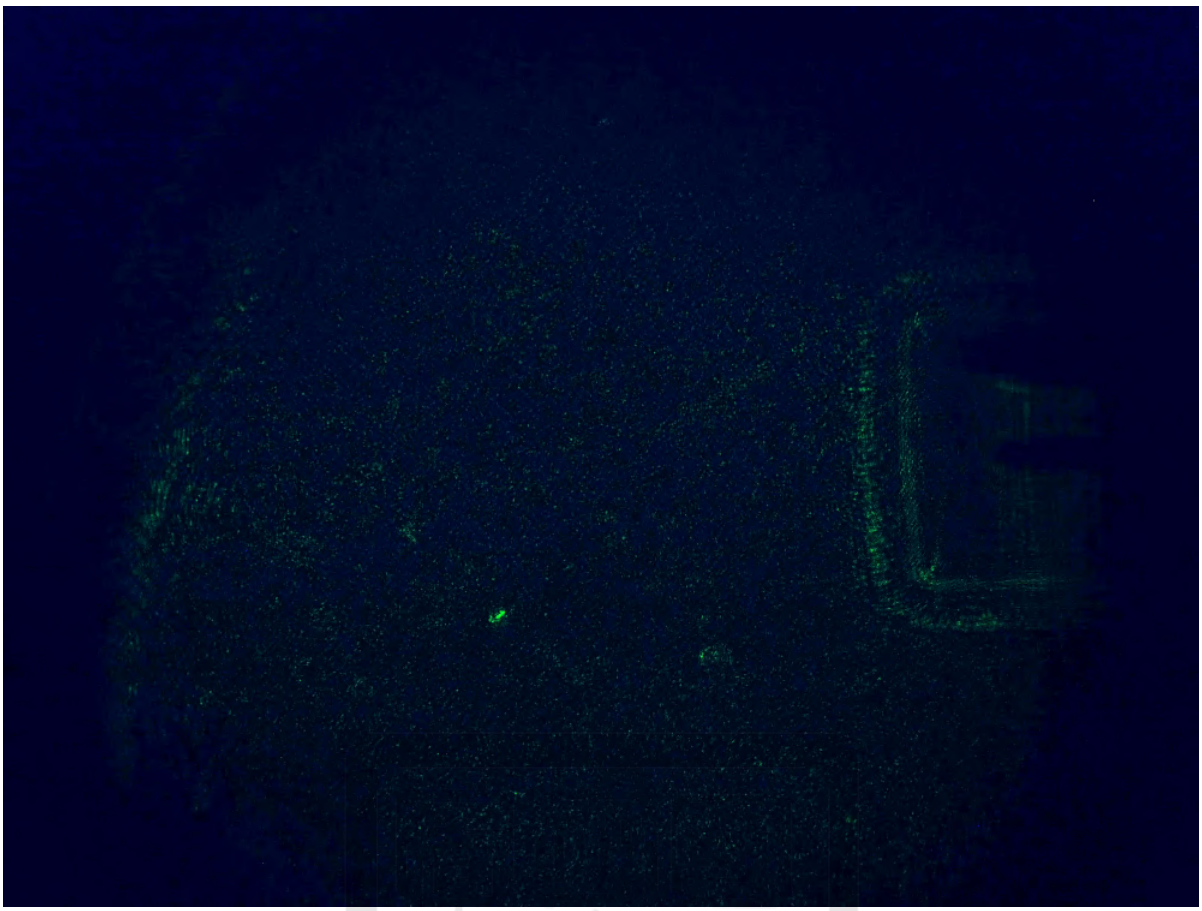

Figure 78: Setting at laser time dealy 90.39 ms schlieren image

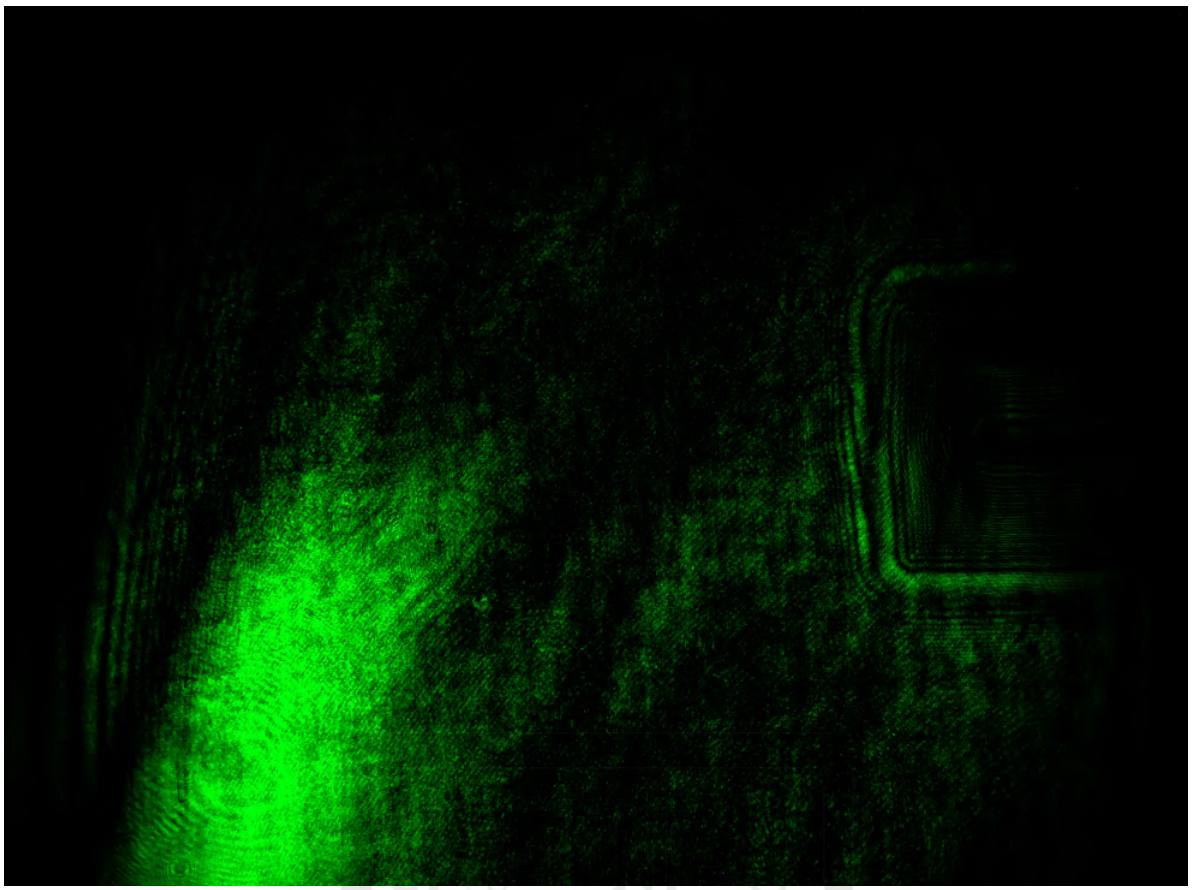

Figure 79: Setting at laser time dealy 100.39 ms schlieren image

A.3 ICDN system design

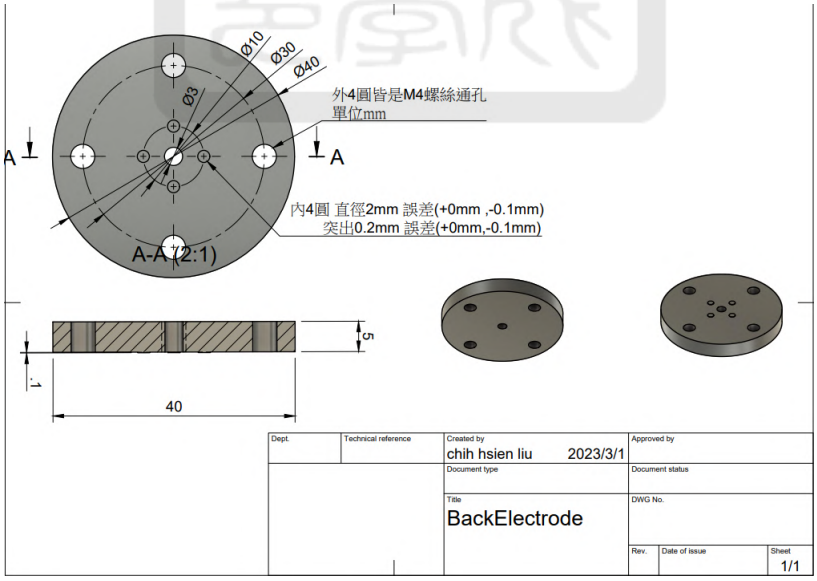

Figure 80: Back electrode design

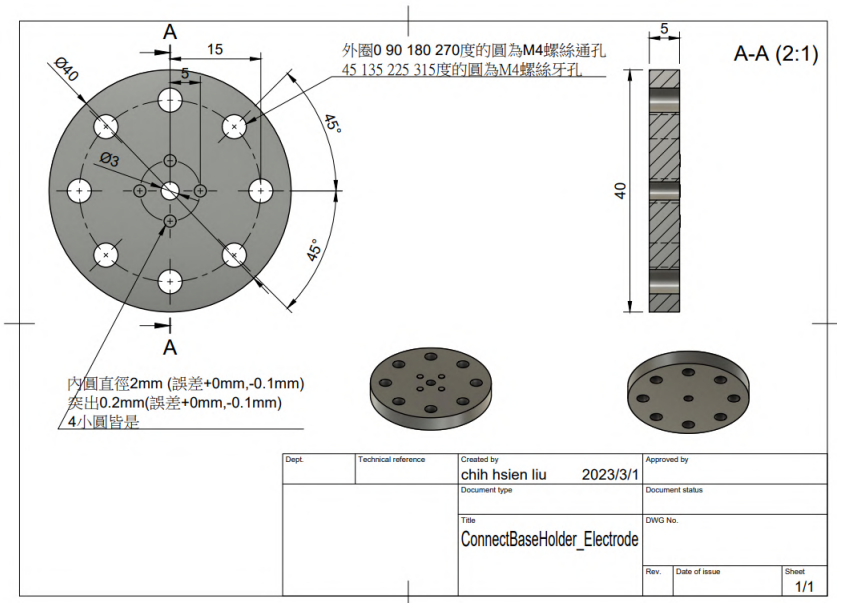

Figure 81: Connect base holder.electrode (Brass) design

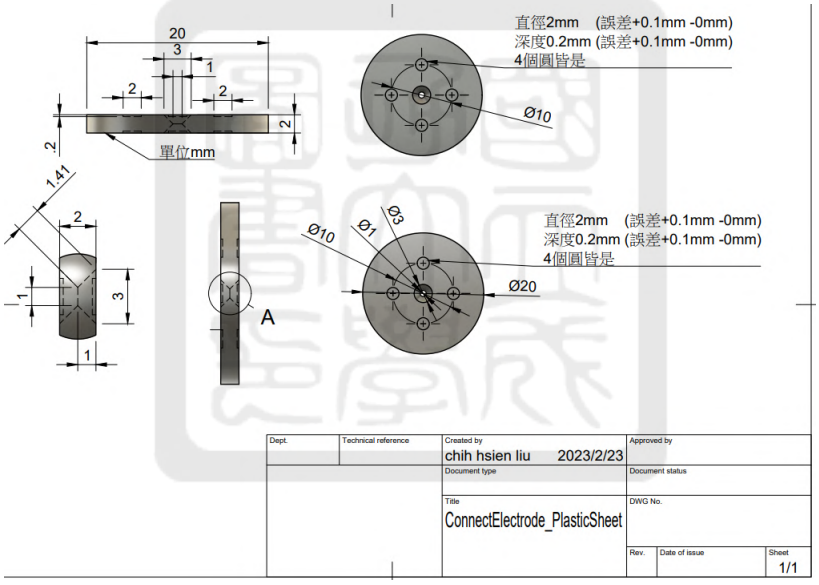

Figure 82: Connect electrode plastic sheet

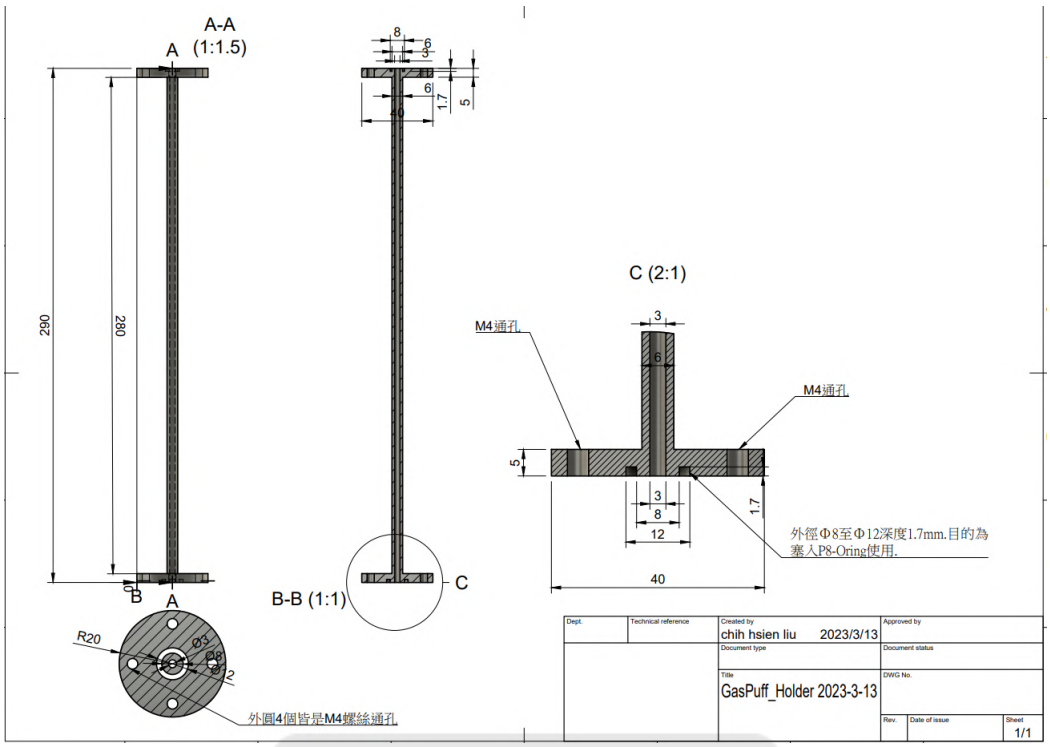

Figure 83: Electrode gas tube assemble design

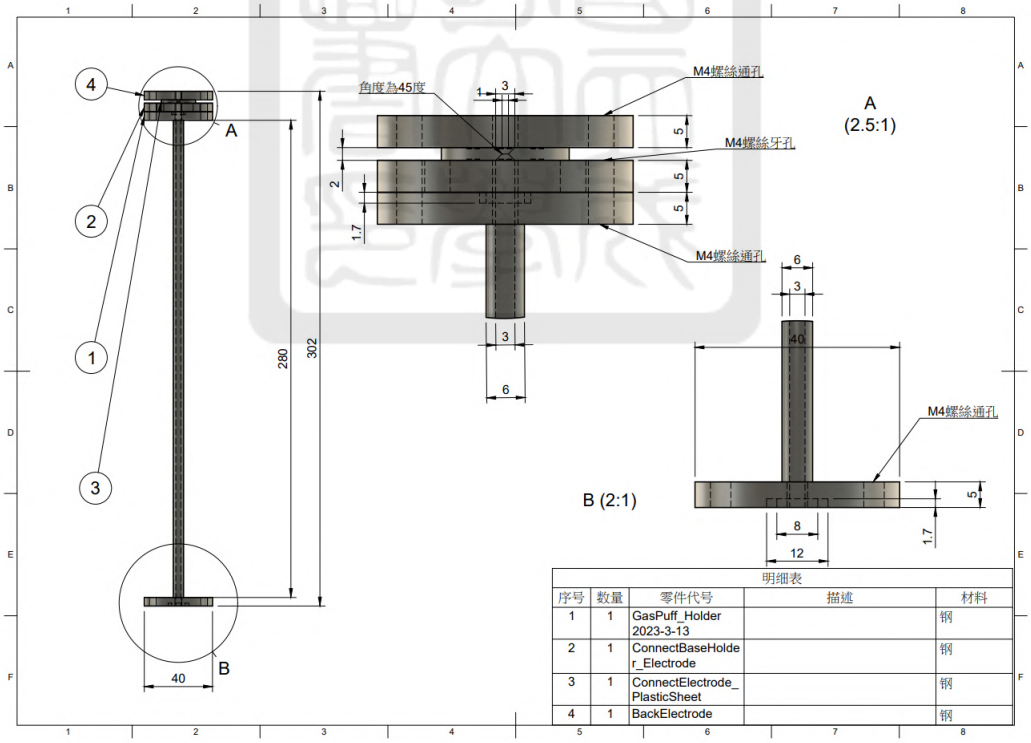

Figure 84: Electrode gas tube assemble design

A.4 super-Gaussing function fitting

A.4.1 High voltage(HV)-laser delay time 20 ms-1 (first data)

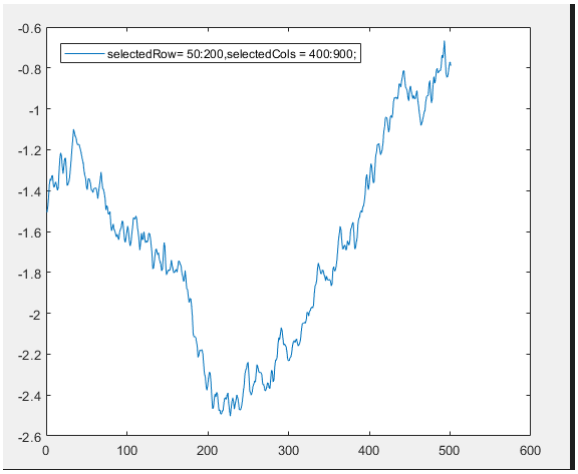

Figure 85: X軸:pixel Y軸:phase. Plasma plume, 20ms delay, average of cols 400~900, average of row 50~200.

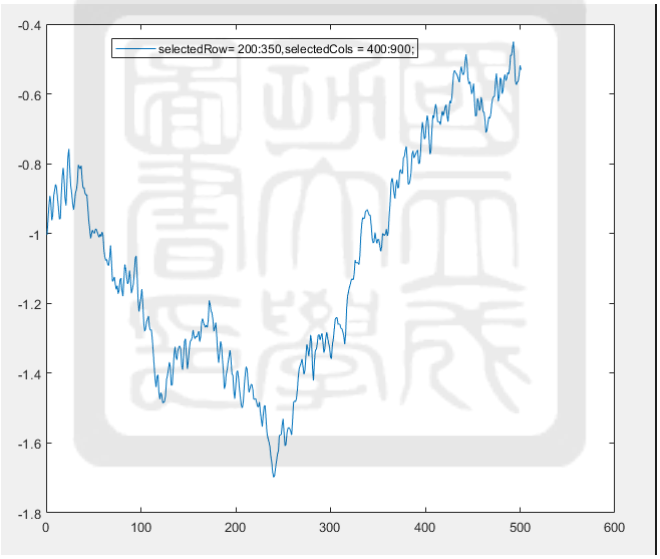

Figure 86: X軸:pixel Y軸:phase.Plasma plume, 20ms delay, average of cols 400~900, average of row 200~350

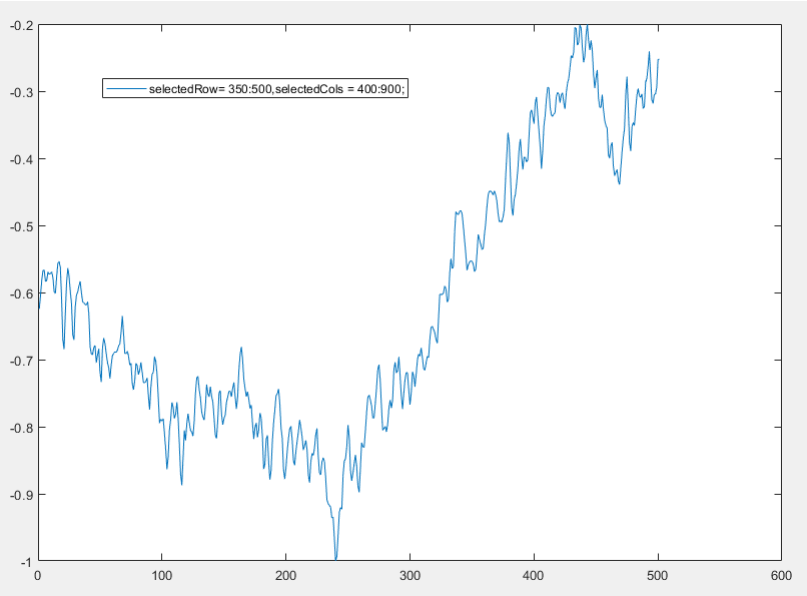

Figure 87: X軸:pixel Y軸:phase. Plasma plume, 20ms delay, average of cols 400~900, average of row 350~500

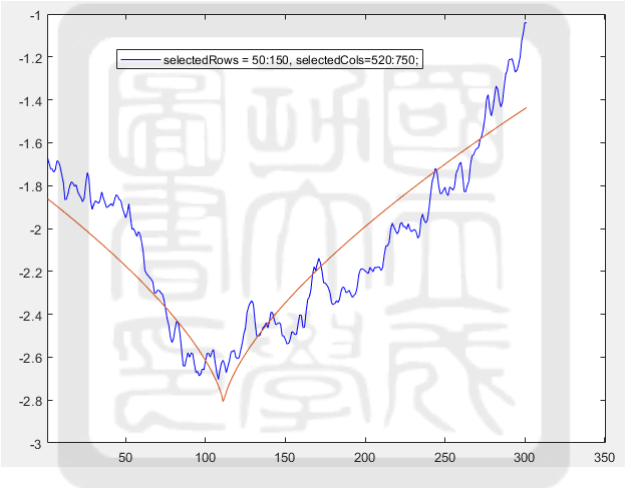

Figure 88: X軸:pixel Y軸:phase Plasma plume, 20ms delay, average of cols 520~750, average of row 50~150

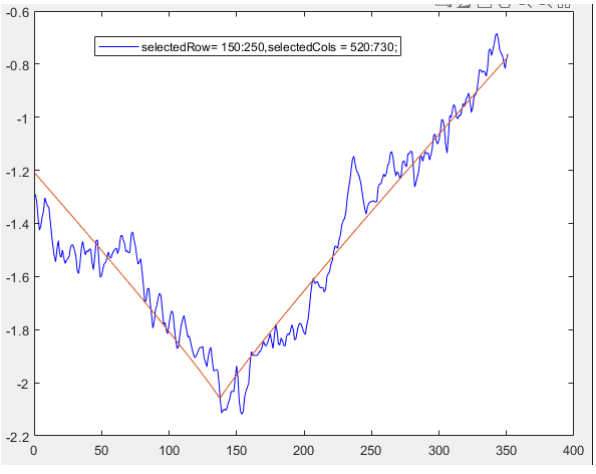

Figure 89: X軸:pixel Y軸:phase. Plasma plume, 20ms delay, average of cols 520~730, average of row 150~250

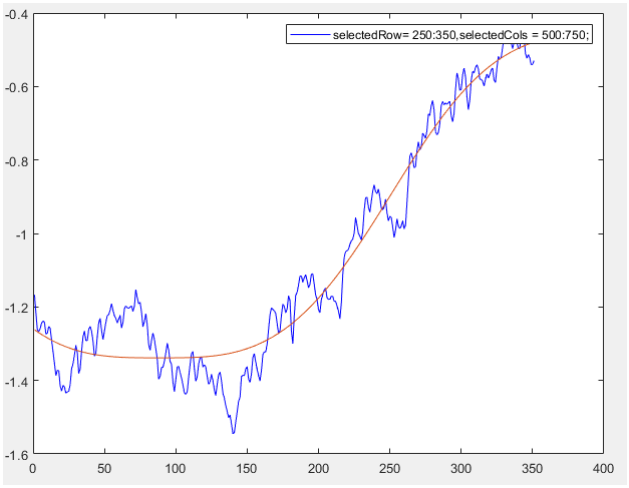

Figure 90: X軸:pixel Y軸:phase. Plasma plume, 20ms delay, average of cols 500~750, average of row 250~350

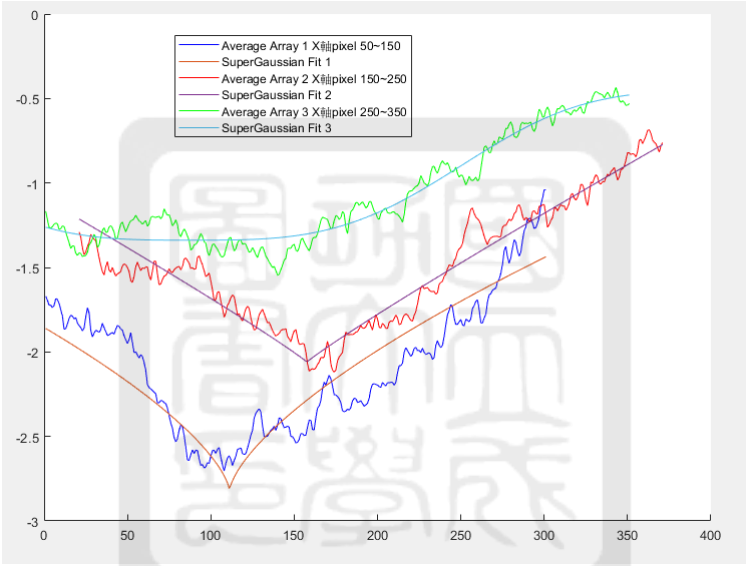

Figure 91: X軸:pixel Y軸:phase. 合併selction three function blue line (50~150), red line (150~250), green line 250~350

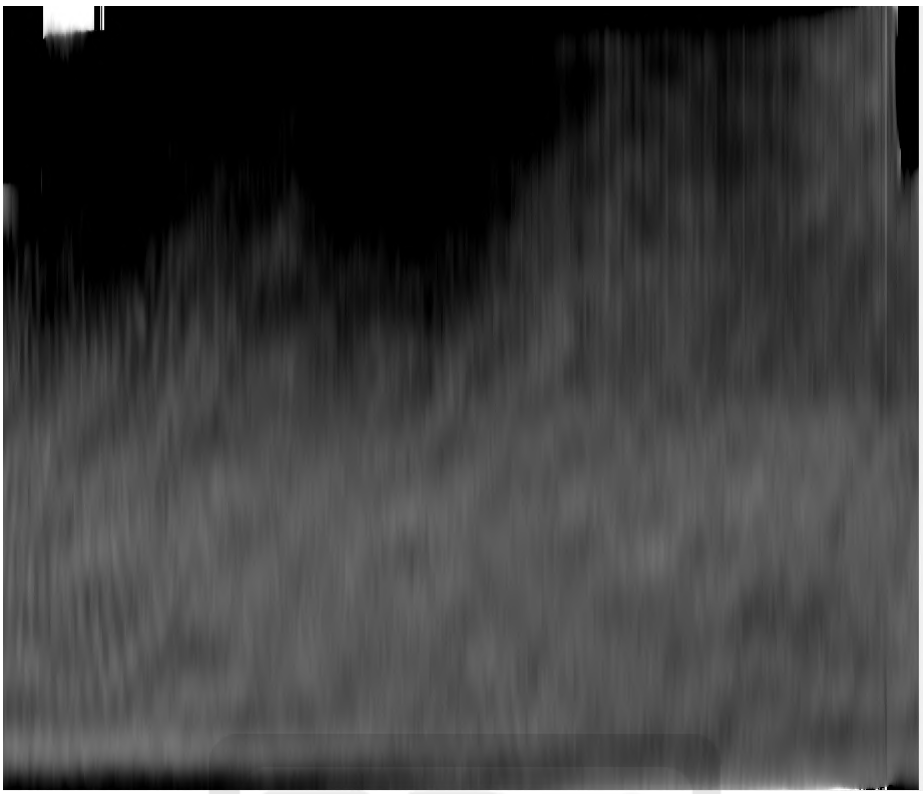

Figure 92: Rotate 90 degree image

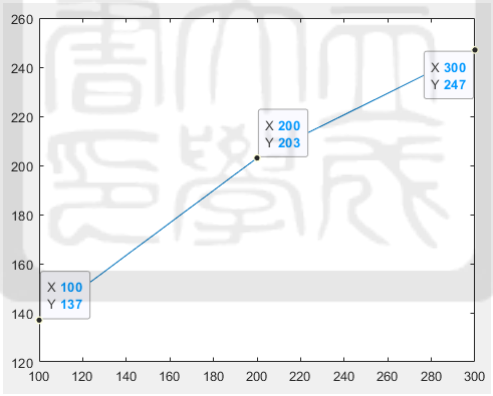

Figure 93: FWHM about selction 50~150 (left), 150~250(middle), 250~350 (right).

A.4.2 HV-20ms-2

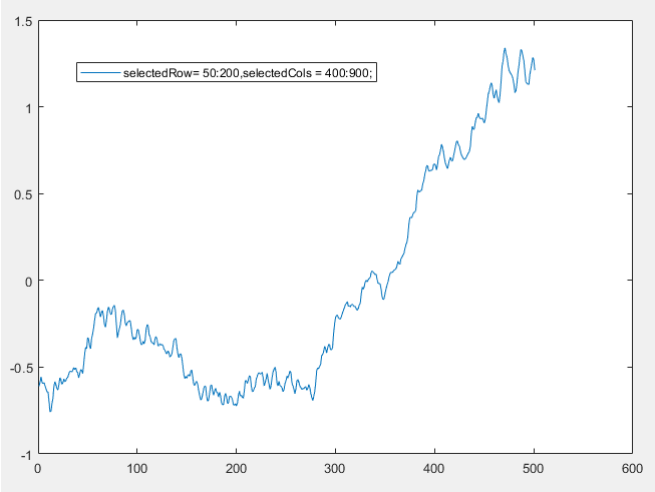

Figure 94: X軸:pixel Y軸:phase. Plasma plume, 20ms delay, average of cols 400~900, average of row 50~200

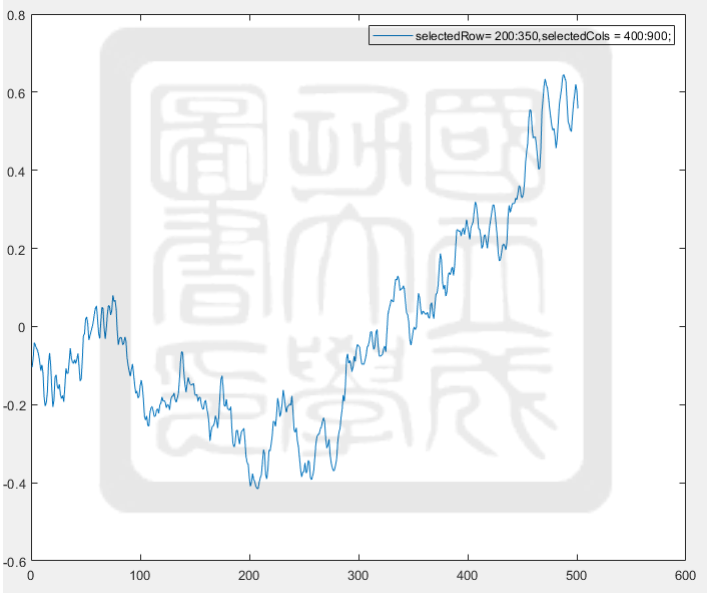

Figure 95: X軸:pixel Y軸:phase. Plasma plume, 20ms delay, average of cols 400~900, average of row 200~350

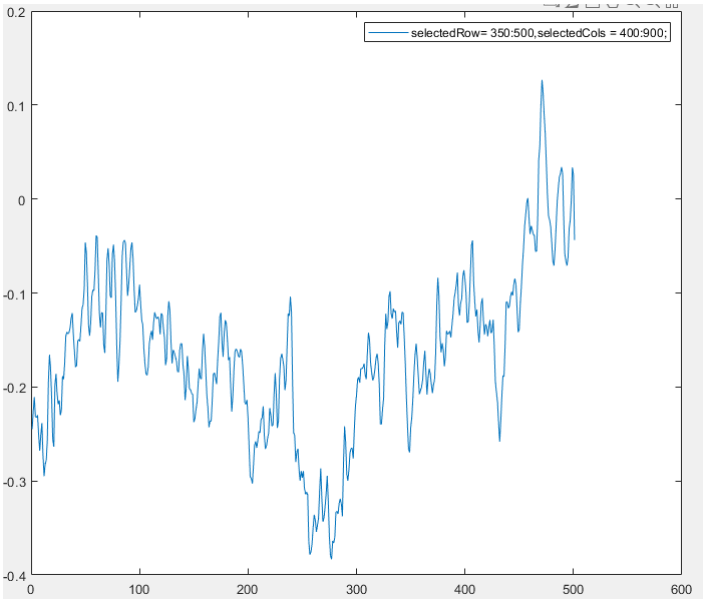

Figure 96: X軸:pixel Y軸:phase. Plasma plume, 20ms delay, average of cols 400~900, average of row 350~500

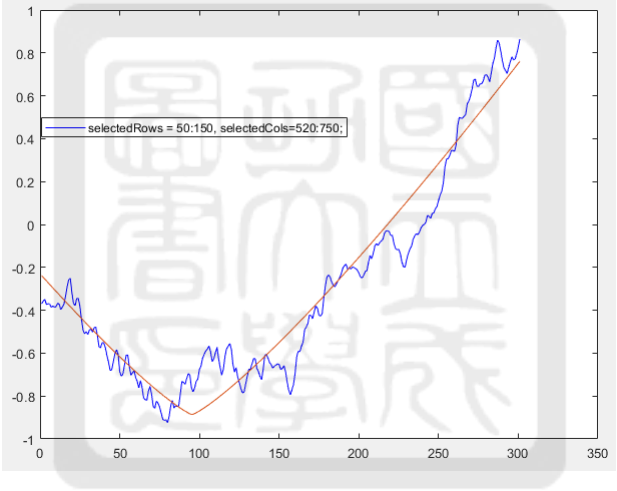

Figure 97: X軸:pixel Y軸:phase. Plasma plume, 20ms delay, average of cols 520~750, average of row 50~150

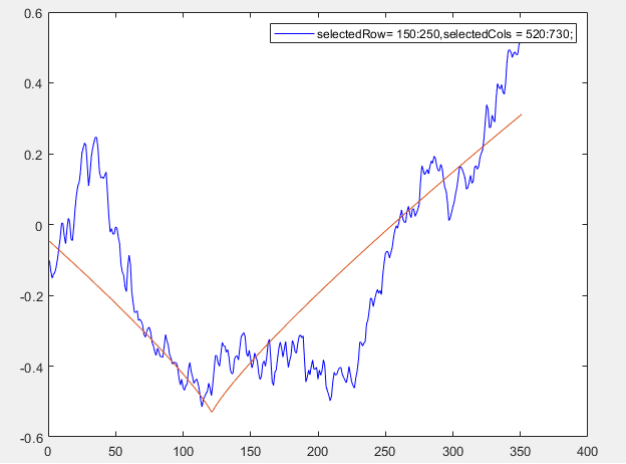

Figure 98: X軸:pixel Y軸:phase. Plasma plume, 20ms delay, average of cols 520~750, average of row 150~730

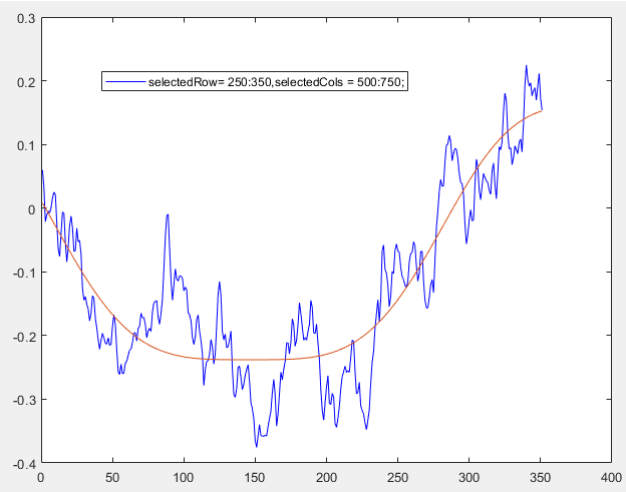

Figure 99: X軸:pixel Y軸:phase. Plasma plume, 20ms delay, average of cols 500~750, average of row 250~350

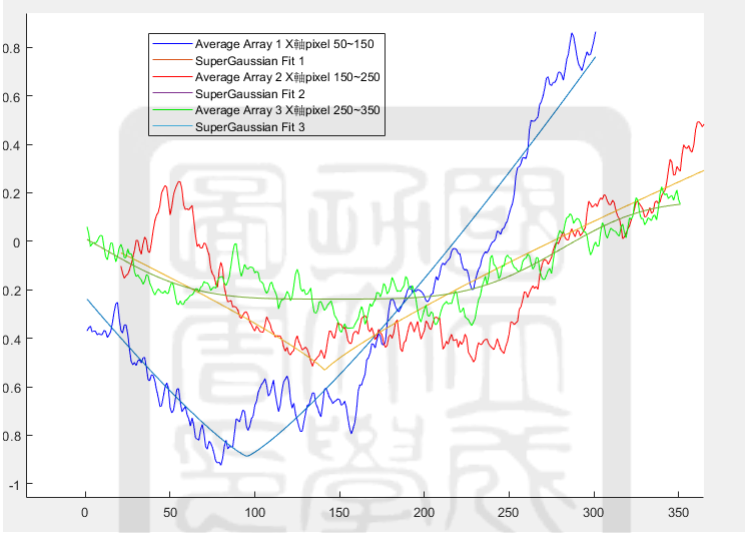

Figure 100: X軸:pixel Y軸:phase. 合併selction three function blue line (50~150), red line (150~250), green line 250~350

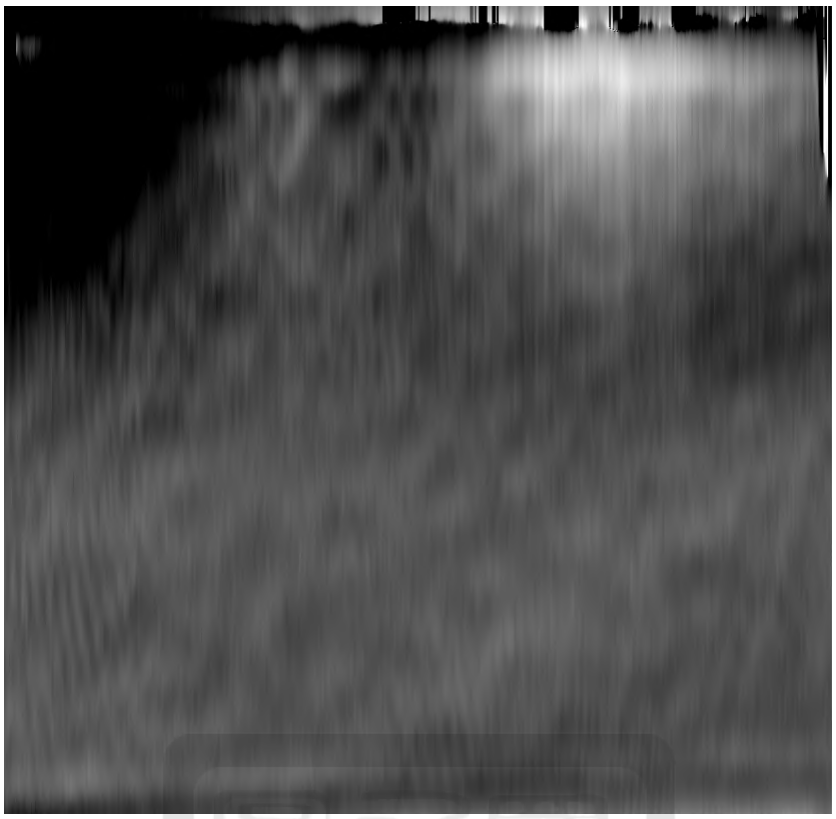

Figure 101: rotate 90 degree image

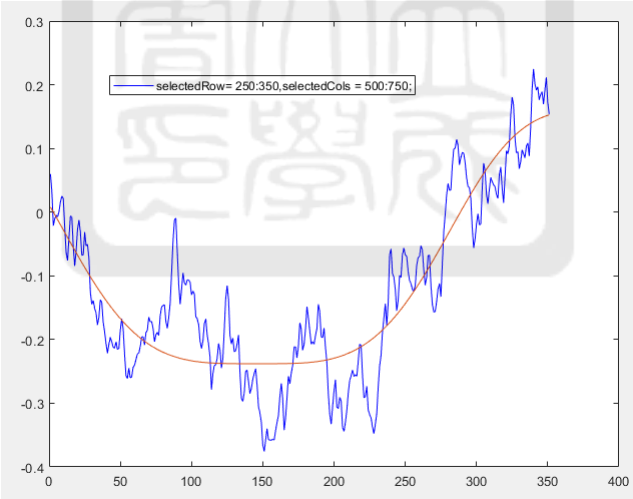

Figure 102: X軸:pixel Y軸:phase Plasma plume, 20ms delay, average of cols 500~750, average of row 250~350

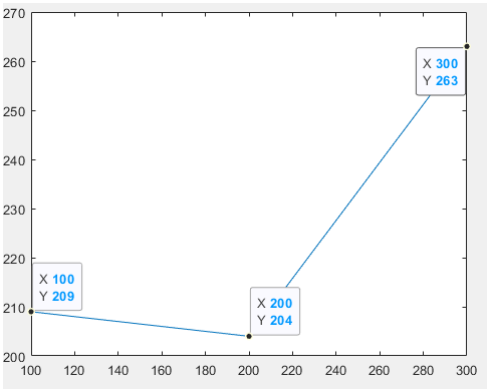

Figure 103: FWHM about selction 50~150 (left), 150~250(middle), 250~350 (right).

A.4.3 HV-30ms-1

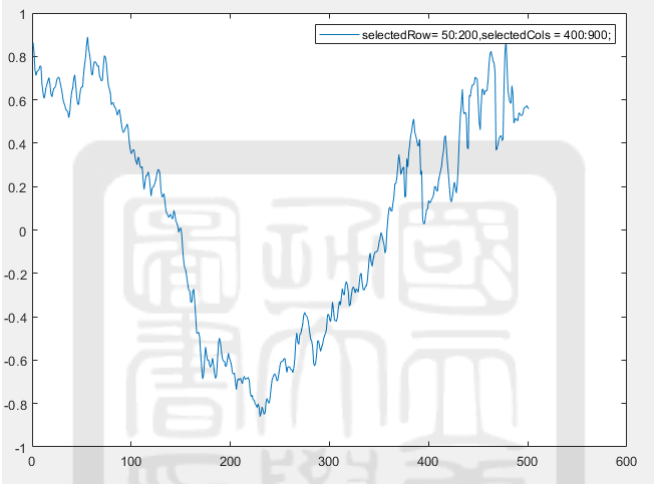

Figure 104: X軸:pixel Y軸:phase. Plasma plume, 30ms delay, average of cols 400~900, average of row 50~200

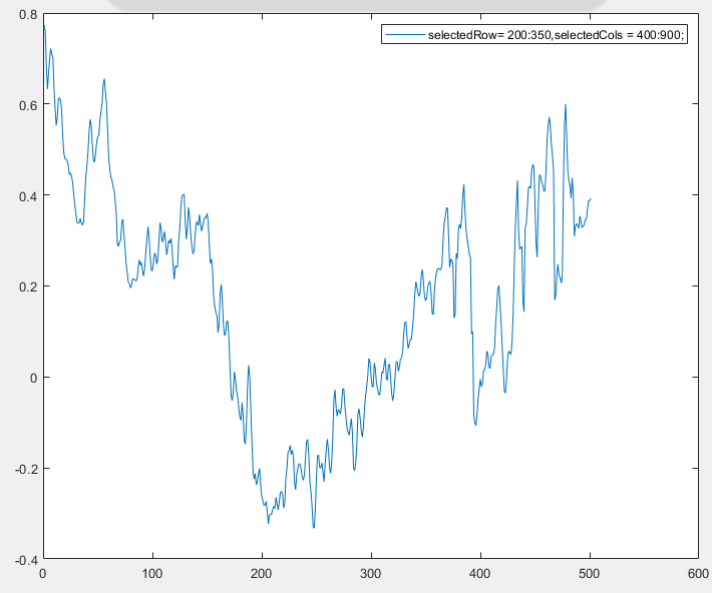

Figure 105: X軸:pixel Y軸:phase. Plasma plume, 30ms delay, average of cols 400~900, average of row 200~350

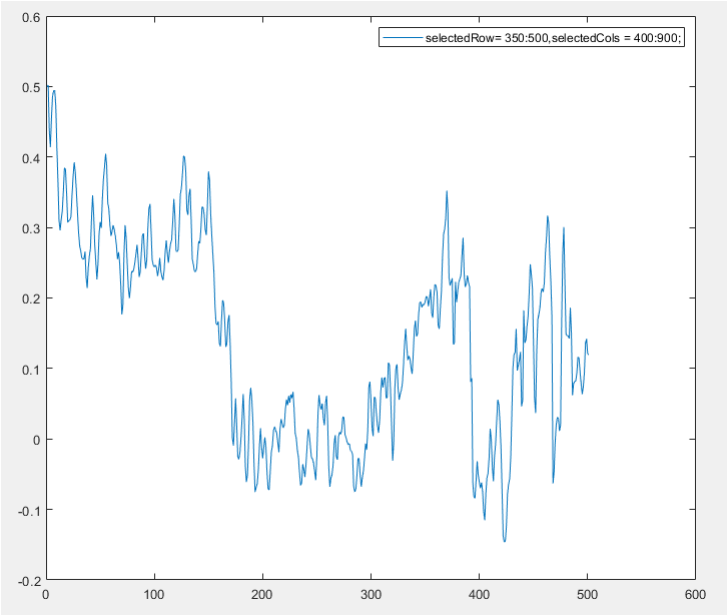

Figure 106: X軸:pixel Y軸:phase. Plasma plume, 30ms delay, average of cols 400~900, average of row 350 ~500

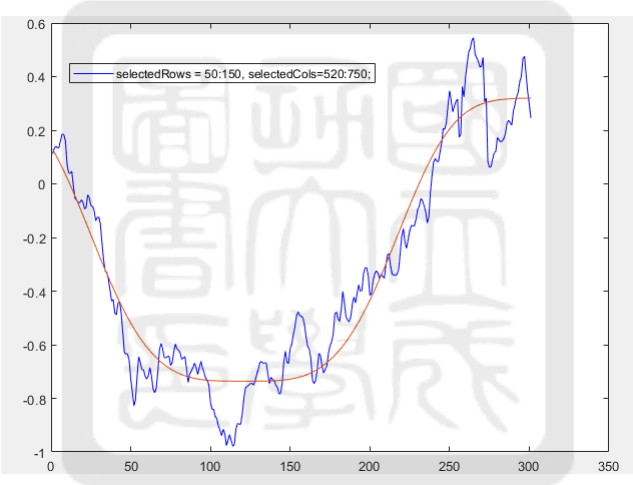

Figure 107: X軸:pixel Y軸:phase. Plasma plume, 30ms delay, average of cols 520~750, average of row 50~150

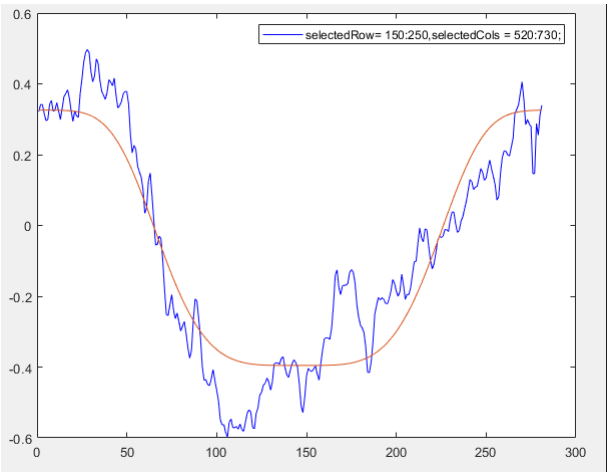

Figure 108: X軸:pixel Y軸:phase. Plasma plume, 30ms delay, average of cols 520~750, average of row 150~250

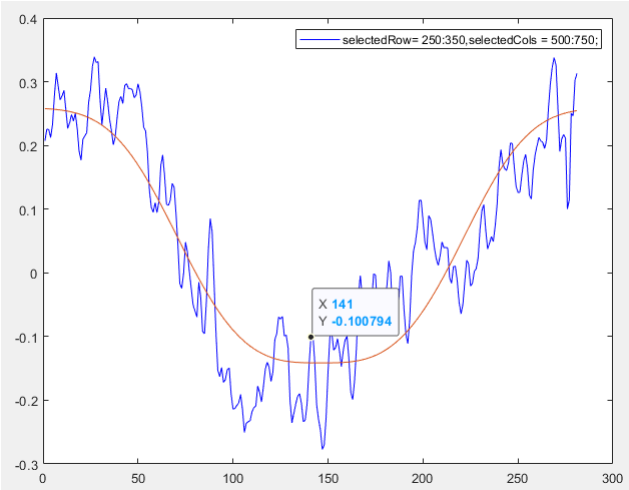

Figure 109: X軸:pixel Y軸:phase. Plasma plume, 30ms delay, average of cols 500~750, average of row 250~350

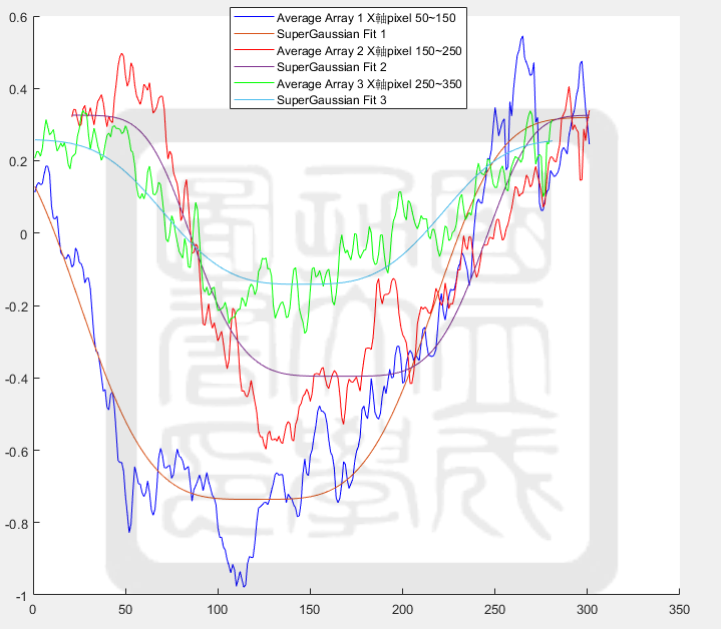

Figure 110: X軸:pixel Y軸:phase. 合併selction three function blue line (50~150), red line (150~250), green line 250~350

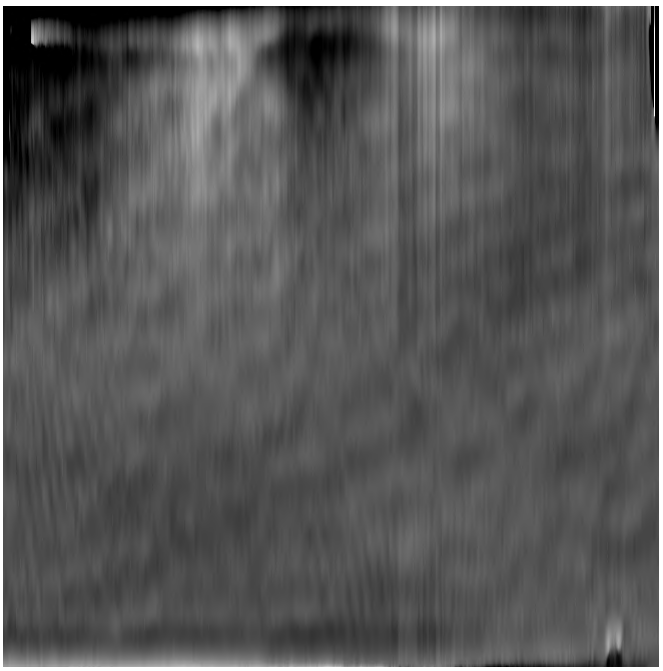

Figure 111: rotate 90 degree image

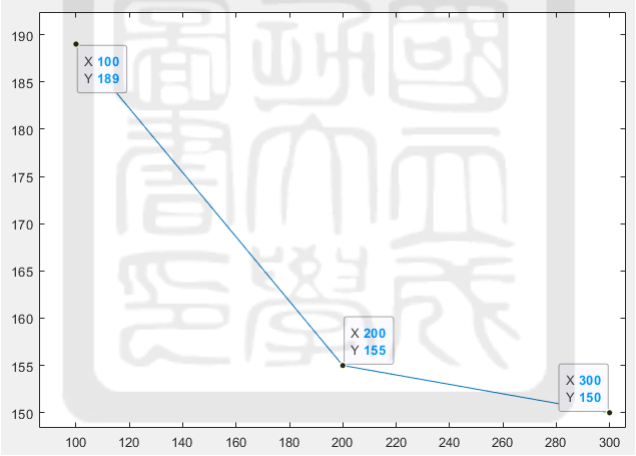

Figure 112: FWHM about row selction 50~150 (left), 150~250(middle), 250~350 (right).

A.4.4 HV-30 ms-2

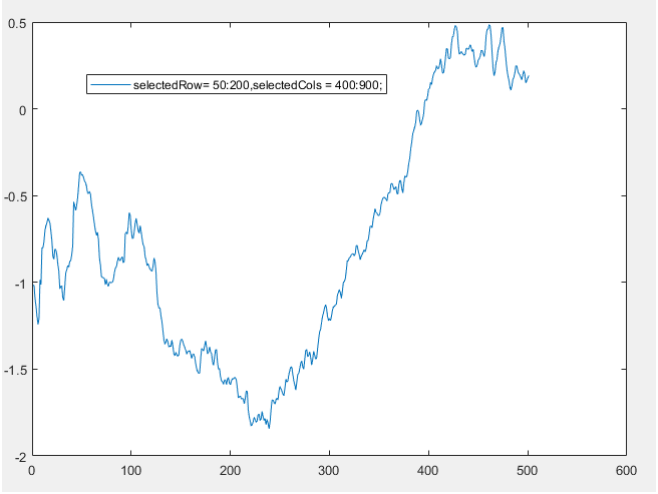

Figure 113: X軸:pixel Y軸:phase Plasma plume, 30ms delay, average of cols 400~900, average of row 50~200

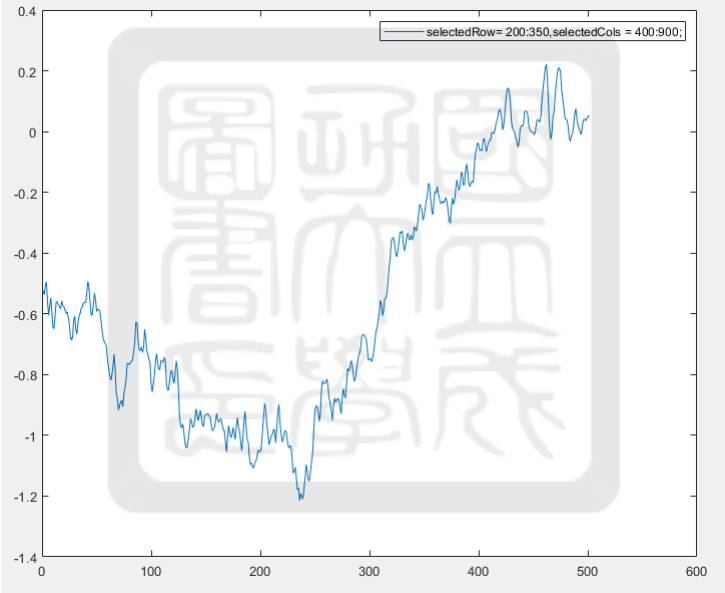

Figure 114: X軸:pixel Y軸:phase. Plasma plume, 30ms delay, average of cols 400~900, average of row 200~350

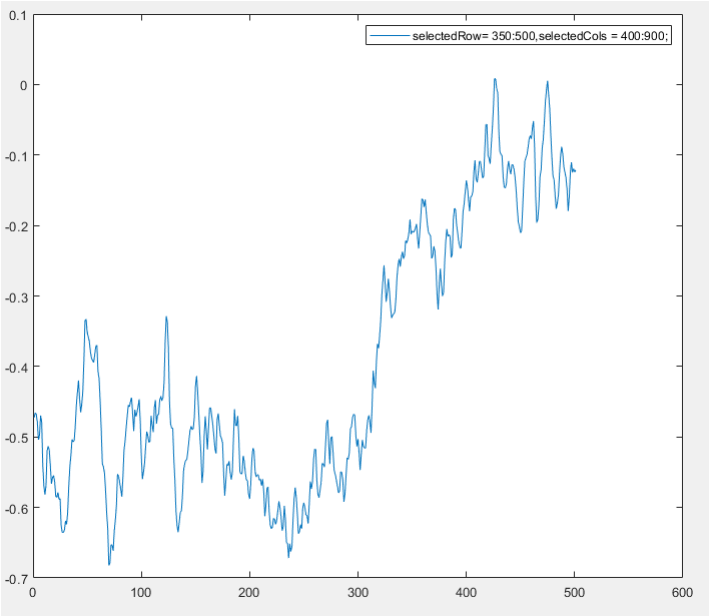

Figure 115: X軸:pixel Y軸:phase. Plasma plume, 30ms delay, average of cols 400~900, average of row 350~500

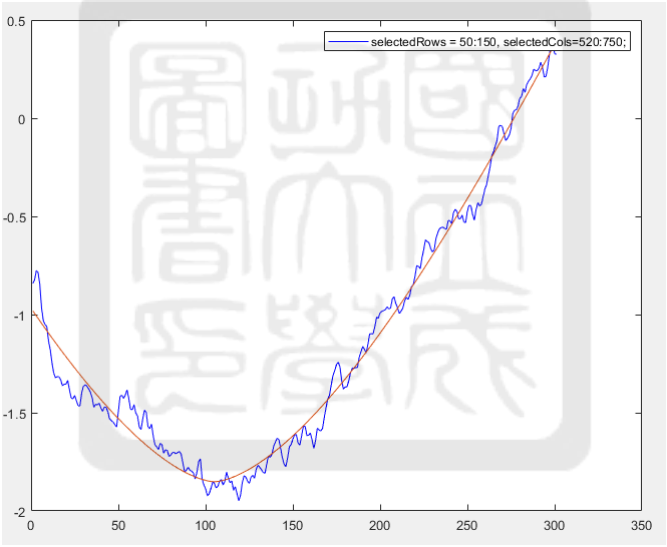

Figure 116: X軸:pixel Y軸:phase. Plasma plume, 30ms delay, average of cols 520~750, average of row 50~150

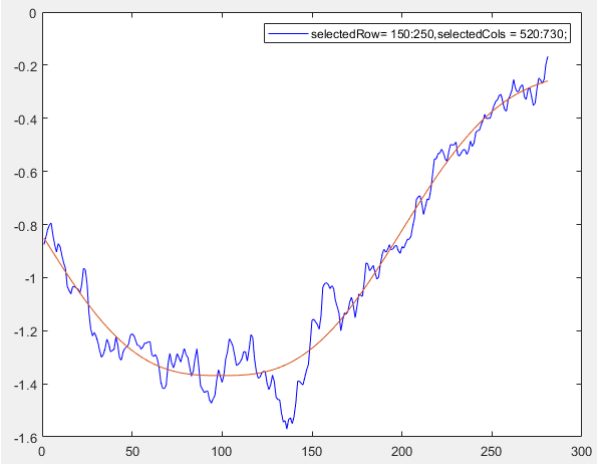

Figure 117: X軸:pixel Y軸:phase. Plasma plume, 30ms delay, average of cols 520~750, average of row 150~250

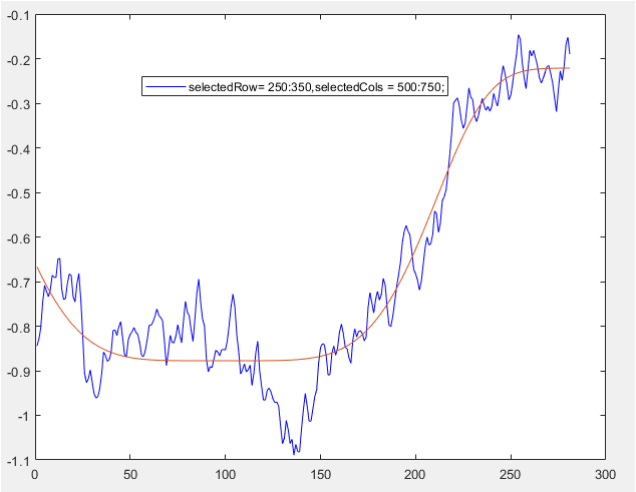

Figure 118: X軸:pixel Y軸:phase. Plasma plume, 30ms delay, average of cols 500~750, average of row 250~350

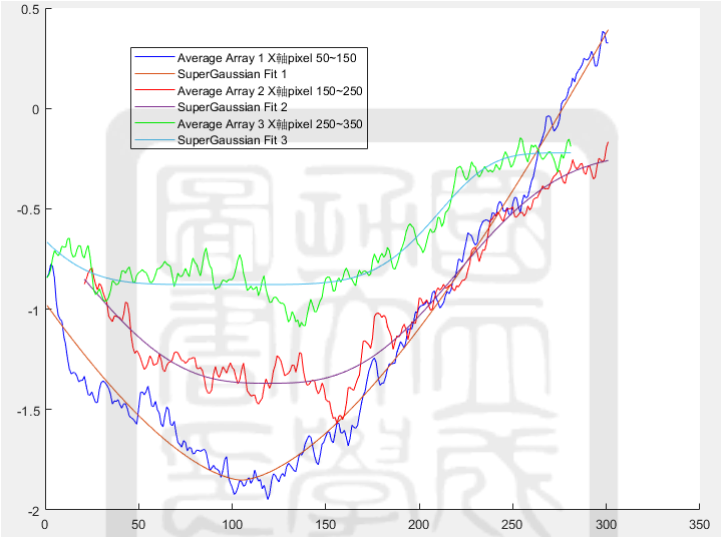

Figure 119: X軸:pixel Y軸:phase. 合併selction three function blue line (50~150), red line (150~250), green line 250~350

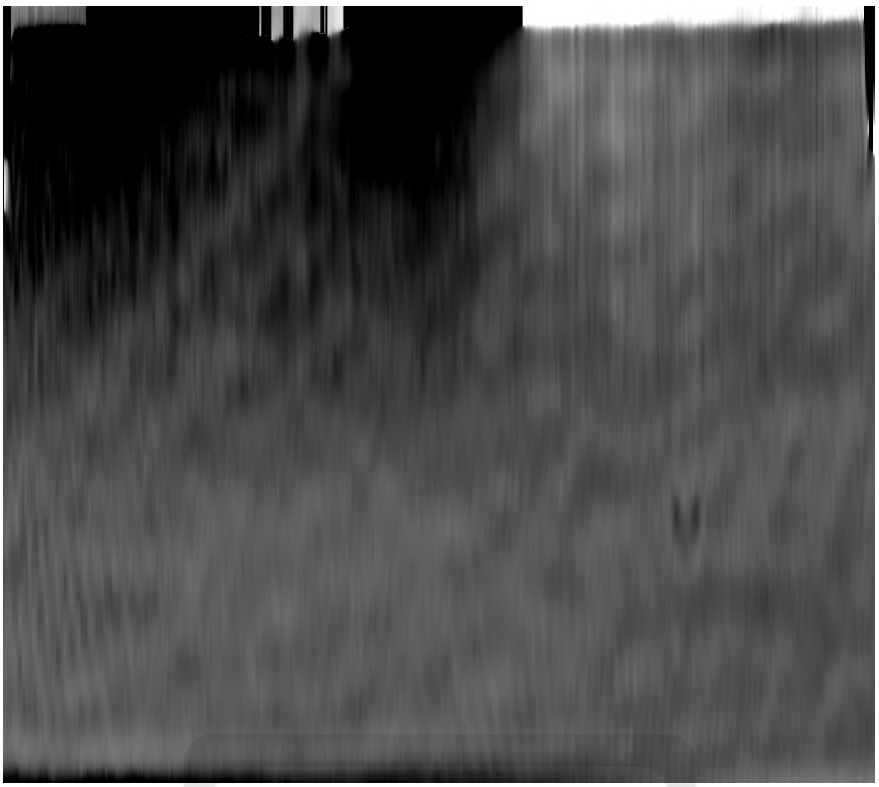

Figure 120: rotate 90 degree image

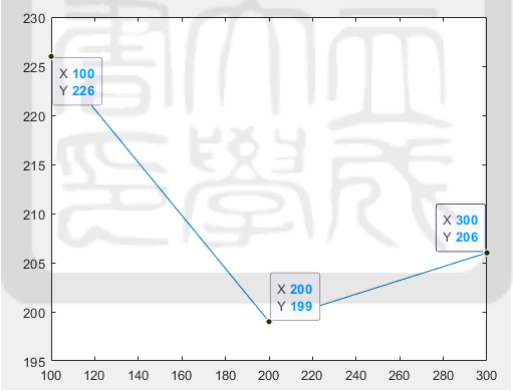

Figure 121: y軸:FWHM pixel. FWHM about row selction 50~150 (left), 150~250(middle), 250~350 (right).

A.4.5 HV-40 ms

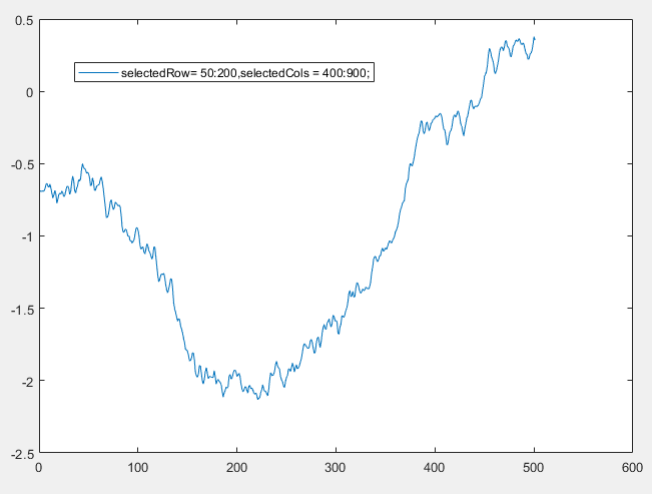

Figure 122: X軸:pixel Y軸:phase. Plasma plume, 40ms delay, average of cols 400~900, average of row 50~200

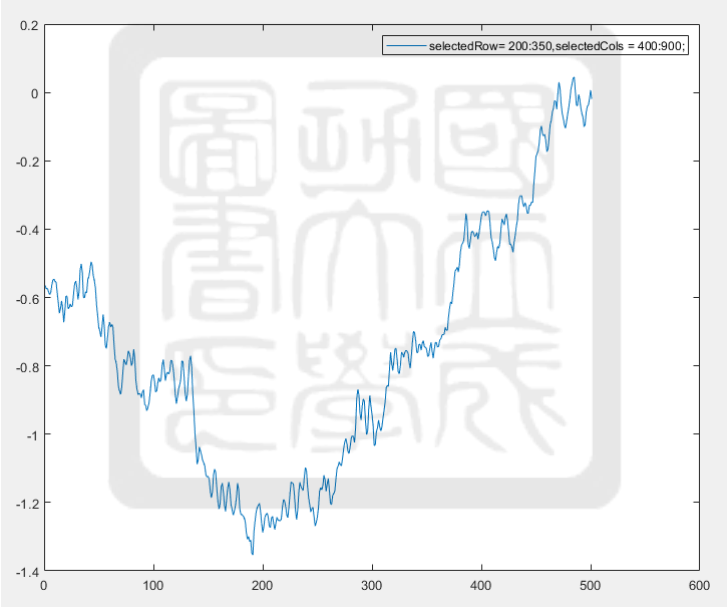

Figure 123: X軸:pixel Y軸:phase. Plasma plume, 40ms delay, average of cols 400~900, average of row 200~350

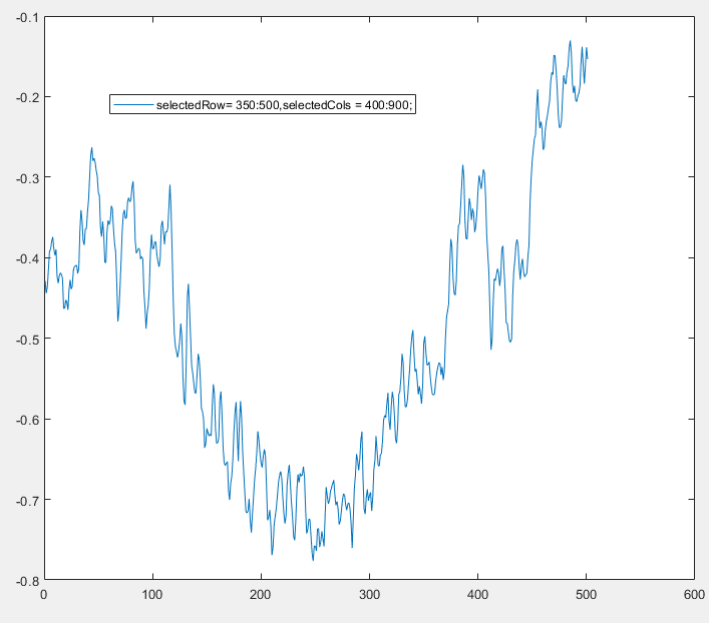

Figure 124: X軸:pixel Y軸:phase. Plasma plume, 40ms delay, average of cols 400~900, average of row 350~500

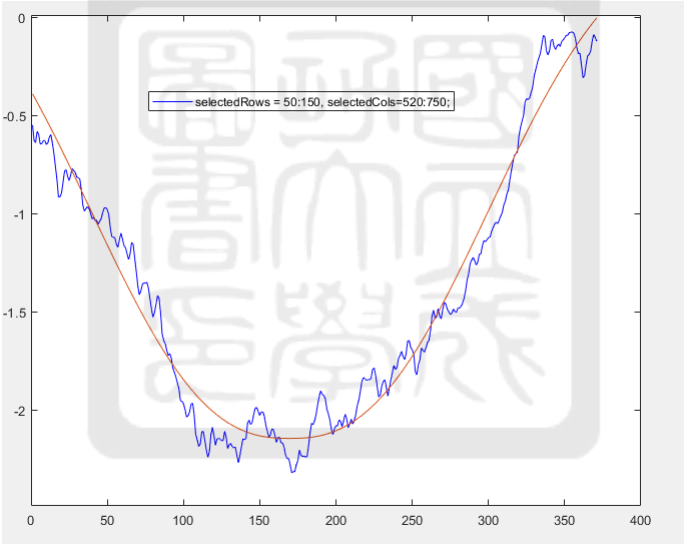

Figure 125: X軸:pixel Y軸:phase. Plasma plume, 40ms delay, average of cols 520~750, average of row 50~150

Figure 126: X軸:pixel Y軸:phase. Plasma plume, 40ms delay, average of cols 520~750, average of row 150~250

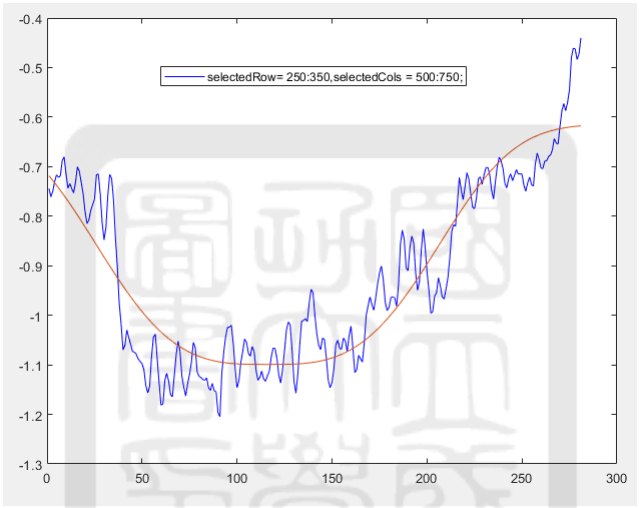

Figure 127: X軸:pixel Y軸:phase Plasma plume, 40ms delay, average of cols 500~750, average of row 250~350

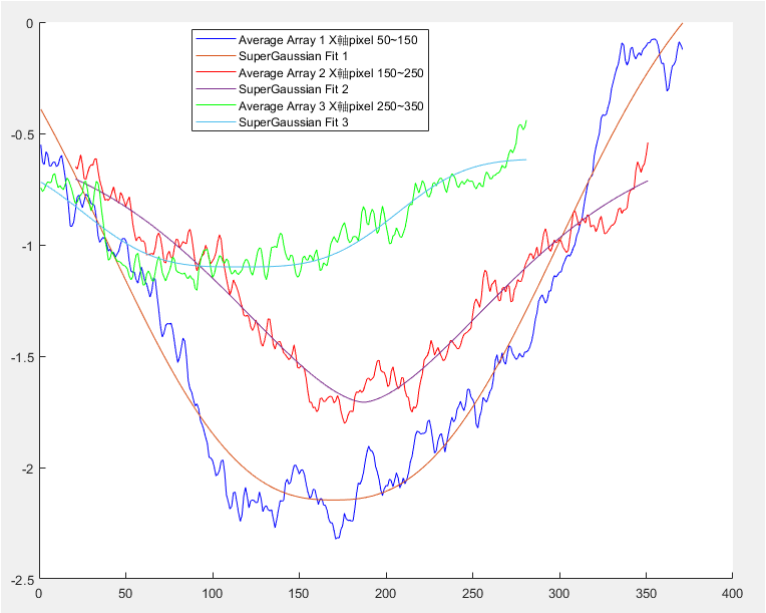

Figure 128: X軸:pixel Y軸:phase. 合併selction three function blue line (50~150), red line (150~250), green line 250~350

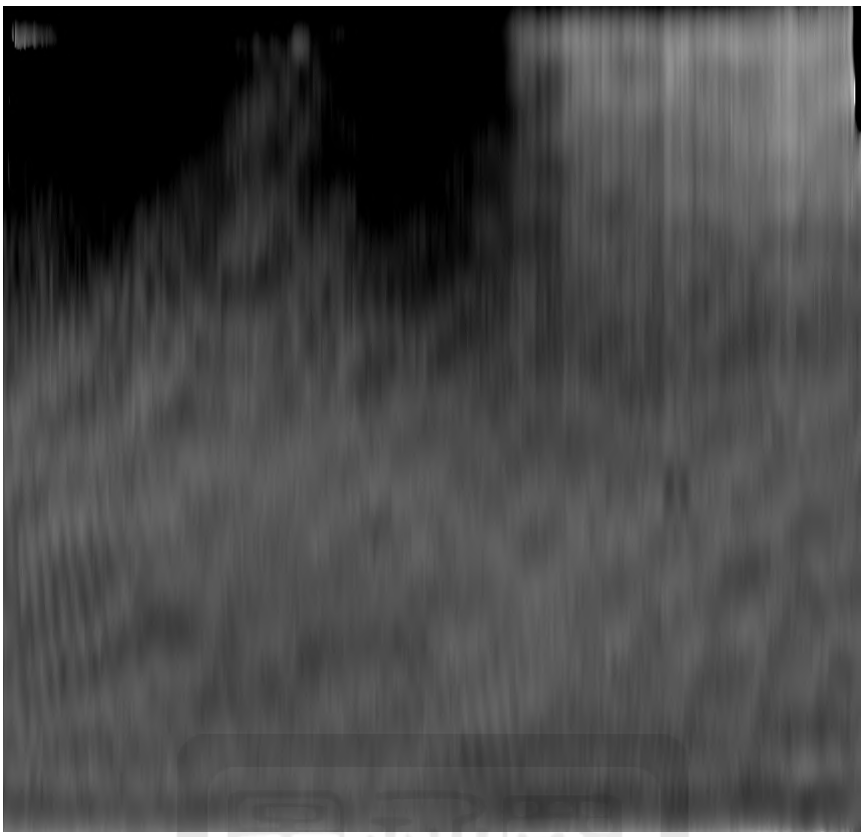

Figure 129: rotate 90 degree image

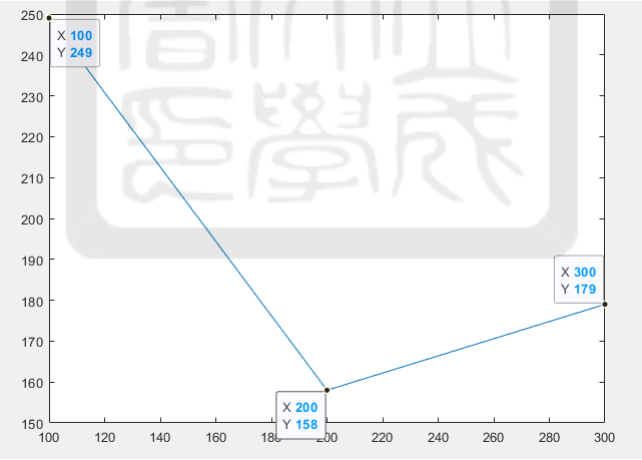

Figure 130: y軸:FWHM pixel. FWHM about row selction 50~150 (left), 150~250(middle), 250~350 (right).

A.4.6 No high voltage(HV)-20 ms-1

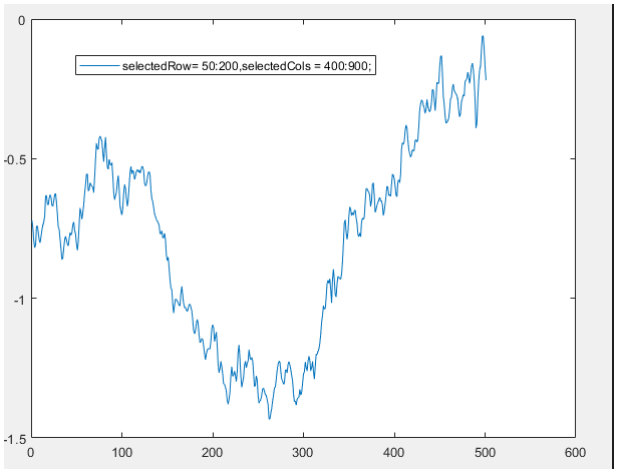

Figure 131: X軸:pixel Y軸:phase. Gas puff, 20ms delay, average of cols 400~900, average of row 50~200

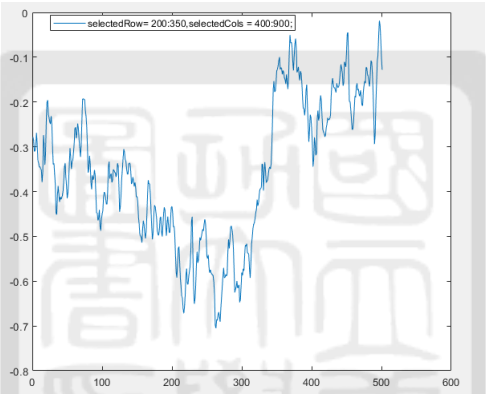

Figure 132: X軸:pixel Y軸:phase. Gas puff, 20ms delay, average of cols 400~900, average of row 200~350

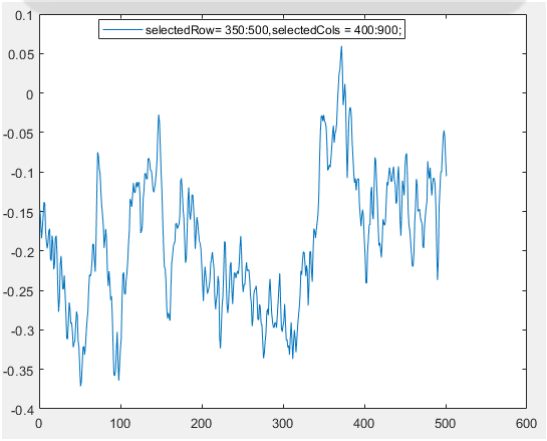

Figure 133: X軸:pixel Y軸:phase. Gas puff, 20ms delay, average of cols 400~900, average of row 350~500

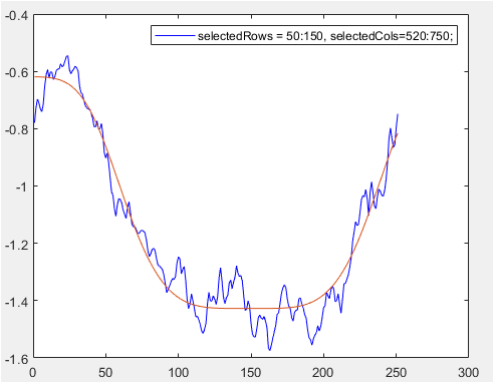

Figure 134: X軸:pixel Y軸:phase. Gas puff, 20ms delay, average of cols 520~750, average of row 50~150

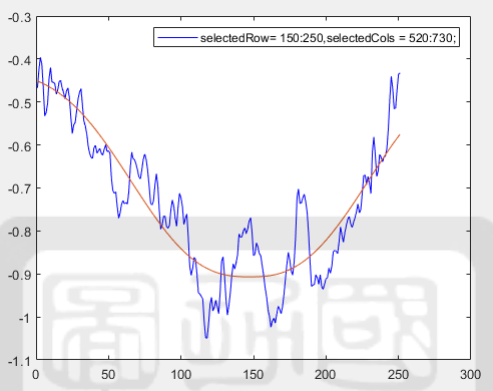

Figure 135: X軸:pixel Y軸:phase. Gas puff, 20ms delay, average of cols 520~750, average of row 150~250

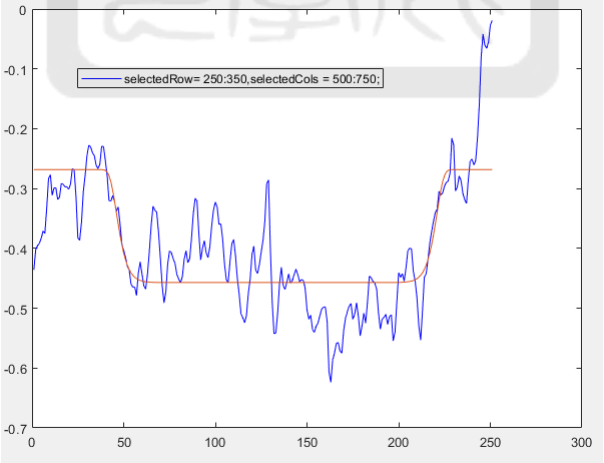

Figure 136: X軸:pixel Y軸:phase. Gas puff, 20ms delay, average of cols 500~750, average of row 250~350

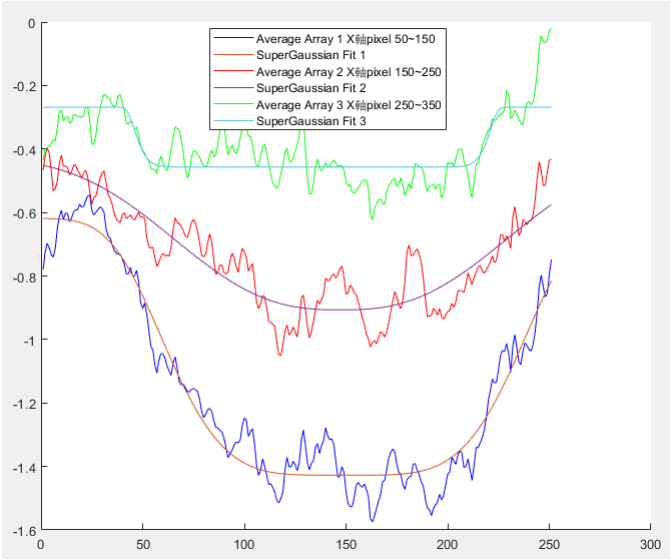

Figure 137: X軸:pixel Y軸:phase. 合併selction three function blue line (50~150), red line (150~250), green line 250~350

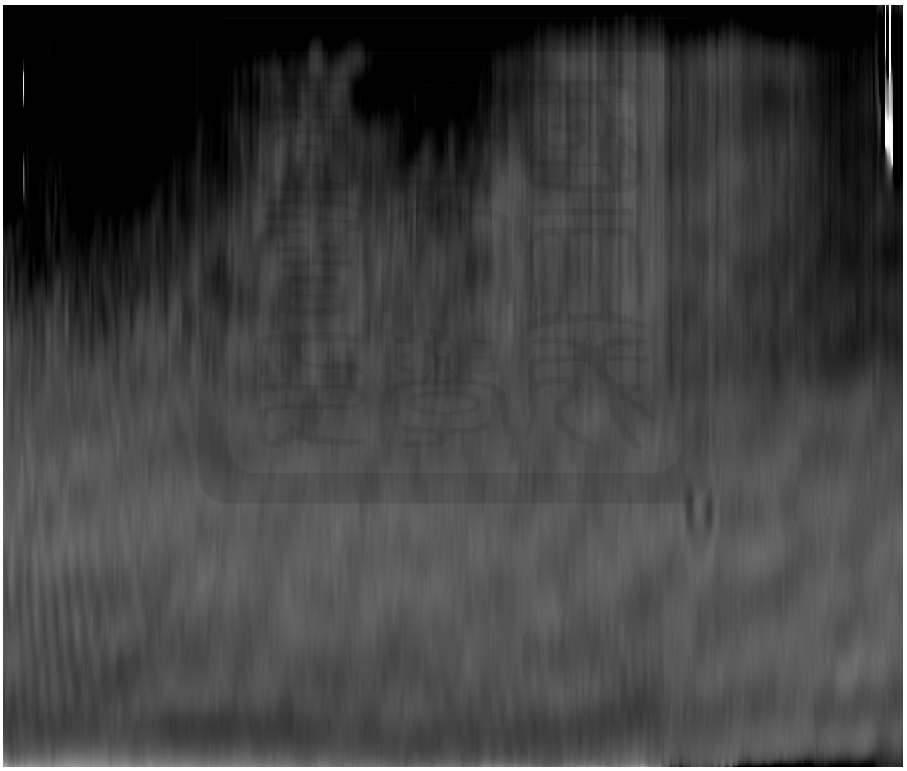

Figure 138: rotate 90 degree image

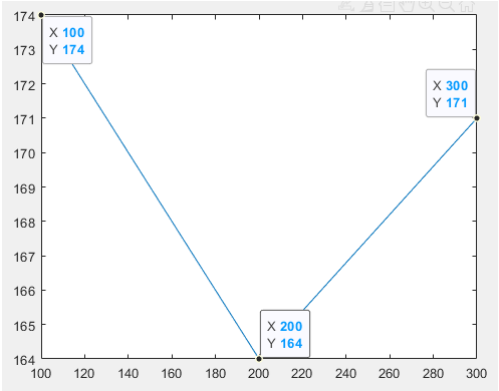

Figure 139: y軸:FWHM pixel. FWHM about row selction 50~150 (left), 150~250(middle), 250~350 (right).

A.4.7 No HV-20 ms-2

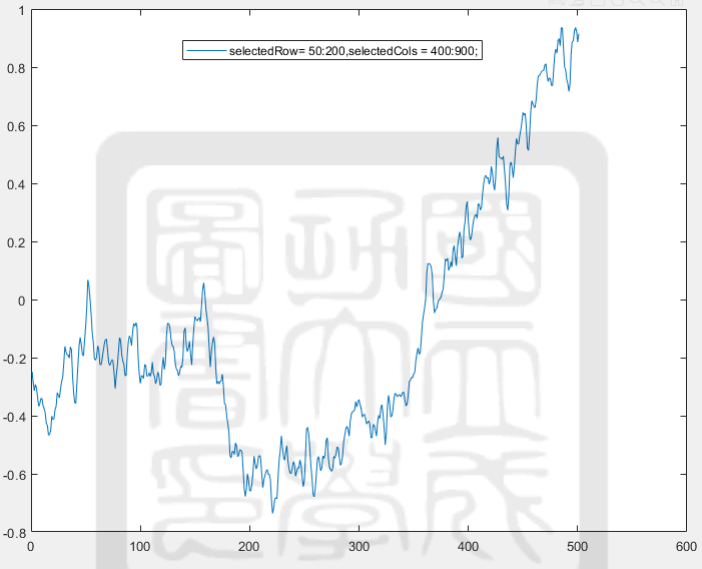

Figure 140: X軸:pixel Y軸:phase. Gas puff, 20ms delay, average of cols 400~900, average of row 50~200

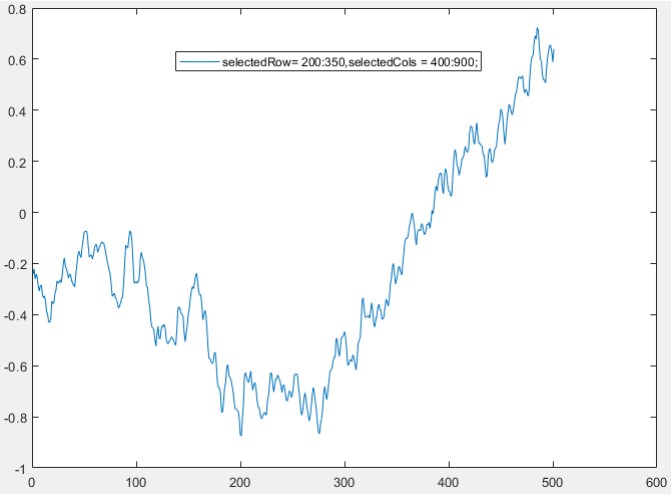

Figure 141: X軸:pixel Y軸:phase. Gas puff, 20ms delay, average of cols 400~900, average of row 200~350

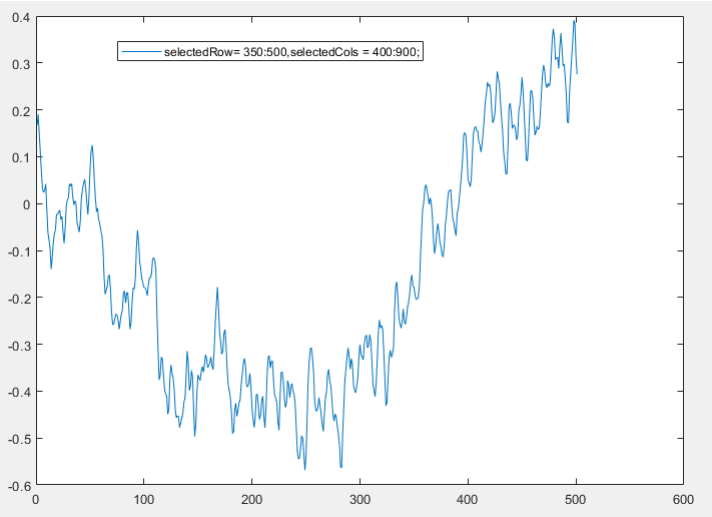

Figure 142: X軸:pixel Y軸:phase. Gas puff, 20ms delay, average of cols 400~900, average of row 350~500

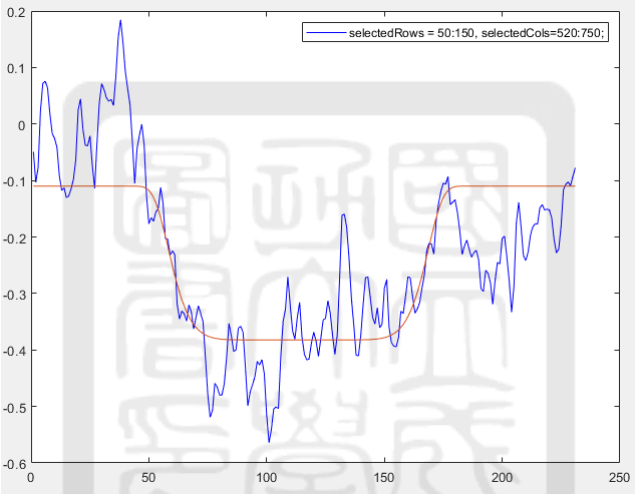

Figure 143: X軸:pixel Y軸:phase. Gas puff, 20ms delay, average of cols 520~750, average of row 50~150

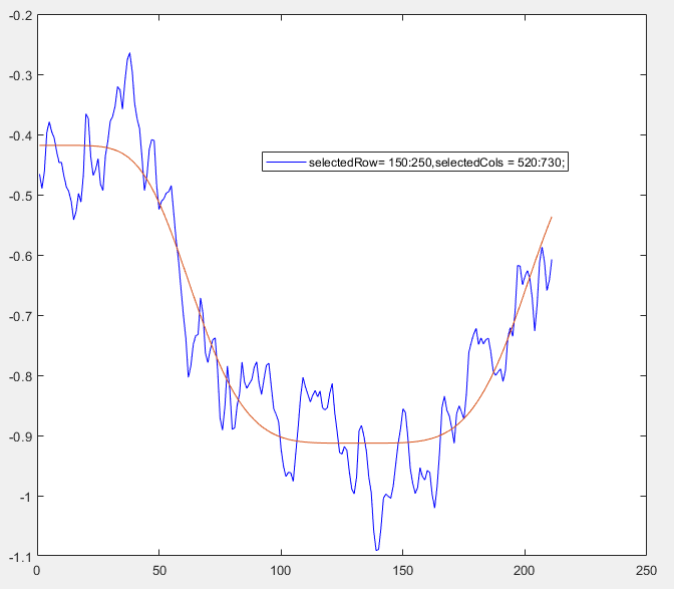

Figure 144: X軸:pixel Y軸:phase. Gas puff, 20ms delay, average of cols 520~750, average of row 150~250

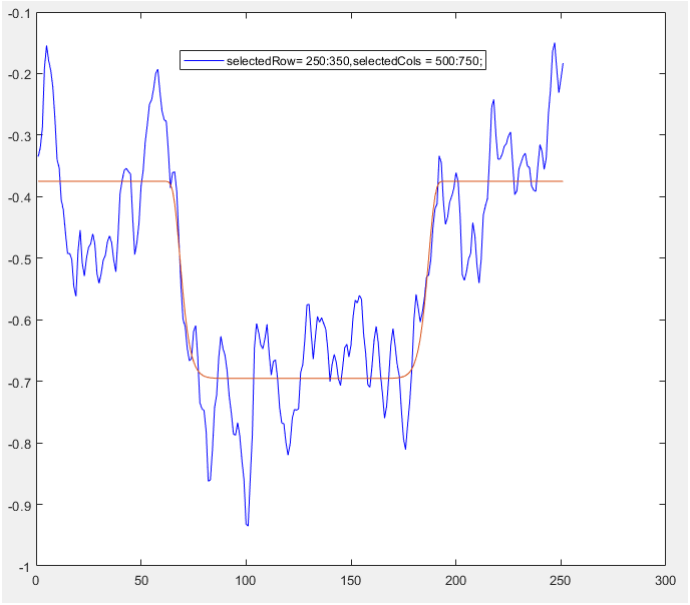

Figure 145: X軸:pixel Y軸:phase. Gas puff, 20ms delay, average of cols 500~750, average of row 250~350

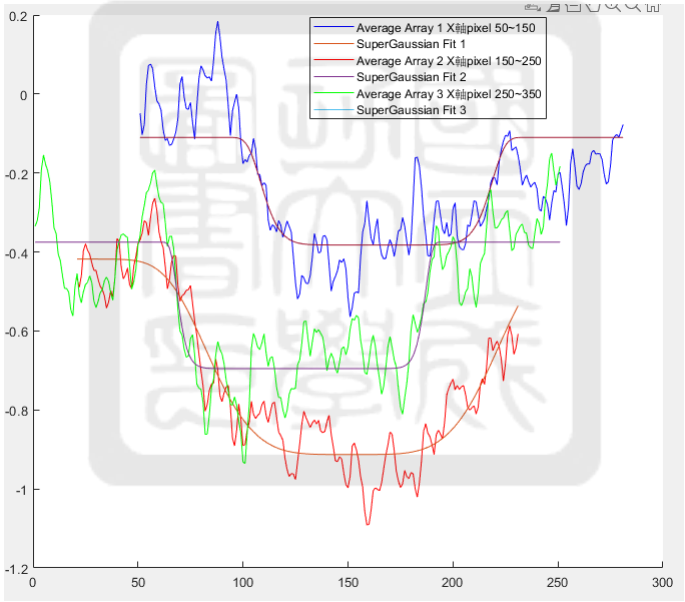

Figure 146: X軸:pixel Y軸:phase. 合併selction three function blue line (50~150), red line (150~250), green line 250~350

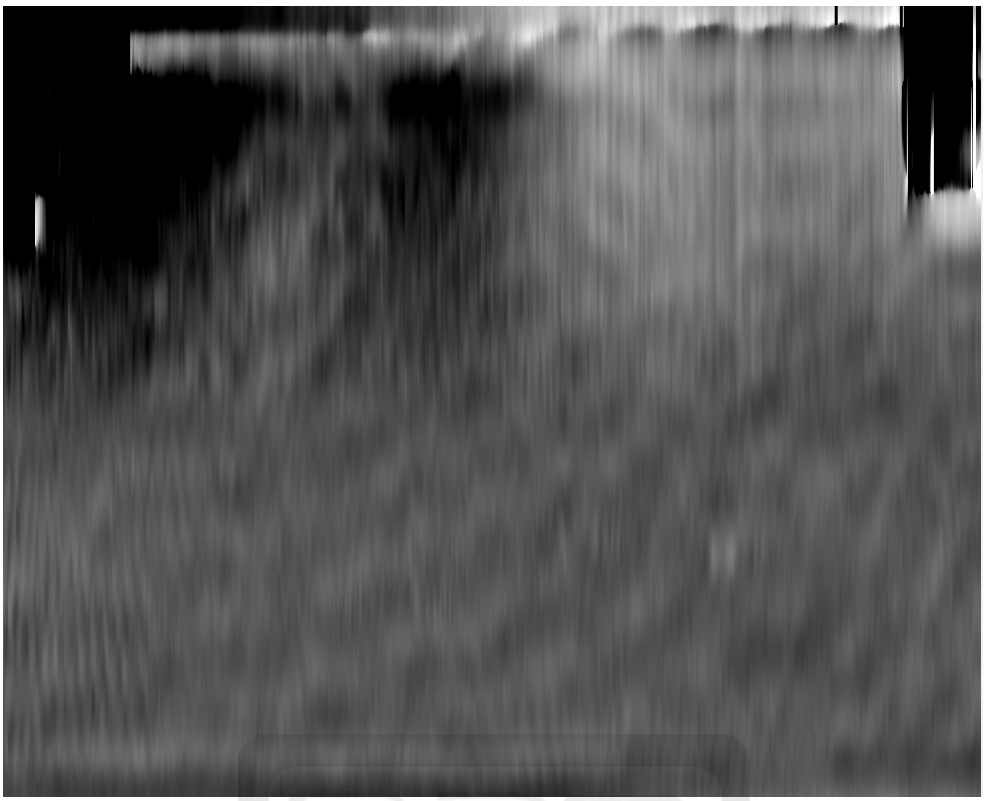

Figure 147: rotate 90 degree image

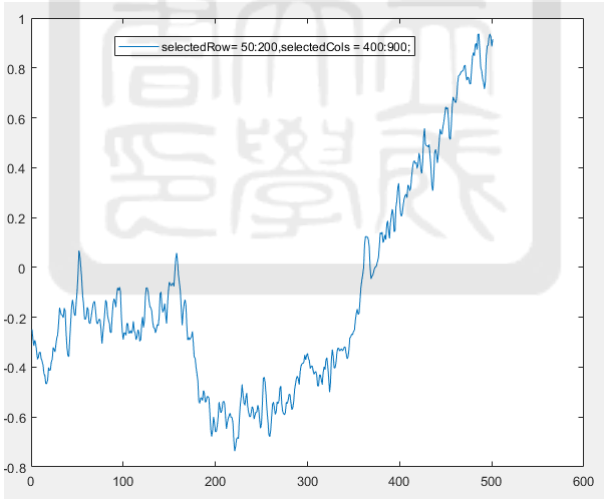

Figure 148: y軸:FWHM pixel. FWHM about row selction 50~150 (left), 150~250(middle), 250~350 (right).

A.4.8 No HV-20 ms -3

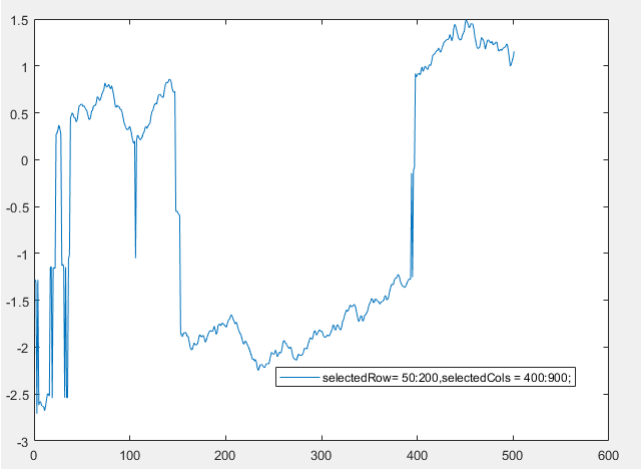

Figure 149: X軸:pixel Y軸:phase. Gas puff, 20ms delay, average of cols 400~900, average of row 50~150

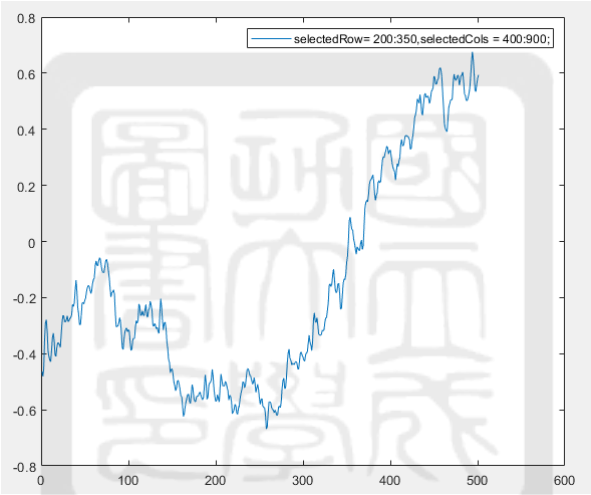

Figure 150: X軸:pixel Y軸:phase. Gas puff, 20ms delay, average of cols 400~900, average of row 200~350

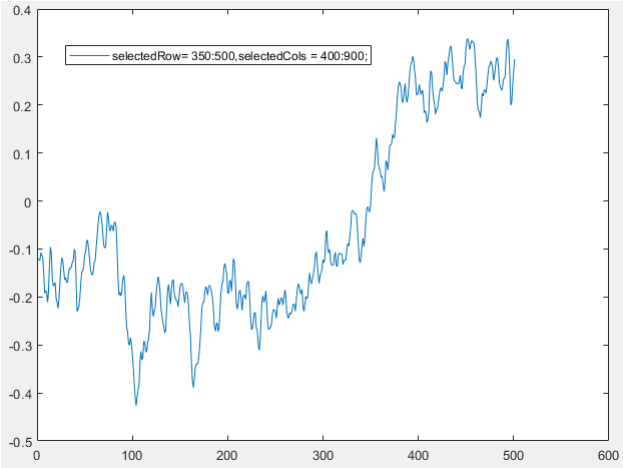

Figure 151: X軸:pixel Y軸:phase. Gas puff, 20ms delay, average of cols 400~900, average of row 350~500

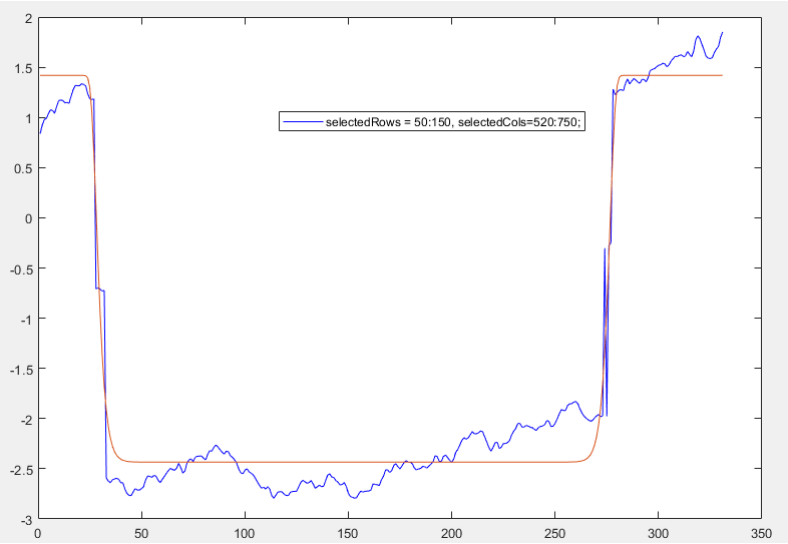

Figure 152: X軸:pixel Y軸:phase. Gas puff, 20ms delay, average of cols 520~750, average of row 50~150

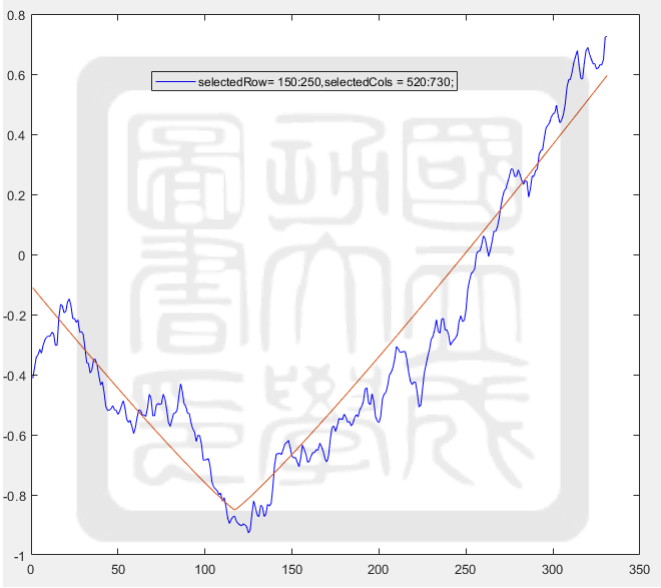

Figure 153: X軸:pixel Y軸:phase. Gas puff, 20ms delay, average of cols 520~750, average of row 150~250

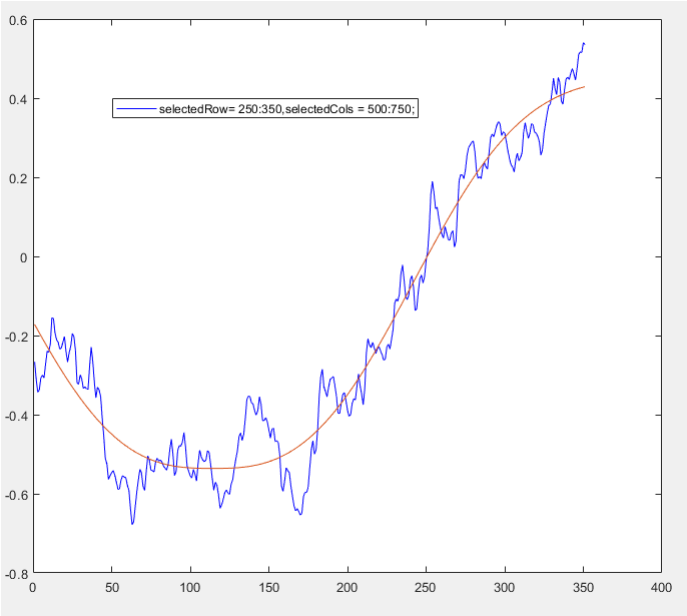

Figure 154: X軸:pixel Y軸:phase. Gas puff, 20ms delay, average of cols 500~750, average of row 250~350

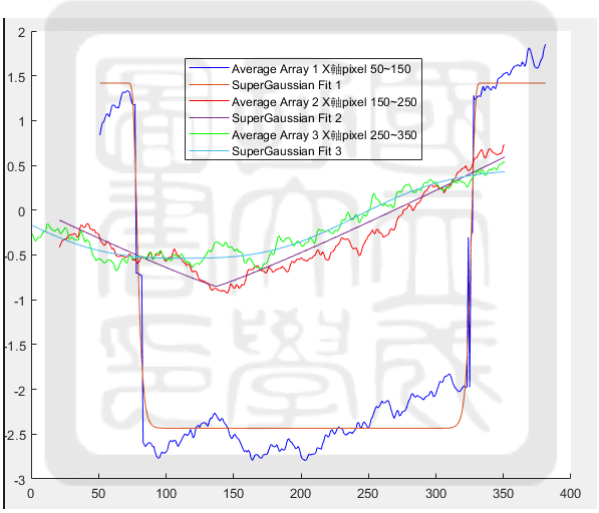

Figure 155: X軸:pixel Y軸:phase. 合併selction three function blue line (50~150), red line (150~250), green line 250~350

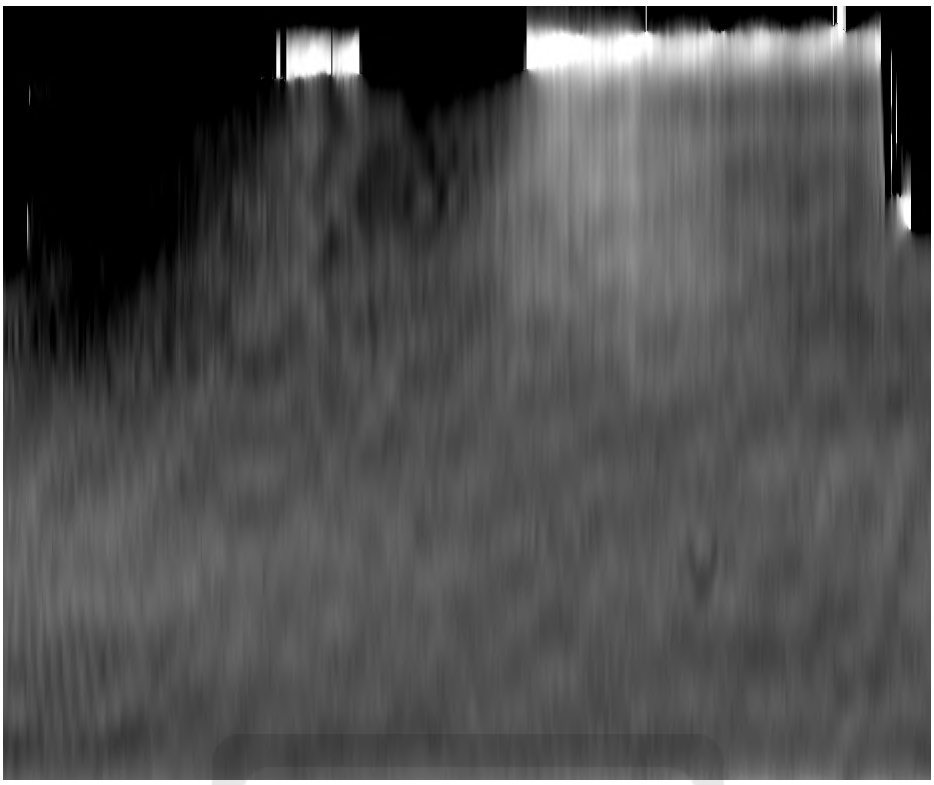

Figure 156: rotate 90 degree image

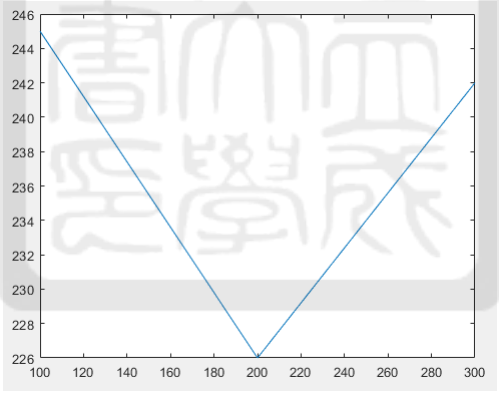

Figure 157: y軸:FWHM pixel. FWHM about row selction 50~150 (left), 150~250(middle), 250~350 (right).

A.4.9 No HV- 20 ms-4

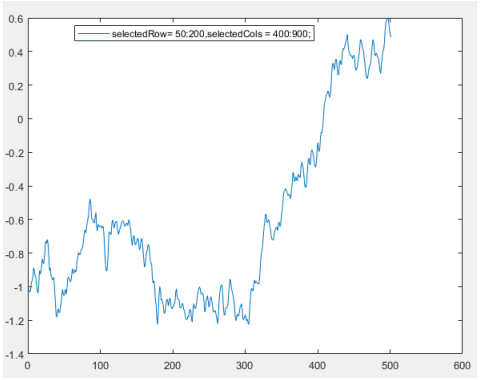

Figure 158: X軸:pixel Y軸:phase. Gas puff, 20ms delay, average of cols 400~900, average of row 50~200

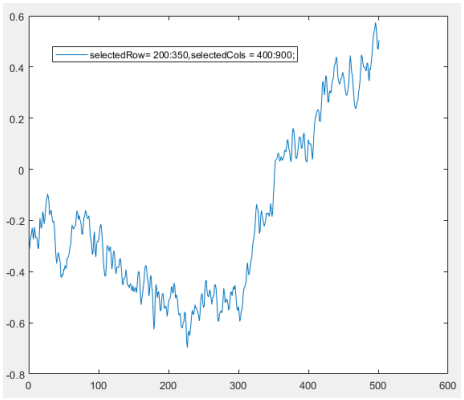

Figure 159: X軸:pixel Y軸:phase. Gas puff, 20ms delay, average of cols 400~900, average of row 200~350

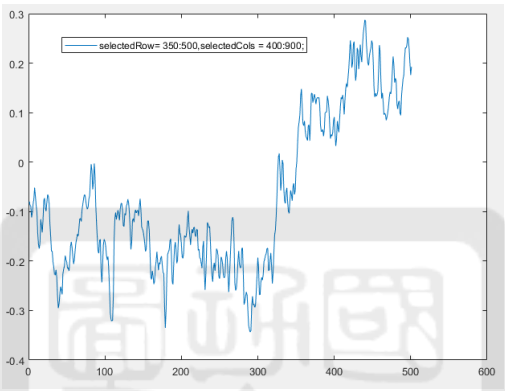

Figure 160: X軸:pixel Y軸:phase. Gas puff, 20ms delay, average of cols 400~900, average of row 350~500

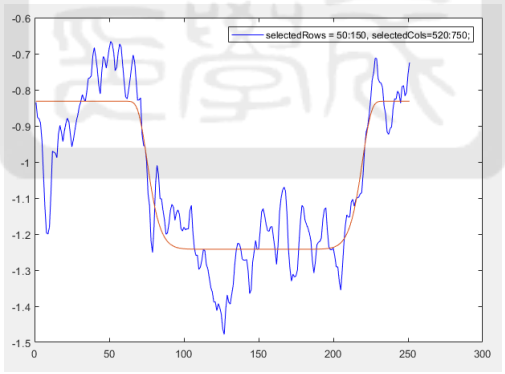

Figure 161: X軸:pixel Y軸:phase. Gas puff, 20ms delay, average of cols 520~750, average of row 50~150

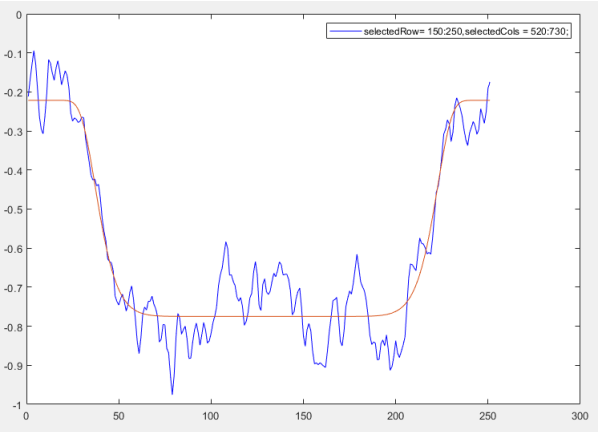

Figure 162: X軸:pixel Y軸:phase. Gas puff, 20ms delay, average of cols 520~750, average of row 150~250

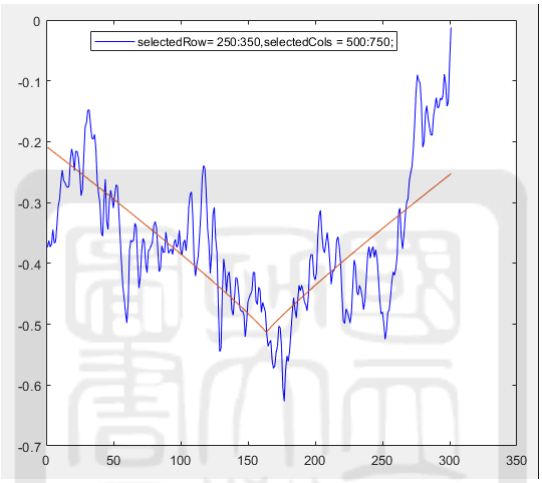

Figure 163: X軸:pixel Y軸:phase. Gas puff, 20ms delay, average of cols 500~750, average of row 250~350

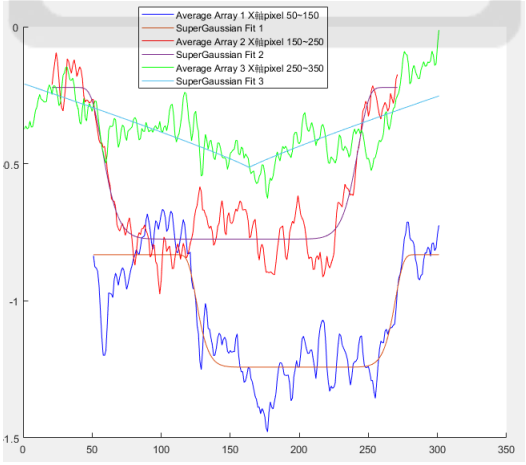

Figure 164: X軸:pixel Y軸:phase. 合併selction three function blue line (50~150), red line (150~250), green line 250~350

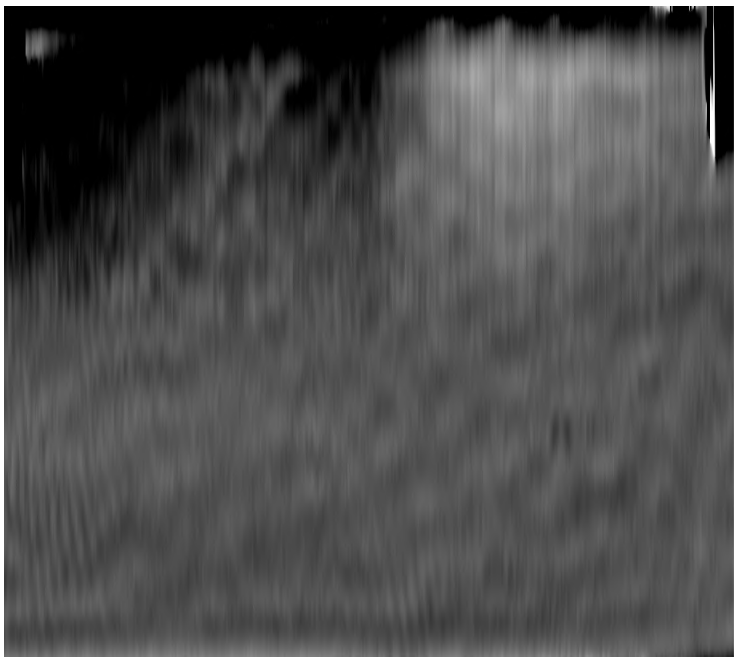

Figure 165: rotate 90 degree image

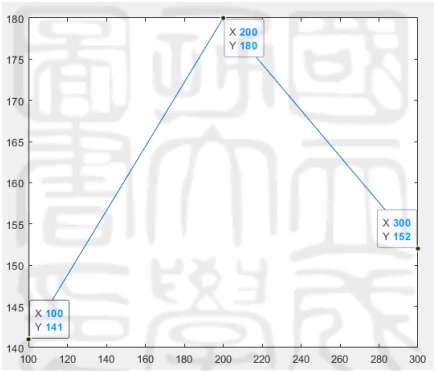

Figure 166: y軸:FWHM pixel. FWHM about row selction 50~150 (left), 150~250(middle), 250~350 (right).

A.4.10 No HV-30 ms-1

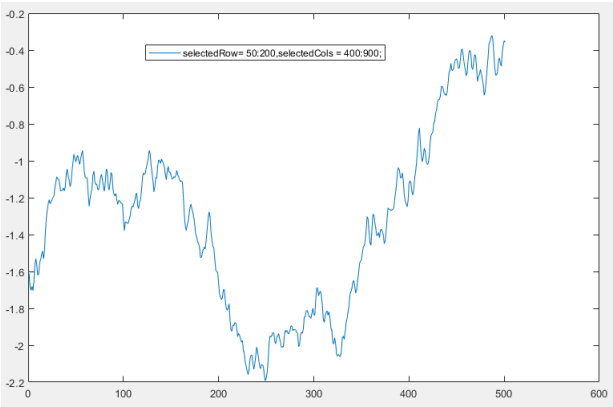

Figure 167: X軸:pixel Y軸:phase. Gas puff, 30ms delay, average of cols 400~900, average of row 50~150

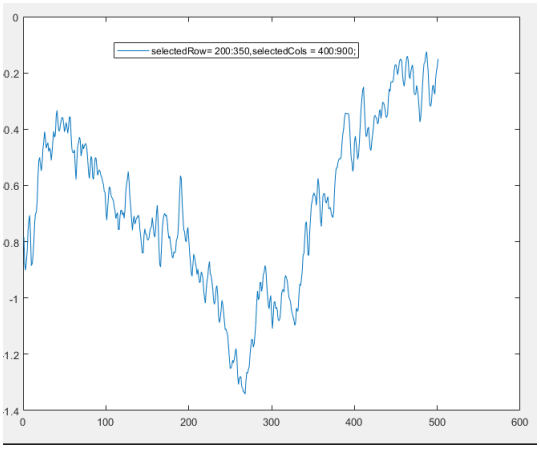

Figure 168: X軸:pixel Y軸:phase. Gas puff, 30ms delay, average of cols 400~900, average of row 200~350

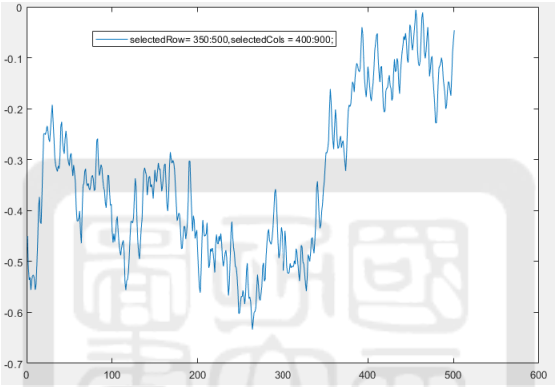

Figure 169: X軸:pixel Y軸:phase. Gas puff, 30ms delay, average of cols 400~900, average of row 350~500

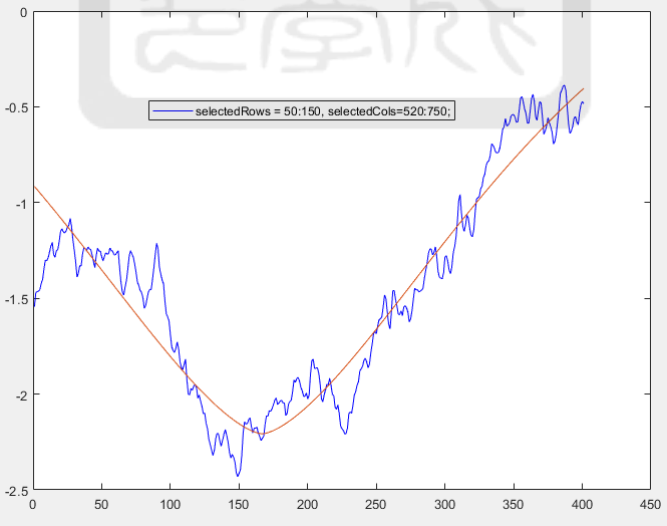

Figure 170: X軸:pixel Y軸:phase. Gas puff, 30ms delay, average of cols 520~750, average of row 50~150

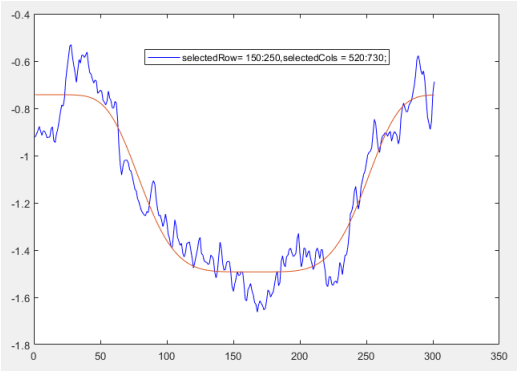

Figure 171: X軸:pixel Y軸:phase. Gas puff, 30ms delay, average of cols 520~750, average of row 150~250

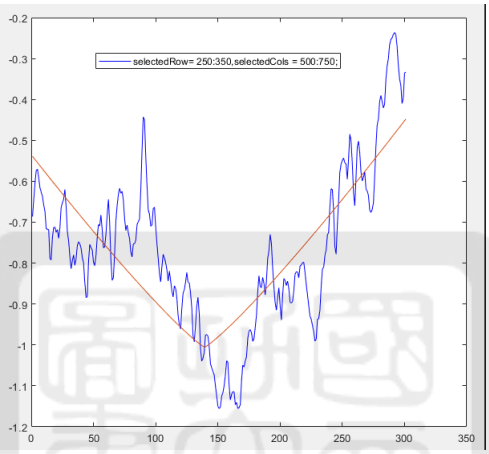

Figure 172: X軸:pixel Y軸:phase. Gas puff, 30ms delay, average of cols 500~750, average of row 250~350

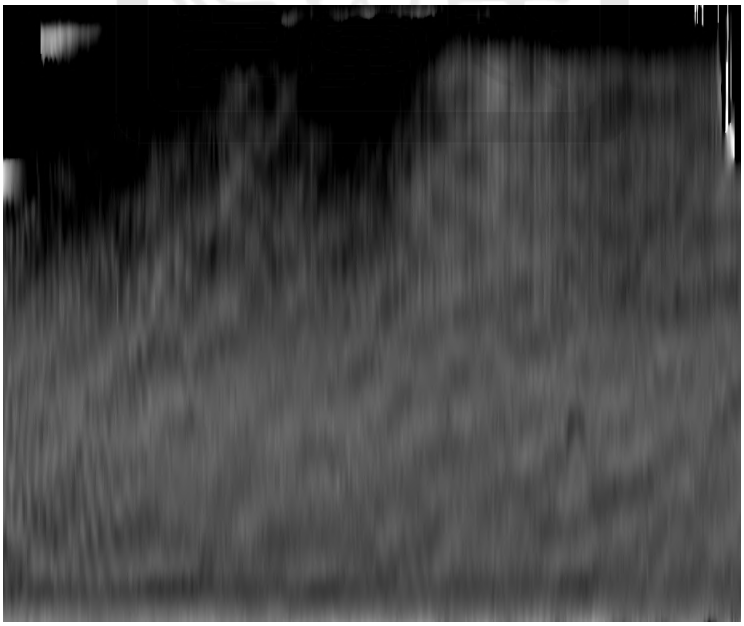

Figure 173: rotate 90 degree image

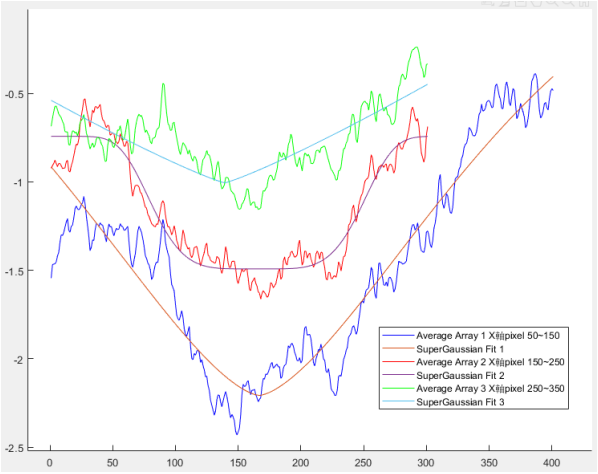

Figure 174: X軸:pixel Y軸:phase. 合併selction three function blue line (50~150), red line (150~250), green line 250~350

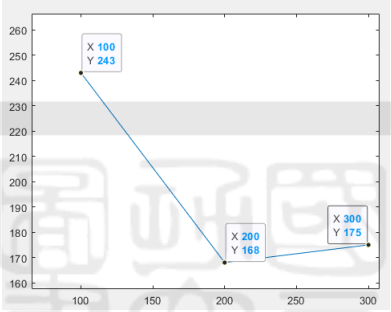

Figure 175: y軸:FWHM pixel. FWHM about row selction 50~150 (left), 150~250(middle), 250~350 (right).

A.4.11 No HV-30 ms-2

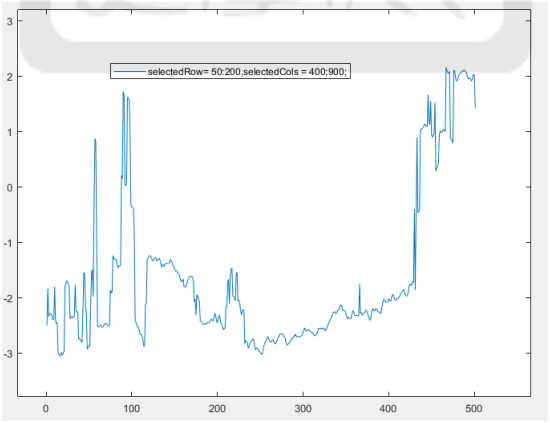

Figure 176: X軸:pixel Y軸:phase. Gas puff, 30ms delay, average of cols 400~900, average of row 50~200

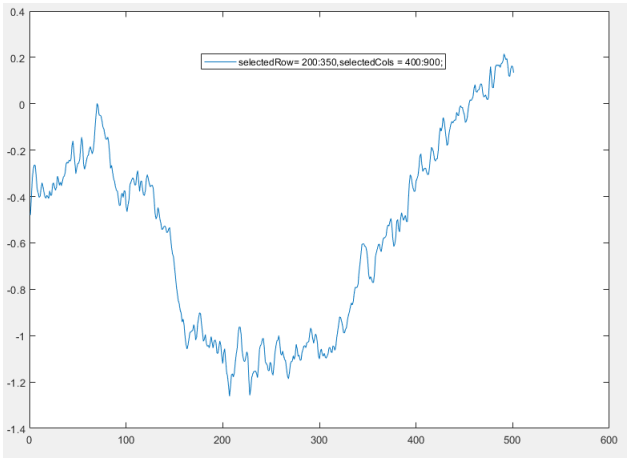

Figure 177: X軸:pixel Y軸:phase. Gas puff, 30ms delay, average of cols 400~900, average of row 200~350

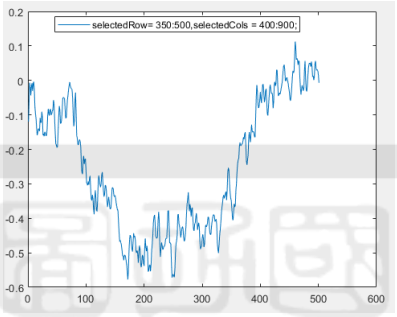

Figure 178: X軸:pixel Y軸:phase. Gas puff, 30ms delay, average of cols 400~900, average of row 350~500

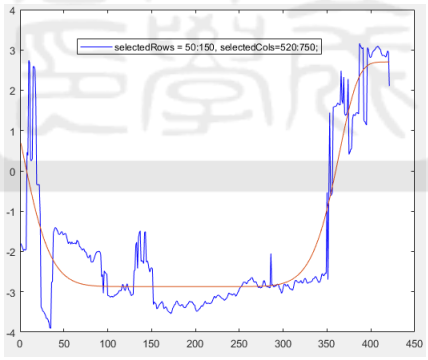

Figure 179: X軸:pixel Y軸:phase. Gas puff, 30ms delay, average of cols 520~750, average of row 50~150

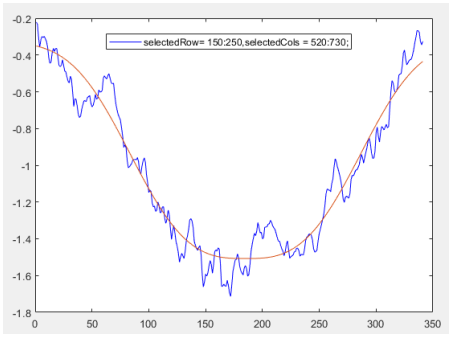

Figure 180: X軸:pixel Y軸:phase. Gas puff, 30ms delay, average of cols 520~750, average of row 150~250

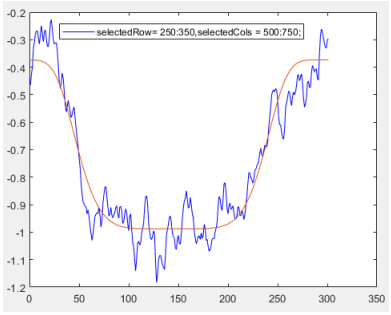

Figure 181: X軸:pixel Y軸:phase. Gas puff, 30ms delay, average of cols 500~750, average of row 250~350

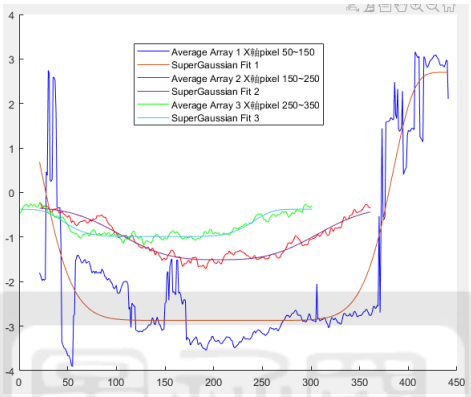

Figure 182: X軸:pixel Y軸:phase. 合併selction three function blue line (50~150), red line (150~250), green line 250~350

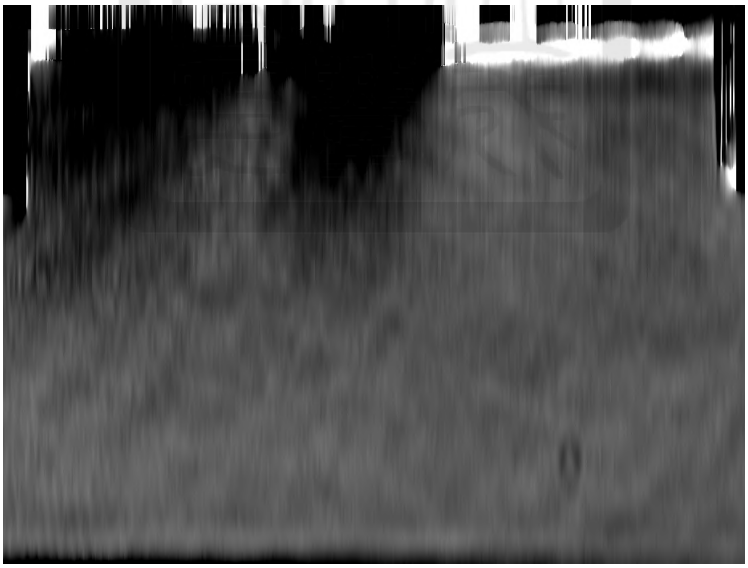

Figure 183: rotate 90 degree image

A.4.12 No HV- 30 ms-3

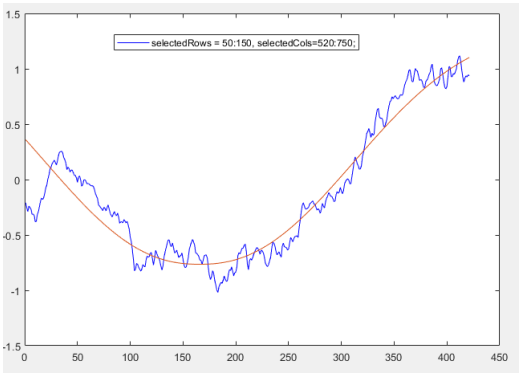

Figure 184: X軸:pixel Y軸:phase. Gas puff, 30ms delay, average of cols 520~750, average of row 50~150

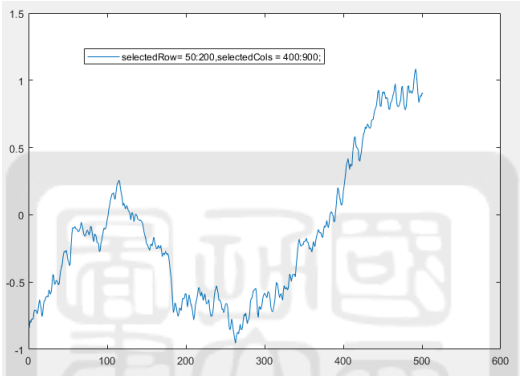

Figure 185: X軸:pixel Y軸:phase. Gas puff, 30ms delay, average of cols 400~900, average of row 50~200

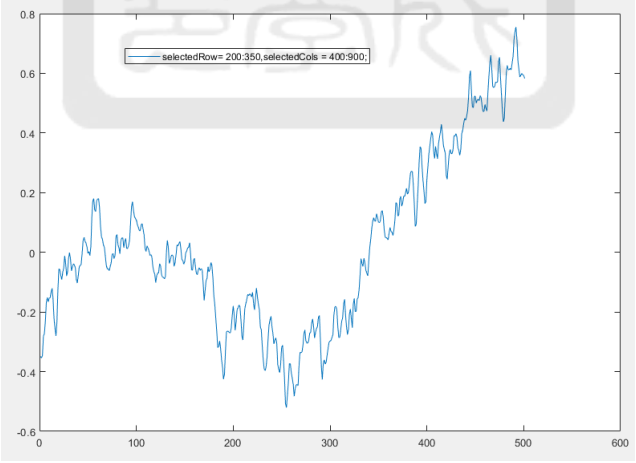

Figure 186: X軸:pixel Y軸:phase

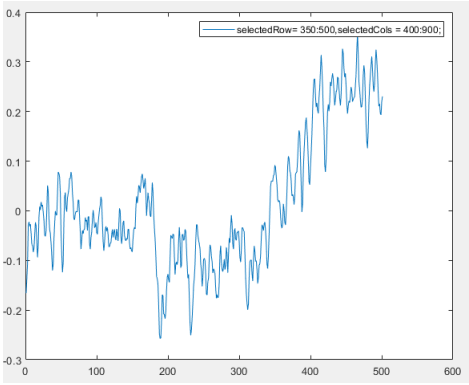

Figure 187: X軸:pixel Y軸:phase. Gas puff, 30ms delay, average of cols 400~900, average of row 200~350

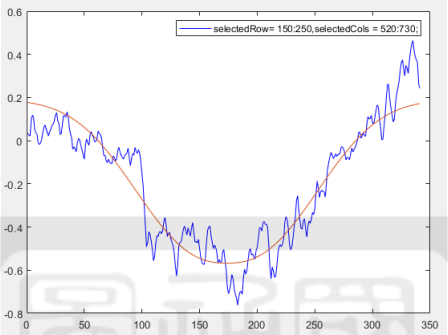

Figure 188: X軸:pixel Y軸:phase. Gas puff, 30ms delay, average of cols 520~730, average of row 150~250

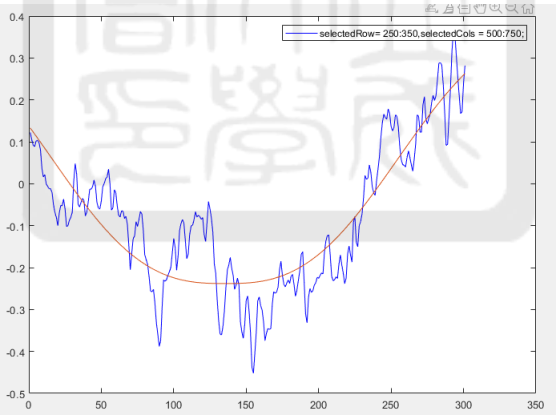

Figure 189: X軸:pixel Y軸:phase. Gas puff, 30ms delay, average of cols 500~750, average of row 250~350

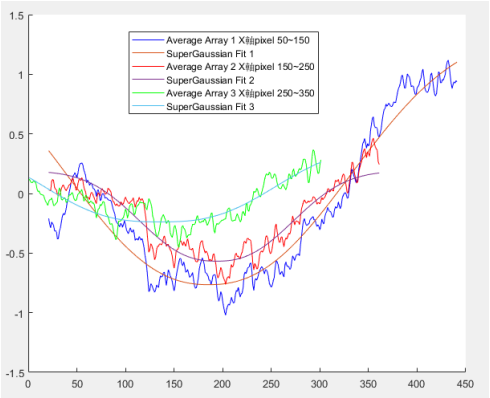

Figure 190: X軸:pixel Y軸:phase. 合併selction three function blue line (50~150), red line (150~250), green line 250~350

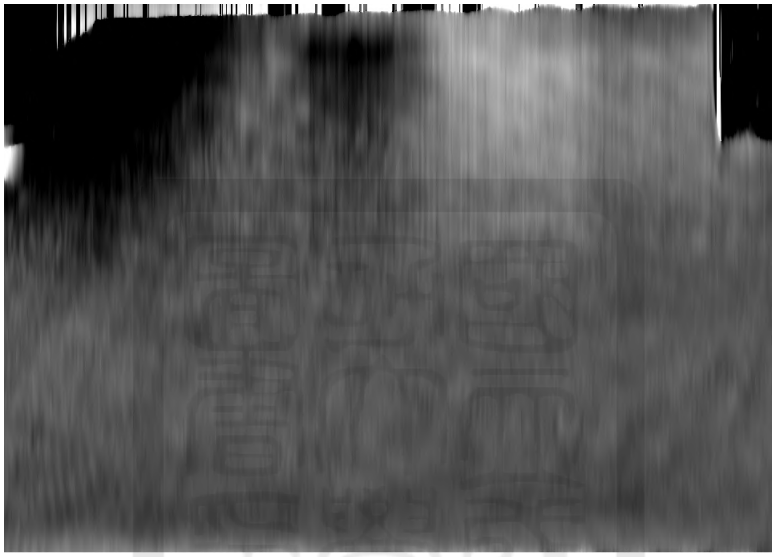

Figure 191: rotate 90 degree image

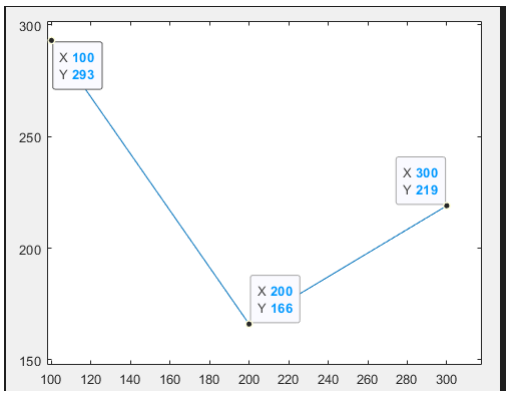

Figure 192: y軸:FWHM pixel. FWHM about row selction 50~150 (left), 150~250(middle), 250~350 (right).

A.4.13 No HV-30 ms-4

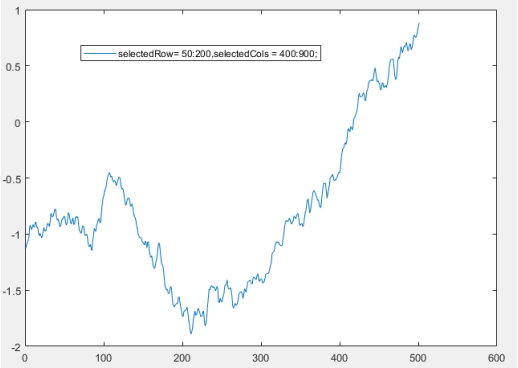

Figure 193: X軸:pixel Y軸:phase. Gas puff, 30ms delay, average of cols 400~900, average of row 50~200

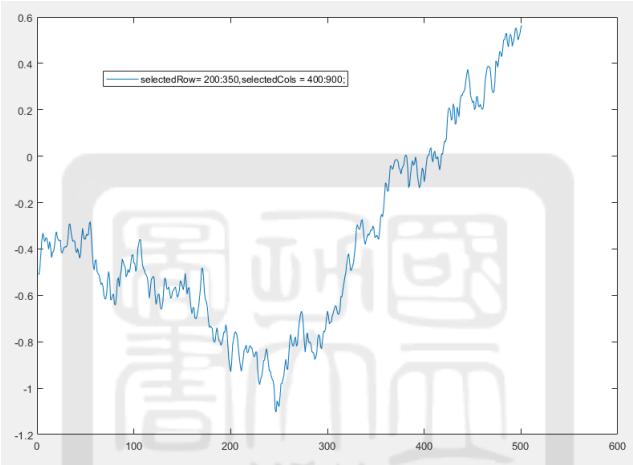

Figure 194: X軸:pixel Y軸:phase. Gas puff, 30ms delay, average of cols 400~900, average of row 200~350

Figure 195: X軸:pixel Y軸:phase. Gas puff, 30ms delay, average of cols 400~900, average of row 350~500

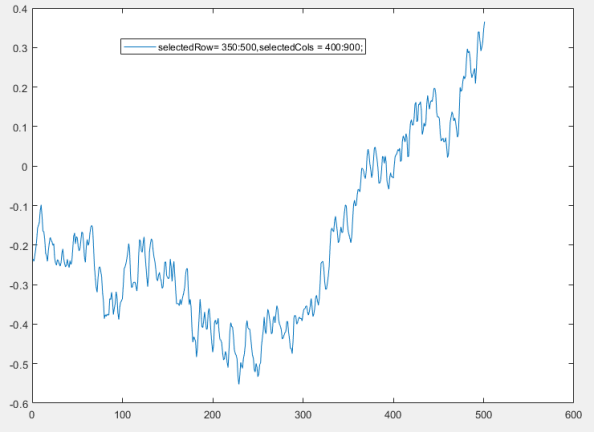

X軸:pixel Y軸:phase

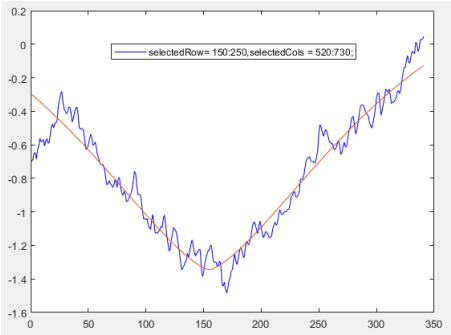

Figure 196: X軸:pixel Y軸:phase. Gas puff, 30ms delay, average of cols 520~730, average of row 150~250

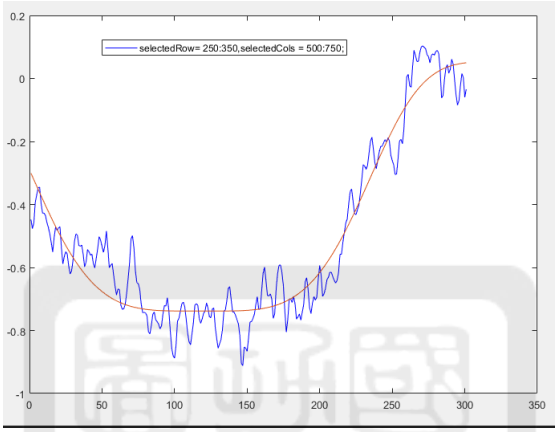

Figure 197: X軸:pixel Y軸:phase. Gas puff, 30ms delay, average of cols 500~730, average of row 250~350

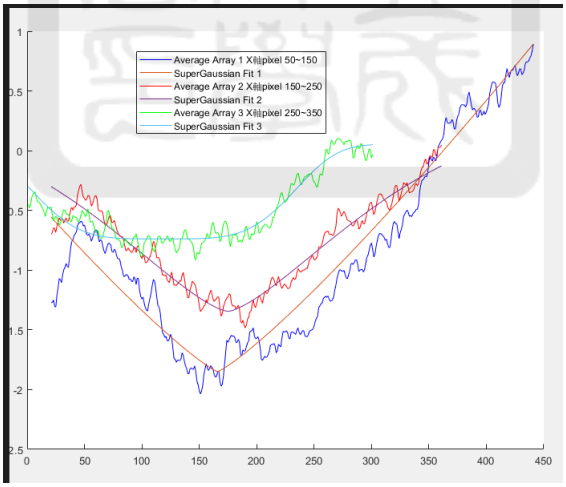

Figure 198: X軸:pixel Y軸:phase. 合併selction three function blue line (50~150), red line (150~250), green line 250~350

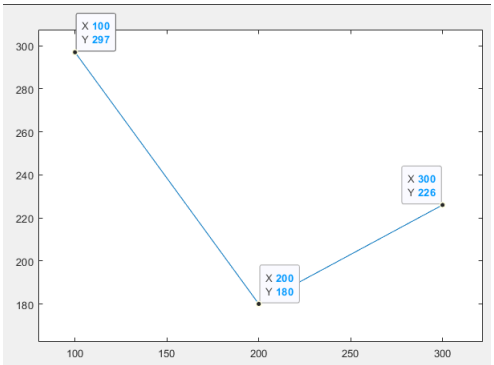

Figure 199: y軸:FWHM pixel. FWHM about row selction 50~150 (left), 150~250(middle), 250~350 (right).

A.4.14 No HV-30 ms-5

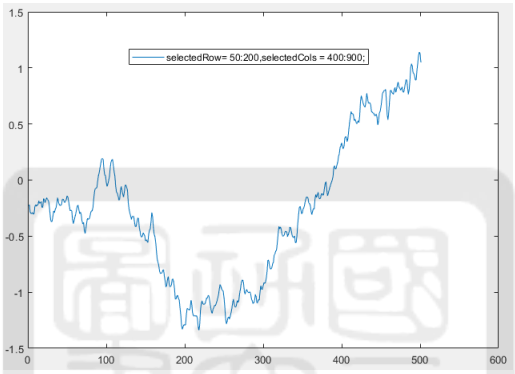

Figure 200: X軸:pixel Y軸:phase. Gas puff, 30ms delay, average of cols 400~900, average of row 50~200

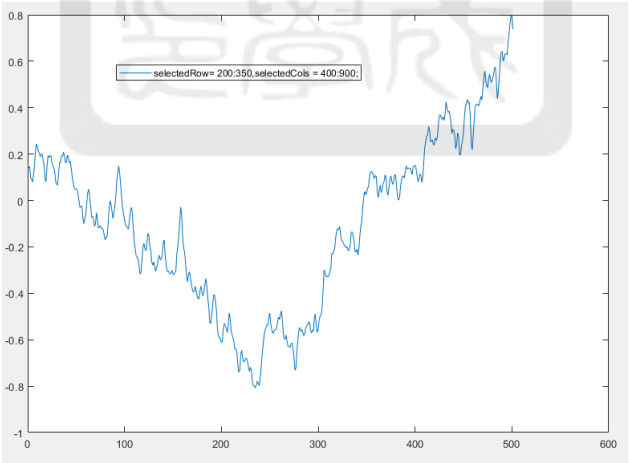

Figure 201: X軸:pixel Y軸:phase. Gas puff, 30ms delay, average of cols 400~900, average of row 200~350

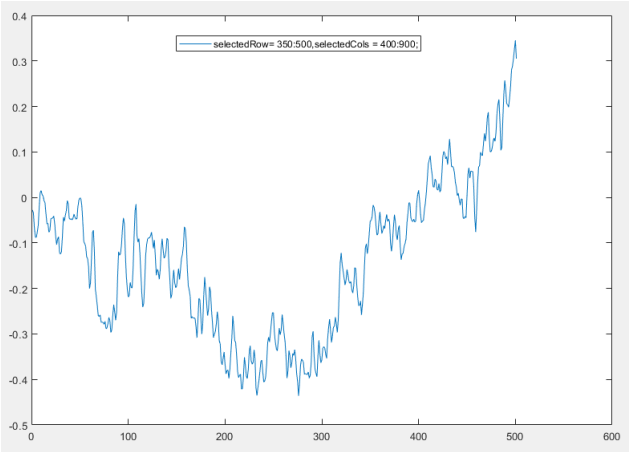

Figure 202: X軸:pixel Y軸:phase. Gas puff, 30ms delay, average of cols 400~900, average of row 350~500

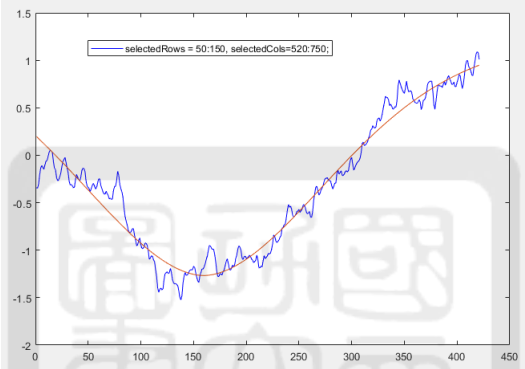

Figure 203: X軸:pixel Y軸:phase. Gas puff, 30ms delay, average of cols 520~750, average of row 50~150

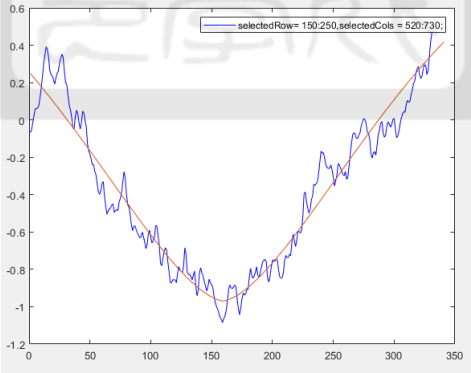

Figure 204: X軸:pixel Y軸:phase. Gas puff, 30ms delay, average of cols 520~750, average of row 150~250

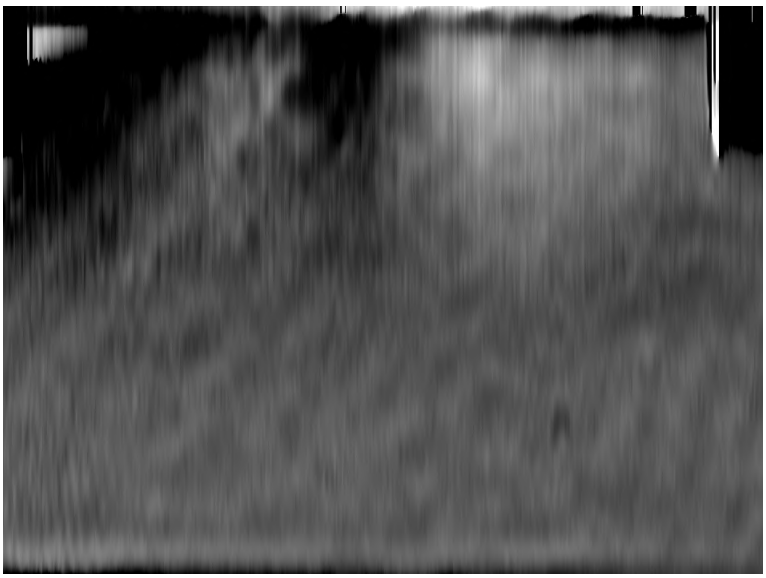

Figure 205: rotate 90 degree image

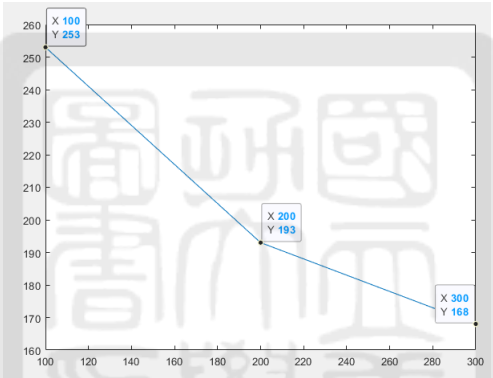

Figure 206: y軸:FWHM pixel. FWHM about row selction 50~150 (left), 150~250(middle), 250~350 (right).

A.4.15 No HV-40 ms-1

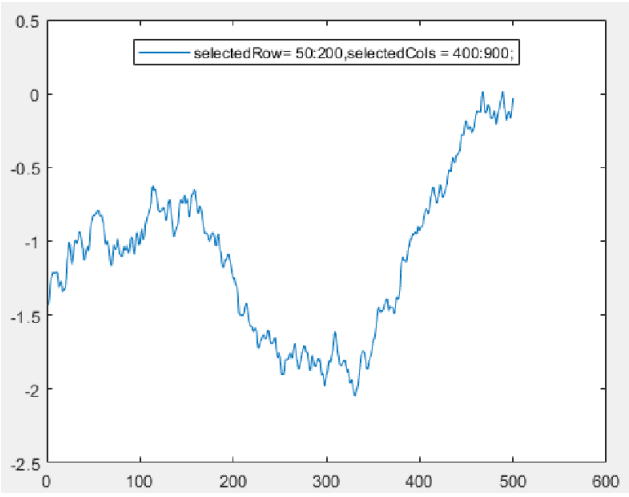

Figure 207: X軸:pixel Y軸:phase. Gas puff, 40ms delay, average of cols 400~900, average of row 50~200

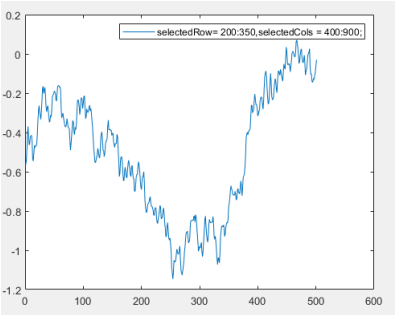

Figure 208: X軸:pixel Y軸:phase. Gas puff, 40ms delay, average of cols 400~900, average of row 200~350

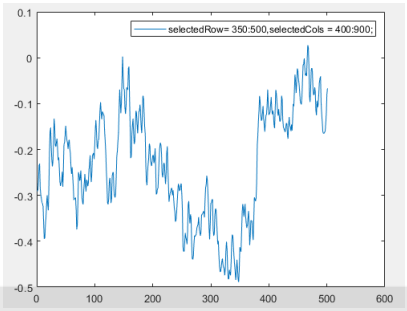

Figure 209: X軸:pixel Y軸:phase. Gas puff, 40ms delay, average of cols 400~900, average of row 350~500

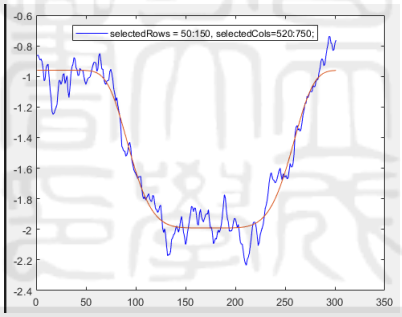

Figure 210: X軸:pixel Y軸:phase. Gas puff, 40ms delay, average of cols 520~750, average of row 50~150

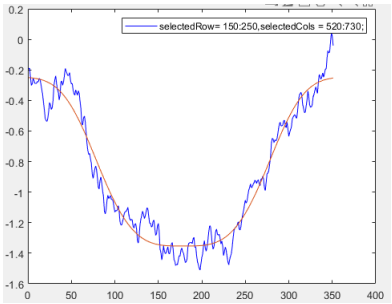

Figure 211: X軸:pixel Y軸:phase. Gas puff, 40ms delay, average of cols 520~750, average of row 150~250

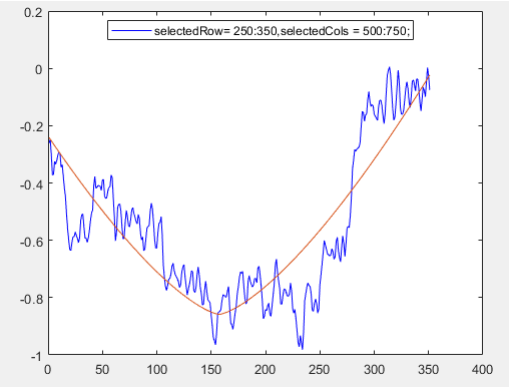

Figure 212: X軸:pixel Y軸:phase. Gas puff, 40ms delay, average of cols 500~750, average of row 250~350

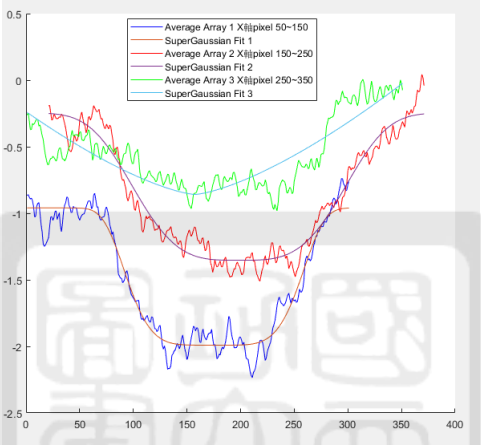

Figure 213: X軸:pixel Y軸:phase. 合併selction three function blue line (50~150), red line (150~250), green line 250~350

00

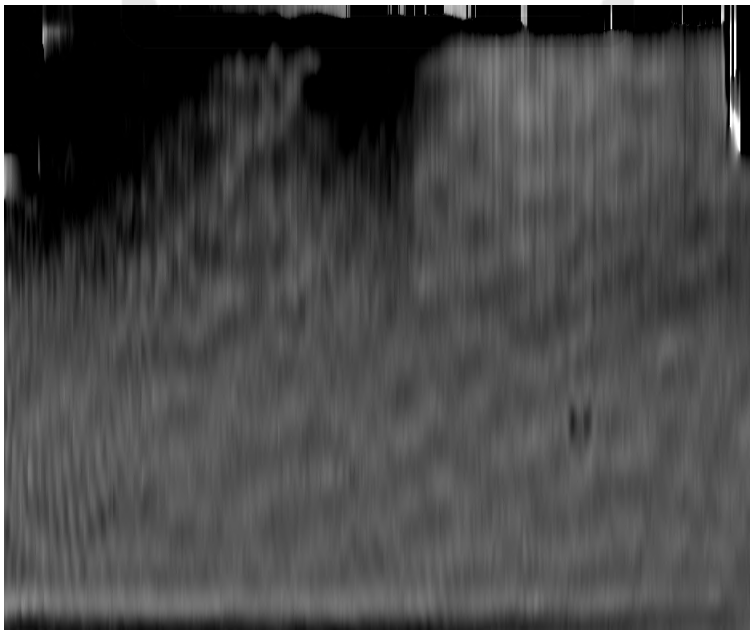

Figure 214: rotate 90 degree image

A.4.16 No HV-40 ms-2

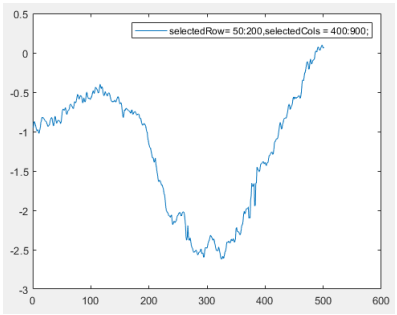

Figure 215: X軸:pixel Y軸:phase. Gas puff, 40ms delay, average of cols 400~900, average of row 50~200

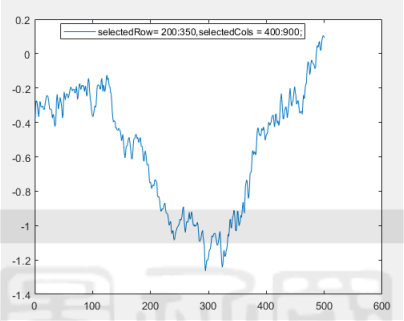

Figure 216: X軸:pixel Y軸:phase. Gas puff, 40ms delay, average of cols 400~900, average of row 200~350

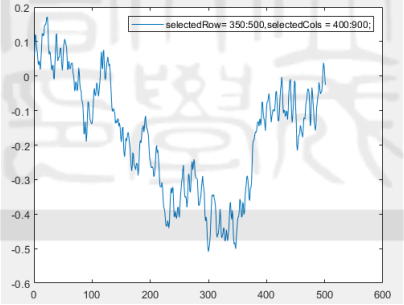

Figure 217: X軸:pixel Y軸:phase. Gas puff, 40ms delay, average of cols 400~900, average of row 350~500

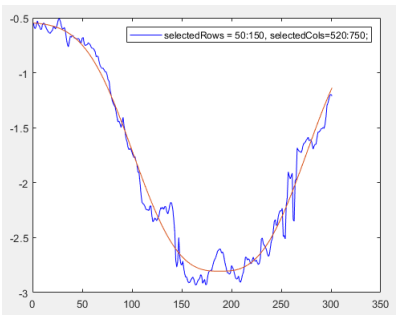

Figure 218: X軸:pixel Y軸:phase. Gas puff, 40ms delay, average of cols 520~750, average of row 50~150

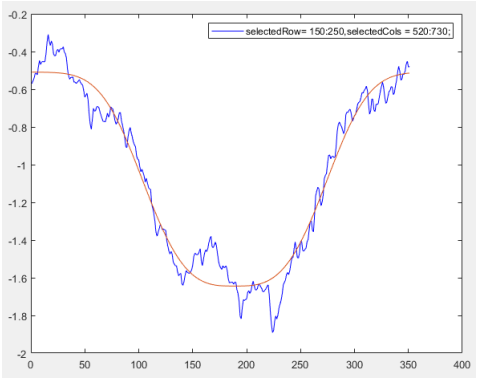

Figure 219: X軸:pixel Y軸:phase. Gas puff, 40ms delay, average of cols 520~750, average of row 150~250

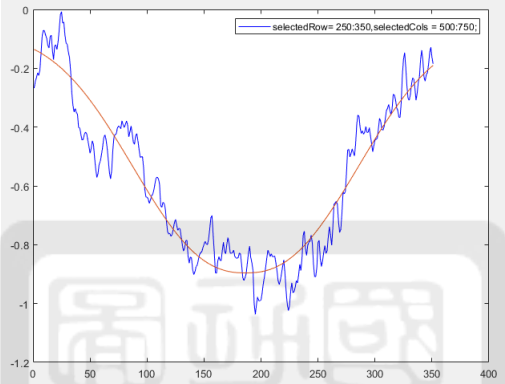

Figure 220: X軸:pixel Y軸:phase. Gas puff, 40ms delay, average of cols 500~750, average of row 250~350

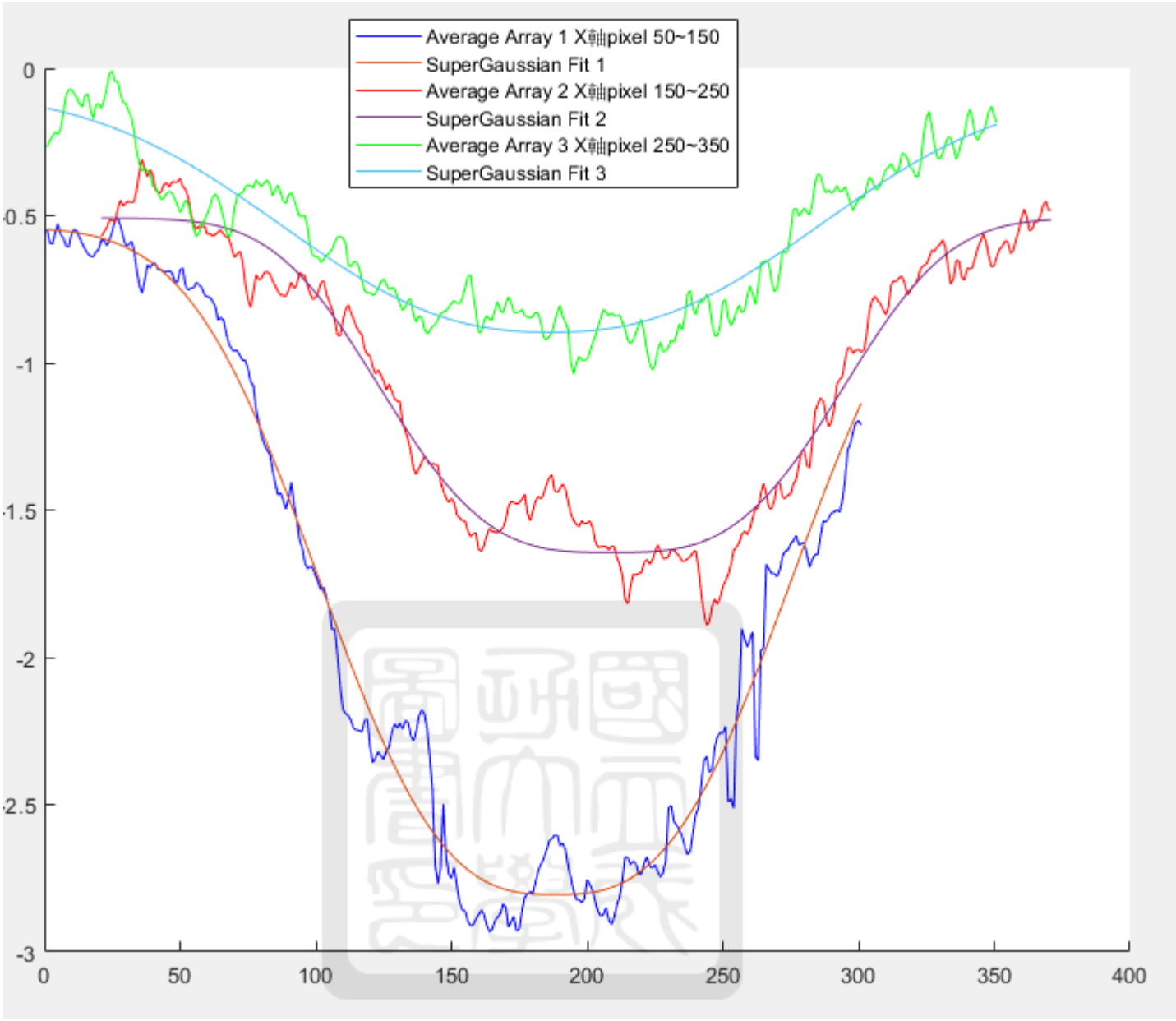

Figure 221: X軸:pixel Y軸:phase. 合併selction three function blue line (50~150), red line (150~250), green line 250~350

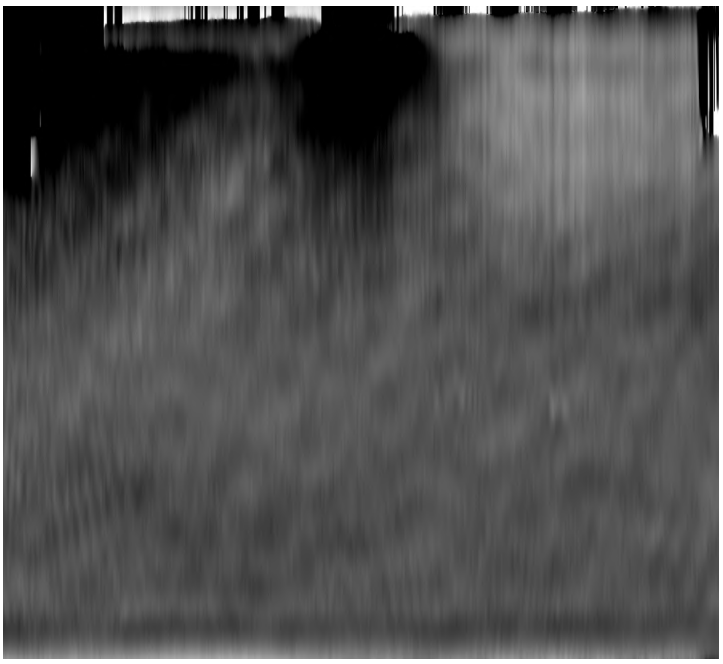

Figure 222: rotate 90 degree image

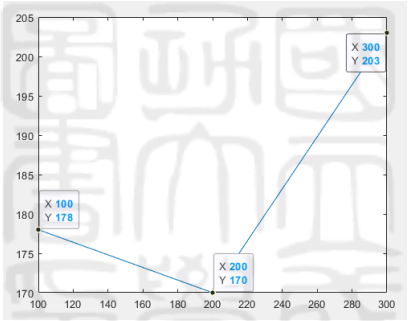

Figure 223: y軸:FWHM pixel. FWHM about row selction 50~150 (left), 150~250(middle), 250~350 (right).

A.4.17 No HV-40 ms -3

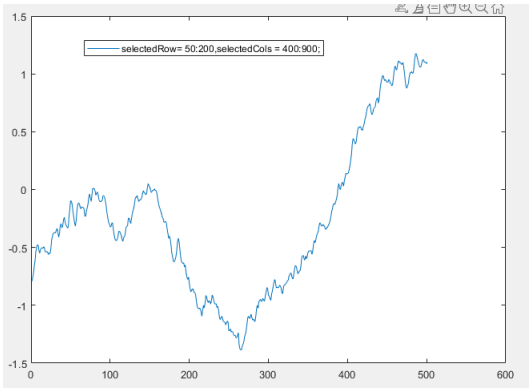

Figure 224: X軸:pixel Y軸:phase. Gas puff, 40ms delay, average of cols 400~900, average of row 50~200

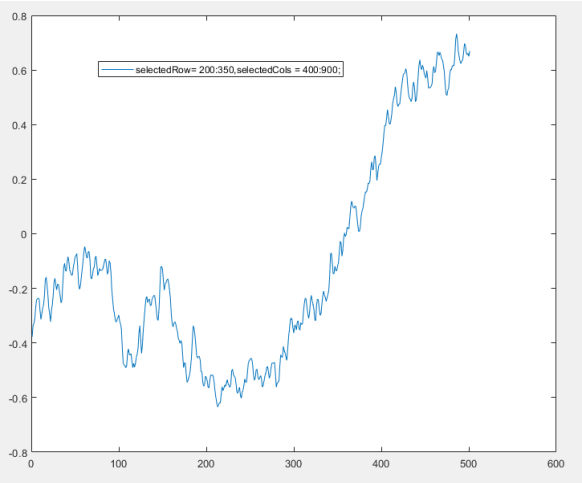

Figure 225: X軸:pixel Y軸:phase. Gas puff, 40ms delay, average of cols 400~900, average of row 200~350

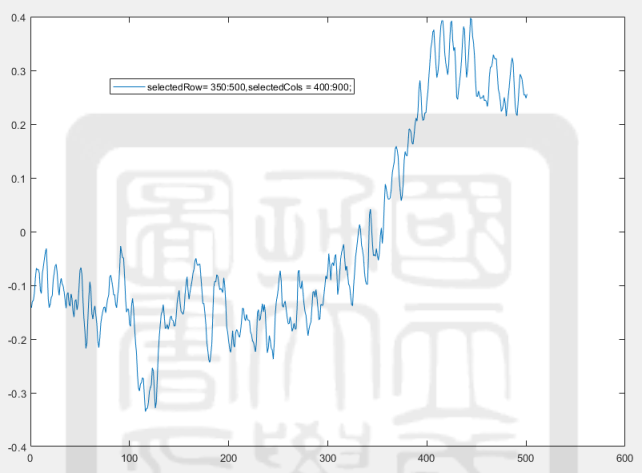

Figure 226: X軸:pixel Y軸:phase. Gas puff, 40ms delay, average of cols 400~900, average of row 350~500

Figure 227: X軸:pixel Y軸:phase. Gas puff, 40ms delay, average of cols 520~750, average of row 50~150

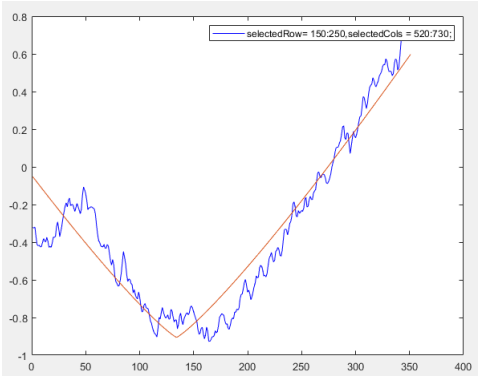

Figure 228: X軸:pixel Y軸:phase. Gas puff, 40ms delay, average of cols 520~750, average of row 150~250

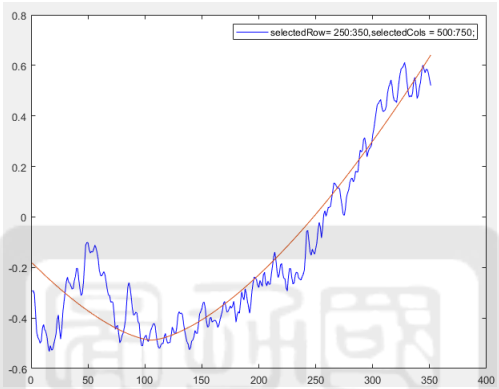

Figure 229: X軸:pixel Y軸:phase. Gas puff, 40ms delay, average of cols 500~750, average of row 250~350

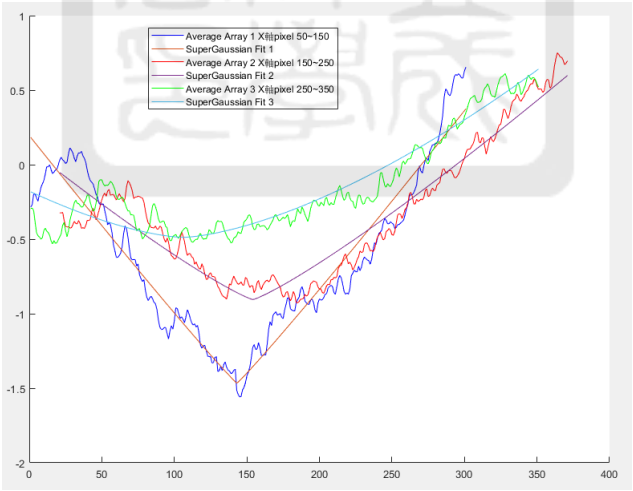

Figure 230: X軸:pixel Y軸:phase. 合併selction three function blue line (50~150), red line (150~250), green line 250~350

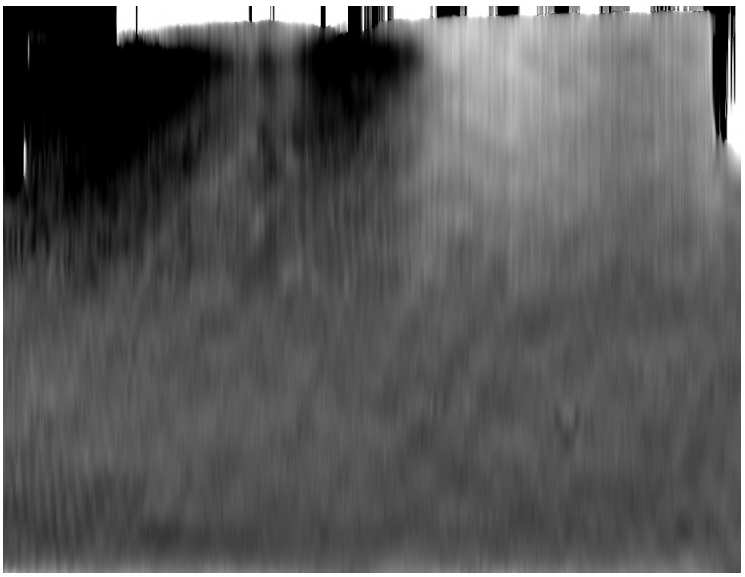

Figure 231: rotate 90 degree image

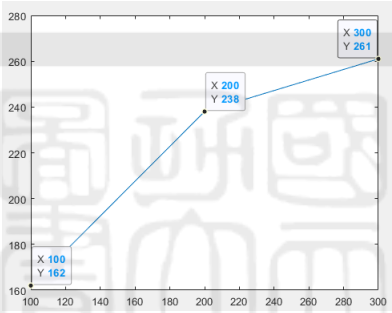

Figure 232: y軸:FWHM pixel. FWHM about row selction 50~150 (left), 150~250(middle), 250~350 (right).

A.5 Nas store record

Table 9: Experiment data record in NAS

Appendix	NAS
8.1	Experiment/2021_cliu/2022-11-15 Analyzer gas pulse valve system 閥門時間測試
8.2	Experiment/2021_cliu/2022-11-22_Gas puff.
	Experiment/2021_cliu/ 2022.12.2
	Experiment/2021_cliu//2022.12.16 convergent nozzle(shadowgraph 10^-3 torr)
8.2	Experiment/2021_cliu/2022.12.27
8.3	Drwaing/2021_cliu/電極
8.4	Experiment/2021_cliu/2023.06.19 分析數據